

Inter-annual variability of CO₂ exchange between pedunculate oak forest (*Quercus robur* L.) and the atmosphere

Anić, Mislav

Doctoral thesis / Disertacija

2019

Degree Grantor / Ustanova koja je dodijelila akademski / stručni stupanj: **University of Zagreb, Faculty of Science / Sveučilište u Zagrebu, Prirodoslovno-matematički fakultet**

Permanent link / Trajna poveznica: <https://um.nsk.hr/um:nbn:hr:217:869952>

Rights / Prava: [In copyright](#) / [Zaštićeno autorskim pravom.](#)

Download date / Datum preuzimanja: **2024-06-30**



Repository / Repozitorij:

[Repository of the Faculty of Science - University of Zagreb](#)





UNIVERSITY OF ZAGREB
FACULTY OF SCIENCE
DEPARTMENT OF GEOPHYSICS

Mislav Anić

**INTER-ANNUAL VARIABILITY OF CO₂
EXCHANGE BETWEEN PEDUNCULATE
OAK FOREST (*Quercus robur* L.) AND
THE ATMOSPHERE**

Doctoral thesis

Zagreb, 2019



UNIVERSITY OF ZAGREB
FACULTY OF SCIENCE
DEPARTMENT OF GEOPHYSICS

Mislav Anić

**INTER-ANNUAL VARIABILITY OF CO₂
EXCHANGE BETWEEN PEDUNCULATE
OAK FOREST (*Quercus robur* L.) AND
THE ATMOSPHERE**

Doctoral thesis

Supervisors:

Dr. Hrvoje Marjanović

Prof. Željko Večenaj

Zagreb, 2019



SVEUČILIŠTE U ZAGREBU
PRIRODOSLOVNO – MATEMATIČKI FAKULTET
GEOFIZIČKI ODSJEK

Mislav Anić

**MEĐUGODIŠNJA VARIJABILNOST
IZMJENE CO₂ IZMEĐU ŠUME HRASTA
LUŽNJAKA (*Quercus robur* L.) I
ATMOSFERE**

DOKTORSKI RAD

Mentori:

dr. sc. Hrvoje Marjanović

doc. dr. sc. Željko Večenaj

Zagreb, 2019.

This thesis was written within the framework of the project EFFectivity (Estimating and Forecasting Forest Ecosystem Productivity by Integrating Field Measurements, Remote Sensing and Modelling). The project was funded by the Croatian Science Foundation (HRZZ-UIP-11-2013-2492).

The thesis was made under the supervision of Dr Hrvoje Marjanović and Dr Željko Večenaj as a part of the doctoral study at the Department of Geophysics, Faculty of Science, University of Zagreb.

Dr Marjanović was born on 13th of June 1973 in Zagreb. In 2000 he graduated Physics at the Faculty of Science, University of Zagreb. Since 2001 he is employed at Croatian Forest Research Institute. In 2009, he defended his PhD thesis (*Modelling tree development and elements of stand structure in young stands of Pedunculate oak (Quercus Robur L.)*) at the Forestry Faculty, University of Zagreb. Since October 2017, Dr Marjanović is Scientific Advisor at Department for Forest Management and Forestry Economics, Croatian Forest Research Institute.

Dr Željko Večenaj was born on 29th of October 1980 in Koprivnica. He graduated Geophysics at the Faculty of Science, University of Zagreb in 2005, at the Department of Geophysics. In 2012, he obtained his PhD (*Characteristics of the bora related turbulence*) at the Faculty of Science, University of Zagreb, Department of Geophysics. Since 2016, Dr Večenaj is Assistant Professor at the Department of Geophysics, Faculty of Science, University of Zagreb.

ACKNOWLEDGEMENTS

First of all, I would like to express my gratitude to Dr Hrvoje Marjanović, the principal investigator and organizer of the whole project EFFectivity within which doctoral thesis was written. His advices and guiding support helped me to cross many obstacles which I encountered during data analysis and writing of manuscripts including this thesis. I am thankful for his patience and for the great deal of trust that he had in me. I am very grateful to Dr Željko Večenaj for his advices and discussions.

Special thanks to Dr Maša Zorana Ostrogović Sever for her generous assistance during writing of this work and for many useful advices and discussions.

Special thanks to Prof. Zoltán Barcza for his generous assistance, discussions, advices on data processing and kind hospitality during my stay in Budapest.

I am very thankful to Prof. Zvezdana Bencetić Klaić and Prof. Branko Grisogono for reading and improving of this dissertation.

Many thanks go to my colleges from Croatian Forest Research Institute, especially Nikolina Milanović and Goran Tijan for their technical support and help with data collection.

At the end, I would like to express my gratitude to my mother and friends for their support, patience and motivation.

LIST OF ABBREVIATIONS

DBH – diameter at breast height

DOY – day of the year

EC – eddy covariance

EGS – end of growing season

GSL – growing season length

GPP – gross primary productivity

NEE – net ecosystem exchange

NEP – net ecosystem productivity

NPP – net primary productivity

NPP_{EC} – NPP estimation with the eddy covariance technique

NPP_{BM} – NPP estimation with the biometric method

NPP_{WBt} – NPP of total (below- and above) wood biomass

NPP_{LF} – NPP of tree foliage and fruits

P – precipitation

R_{ECO} – ecosystem respiration

R_a – autotrophic respiration

R_h – heterotrophic respiration

R_g – global radiation

SGS – start of growing season

SWC – soil water content

T_a – air temperature

T_s – soil temperature

u_* - friction velocity

VPD – vapor pressure deficit

ABSTRACT

Water vapor and carbon dioxide are the main atmospheric constituents which are controlling the Earth's climate. The rapid increase in the atmospheric content of carbon dioxide since the beginning of the industrial revolution is considered as one of the main drivers of the recent climate changes on Earth. Only about 40% of the total anthropogenic emissions of CO₂ remain in the atmosphere, while the rest of the emitted CO₂ is stored in oceans and land. The terrestrial sinks of carbon are global soils and forests. Forests sequester CO₂ from the atmosphere and assimilate carbon into above- and belowground biomass and by that partially offset anthropogenic emission of CO₂ and participate in a regulation of climate. Because of these findings, monitoring of CO₂ exchange between atmosphere and underlying forest ecosystems has gained significant importance. Micrometeorological eddy covariance technique has shown as the most accurate way for direct flux measurement of trace gases, and today it is a standard tool for estimating net ecosystem exchange (*NEE*) of trace gases between the atmosphere and the underlying surface.

Within this research 10-year eddy covariance experiment (2008-2017) was carried out in young pedunculate oak (*Quercus robur* L.) stands (35-44 years old) which are part of the forest complex of the Kupa River basin, about 35 km SW from Zagreb, Croatia. Over the entire study period, Jastrebarsko forest acted as a carbon sink, with an average annual *NEE* of $-319 \pm 30 \text{ g C m}^{-2} \text{ yr}^{-1}$. Estimated *NEE* was partitioned into gross primary production (*GPP*) and ecosystem respiration (*R_{ECO}*). Furthermore, *R_{ECO}* was partitioned into heterotrophic (*R_h*) and autotrophic respiration (*R_a*). Most important carbon flux in forest ecosystems, net primary production (*NPP*), was estimated by subtracting *NEE* from heterotrophic respiration. In this study the causes of inter-annual variability of carbon *NEE* were investigated. Also, the impact of extreme weather events (droughts and floods) on carbon fluxes was investigated. For validation of EC measurements, a biometric estimate of the net primary productivity (*NPP_{BM}*), which was built on periodic measurement and simple modelling, was compared with *NPP_{EC}*. Comparison of *NPP_{EC}* and *NPP_{BM}* showed good agreement ($R^2=0.46$).

Key words: CO₂, *NEE*, *GPP*, *R_{ECO}*, *NPP*, turbulence, eddy covariance, pedunculate oak

TABLE OF CONTENTS

ACKNOWLEDGEMENTS	ii
LIST OF ABBREVIATIONS	iii
ABSTRACT	iv
1. INTRODUCTION	1
1.1 The atmospheric boundary layer	2
1.2 Carbon fluxes in the ecosystem	4
1.3 Eddy covariance technique	6
1.4 Review of previous research.....	10
1.5 Research objectives	13
2. RESEARCH AREA AND MATERIALS	14
2.1. Research area	14
2.2. Experimental site and measurements	16
3. METHODOLOGY	20
3.1 Raw data description and treatment.....	20
3.2 Flux calculation	22
3.2.1 Data quality control.....	23
3.2.2 Time lag compensation	23
3.2.3 Coordinate rotation	24
3.2.4 Flux determination	27
3.2.5 Spectral corrections.....	28
3.2.6 WPL correction	30
3.2.7 Self-heating correction (Burba correction)	30
3.2.8 Stationarity test	31
3.2.9 CO ₂ flux storage computation.....	32
3.3 Secondary flux data treatment	32
3.3.1 Absolute limits	32
3.3.2 Secondary CO ₂ flux despiking.....	33
3.4 Night CO ₂ flux error and u^* filtering	34
3.5 Data gap-filling.....	36
3.6 Flux partitioning	37
3.7 Estimation of <i>NPP</i> based on biometric measurements (NPP_{BM}).....	38
3.7.1 <i>NPP</i> of total woody biomass (NPP_{WBt}).....	39

3.7.2 <i>NPP</i> of tree foliage and fruits (NPP_{LF})	43
3.7.3 Modelling within-seasonal dynamics of NPP_{BM}	43
3.8 Meteorological data treatment	46
3.9 Flux footprint.....	47
4. RESULTS AND DISCUSSION.....	49
4.1 Meteorological conditions during the study period 2008-2017.....	49
4.2 Length of growing season.....	54
4.3 Flux footprint analysis	55
4.4 Net ecosystem exchange of CO ₂	56
4.4.1 Diurnal cycle of <i>NEE</i>	56
4.4.2 The annual cycle of <i>NEE</i>	58
4.4.3 Total sums of <i>NEE</i>	59
4.5 Partitioned fluxes of carbon: <i>GPP</i> , <i>NPP</i> and <i>RECO</i>	62
4.6 Inter-annual variability of carbon <i>NEE</i>	68
4.7 <i>NPP</i> estimated with biometric method (NPP_{BM}).....	75
4.8 Comparison of <i>NPP</i> estimates from EC and BM measurements	77
4.9 Comparison with other carbon flux estimates	81
5. CONCLUSIONS.....	83
6. EXTENDED ABSTRACT (in Croatian).....	85
6.1 Uvod	85
6.2 Područje istraživanja i materijali	87
6.3 Metodologija.....	88
6.3.1 Tretiranje sirovih podataka	88
6.3.2 Izračun tokova ugljika EC metodom	88
6.3.3 Izračun neto primarne produkcije EC metodom (NPP_{EC})	90
6.3.4 Izračun neto primarne produkcije biometrijskom metodom (NPP_{BM}).....	90
6.4 Rezultati i diskusija	90
6.4.1 Meteorološki uvjeti u periodu 2008-2017.....	90
6.4.2 Neto izmjena CO ₂ - <i>NEE</i>	91
6.4.3 Razdijeljeni tokovi ugljika <i>GPP</i> , <i>RECO</i> i <i>NPP</i>	92
6.4 Usporedba EC mjerenja s biometrijskim mjerenjima.....	92
6.5 Zaključak	93
REFERENCES	94
CURRICULUM VITAE	106

1. INTRODUCTION

Enhanced exploitation of fossil fuels since the beginning of the industrial revolution led to an increase in the atmospheric content of CO₂ from ~280 ppm at the beginning of 18th century to almost 370 ppm at the end of the 20th century [Schimel 1995]. This increase in the atmospheric concentration of CO₂ influenced by human activity is considered as the main driver of the recent climate changes on Earth [IPCC 2014]. The growth in atmospheric CO₂ concentration became significantly high in the last 60 years (Fig. 1.1). Forest ecosystems have provided mankind with raw material and food for centuries, and in the last few decades their importance was also recognized in terms of their contribution to the regulation of climate. Global forests act as a carbon sink [Pan *et al.* 2011]. They sequester CO₂ from the atmosphere and assimilate carbon into above- and belowground biomass and by that partially offset anthropogenic emission of CO₂ [Janssens *et al.* 2003]. Only about 40% of total anthropogenic emission of CO₂ remains in the atmosphere, while the rest of emitted CO₂ is stored in oceans (30%) and land (30%) [IPCC 2014].

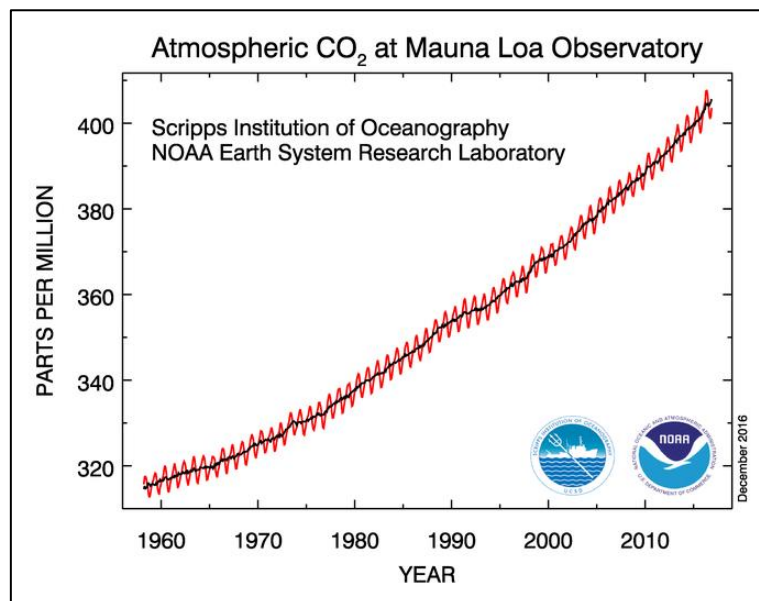


Figure 1.1: Global average atmospheric CO₂ mixing ratio (red line) with long term trend of growth (black line)
(NOAA website 2016)

Typical values of inter-annual variability in the annual rate of growth of atmospheric CO₂ are in the range between 1 and 5 gigatons C yr⁻¹ [Baldocchi *et al.* 2001]. Studies are showing that terrestrial biosphere has an important role in this interannual variability [Keeling 1996]. Canadell *et al.* [2007] have calculated that in the period from 2000 to 2006, global forests were a global sink of carbon of 2.7 Pg C (6 yr)⁻¹. This corresponds to approximately

30% of the total anthropogenic CO₂ emissions during that period. These new learnings about forests ecosystems have opened a new chapter in possible mitigation of the climate changes in the future, but any efforts aimed at managing forests to mitigate increased atmospheric CO₂ require a thorough understanding of the carbon cycle in the forests. However, the potential of forest to act as a carbon sink in the future is uncertain, either due to possible saturation effect [Nabuurs *et al.* 2013], or worse, as a consequences of climate change which would result in directive negative economic impact [Hanewinkel *et al.* 2013]. Thus, monitoring of global forest productivity and understanding year-to-year variability in carbon sequestration became an important task of numerous scientists. Inter-annual variability of forest productivity is a result of the direct response of trees to occurring meteorological conditions [Gough *et al.* 2008], but it also contains a postponed response due to carry-over effect [Urbanski *et al.* 2007, Molen *et al.* 2011]. The postponed response in plants is often explained with the presence of carbon reserve pool, i.e. non-structural carbohydrates (NSC's) that has an important role in overcoming environmental disturbances [Carbone *et al.* 2013, Teets *et al.* 2018].

Development of eddy covariance (EC) technique has greatly facilitated calculation of carbon budgets in the global forests and today EC technique is a widely used standard tool for estimation and monitoring of high frequency (typically half-hourly) carbon and water fluxes within the terrestrial ecosystems [Aubinet *et al.* 2000, Baldocchi *et al.* 2001, 2003]. EC measurements are typically made in the surface layer which is the lowest part of the atmospheric boundary layer (ABL).

1.1 The atmospheric boundary layer

Troposphere, the lowest layer of Earth's atmosphere, can be roughly divided into two parts: a boundary layer near the surface and free atmosphere above it (Fig. 1.2). ABL is the lowest part of the troposphere and it is under direct thermal and mechanical influence of the Earth's surface. These thermal and mechanical surface forcings include heat transfer, transpiration and evaporation, frictional drag, turbulence, pollutant emission and terrain- induced flow modification [Stull, 1988].

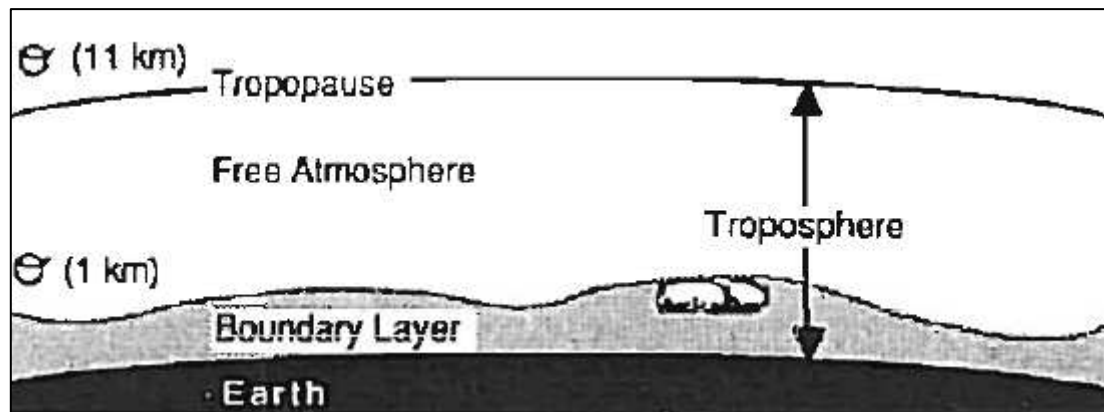


Figure 1.2: Troposphere (from Stull, 1988, page 1)

ABL (Fig. 1.3) is highly variable during the day. In the morning, with the sunrise, starts a heat transfer from the warm surface which destroys the stable nocturnal ABL and the residual layer. A newly formed layer, called mixed layer, is characterized by strong turbulence and is bounded from above by the entrainment zone where the exchange processes between the ABL and the free atmosphere take the place. Dominant mechanisms of turbulence generation in the mixed layer are convection and wind shear. In the case of undisturbed weather conditions, shortly before sunset mixed layer starts to be less turbulent and the stable nocturnal ABL, which is around 100 m deep, starts to develop near the ground. During the night, the stable ABL is capped with the remains of the mixed layer which is now much less turbulent. This layer is called the residual layer and is bounded by a capping inversion on top. The same process is repeating next day after the sunrise [Stull 1988].

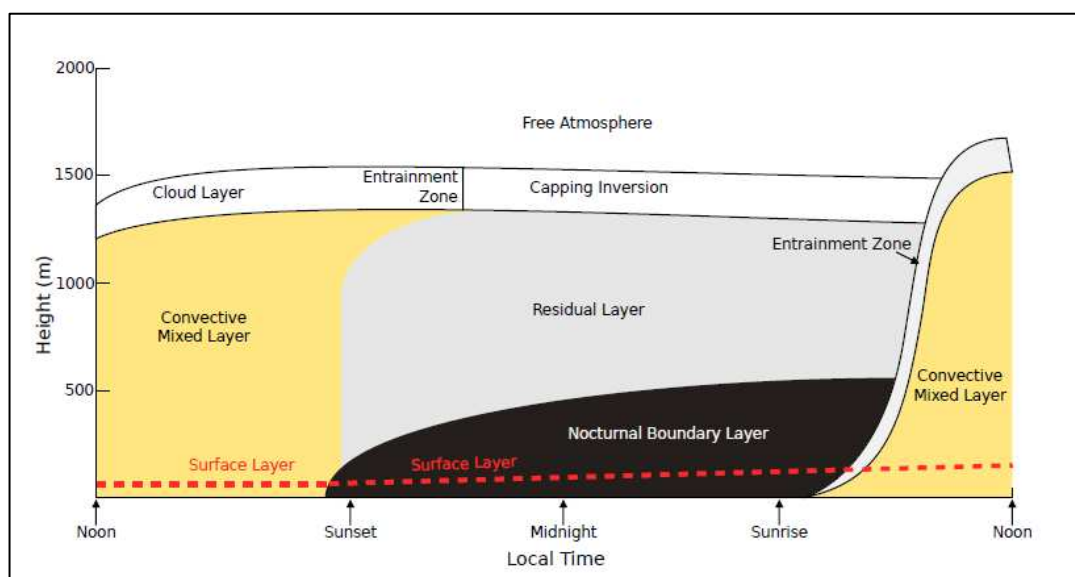
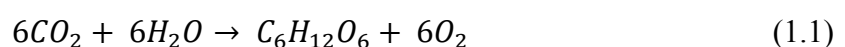


Figure 1.3: The daily cycle of the typical atmospheric boundary layer (from [Babić 2016], page 10)

The depth of ABL also varies in space and time. Under the conditions of strong stable stratification, its thickness can be about 10 m or less. If the stratification is unstable ABL can have a thickness of about 0.5 km over the oceans and 1-4 km over land [e.g. Aubinet *et al.* 2012]. Depending on the underlying surface type, ABL can be divided into several vertical layers. The lowest 5-10% of the ABL occupies atmospheric surface layer which is the “research area” of micrometeorology. The surface layer is one of the main energy-exchange layers in the atmosphere [e.g. Foken 2008]. Atmospheric turbulence is here the dominant transport mechanism and fluxes are approximately constant with height [e.g. Aubinet *et al.* 2012]. Turbulence is a three-dimensional regime of the flow characterized by chaotic changes in pressure and flow velocity which allows the boundary layer to respond to changing surface forcings [e.g. Stull 1988]. Turbulence consists of many different size eddies superimposed on each other. Smaller size eddies are exhibited to strain field of larger eddies. Because of the strain, the vorticity of smaller eddies grows what leads to enhancement of smaller eddies energy at the expense of larger size eddies. So, there is an average energy flux from larger eddies towards smaller ones. On the given wavelength, smaller eddy gains energy from previous larger eddy. This process of energy transfer is called energy cascade [Tennekes and Lumley 1972]. Over the forests, the surface layer can be divided into a roughness sublayer, where the flow consist of turbulence dominated by individual elements and sources and fluxes are not constant with height [e.g. Oke 1987], and into an inertial sublayer where fluxes are almost constant with height and micrometeorological theory can be applied [e.g. Roth 2000]. In the Ekman layer, which sometimes overlies surface layer, fluxes decrease and wind changes direction with the height.

1.2 Carbon fluxes in the ecosystem

Plants absorb CO_2 from the atmosphere and use it in the photosynthesis. Photosynthesis is a chemical process through which plants produce oxygen and glucose ($\text{C}_6\text{H}_{12}\text{O}_6$) from CO_2 and H_2O , using only light as source of energy [e.g. Schulze 2005]. The general equation of photosynthesis is:



In forest ecosystems, carbon is accumulated in live biomass, dead wood and organic matter of forest soil [e.g. Pregitzer and Euskirchen 2004]. These are the three principal

components of the forest ecosystems and they are continuously accumulating and simultaneously losing carbon. Processes of accumulation or loss of carbon are called carbon fluxes. By convention, carbon flux is positive if it leads to an increase in the amount of carbon in certain component of the forest ecosystem, and in the opposite case the carbon flux is negative. Conceptual scheme of the carbon flow through the ecosystem is shown in Fig. 1.4.

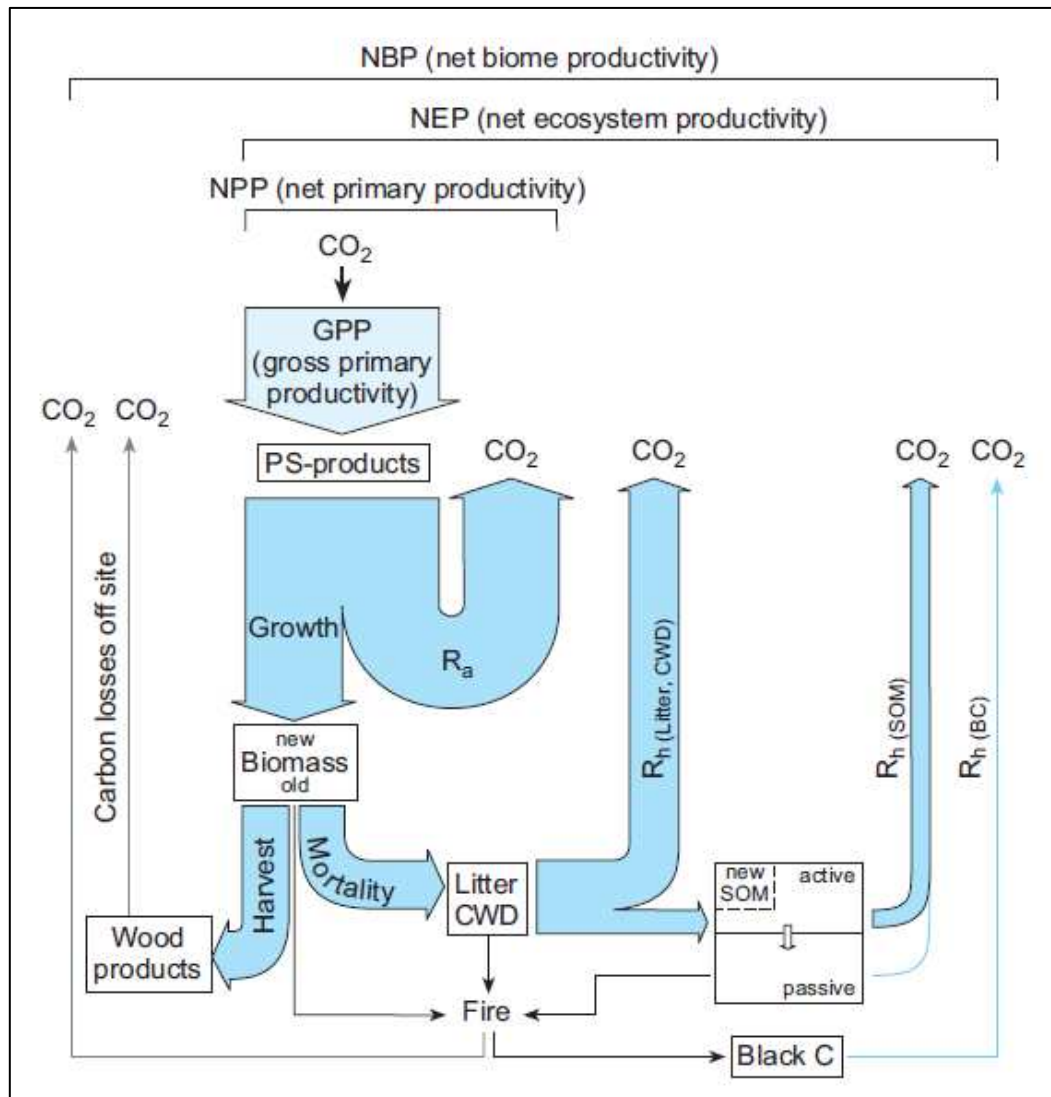


Figure 1.4: Carbon flow through the ecosystem (from [Schulze 2005], page 435)

Gross primary productivity, GPP , is the main positive carbon flux in the ecosystem and it denotes CO_2 assimilation by photosynthesis. The main negative carbon flux, **ecosystem respiration** – R_{ECO} , denotes the amount of carbon which is released from the ecosystem through the respiration processes. R_{ECO} is a sum of the respiration of the plants (autotrophic respiration, R_a) and decomposition of dead organic matter (heterotrophic respiration, R_h):

$$R_{ECO} = R_a + R_h \quad (1.2)$$

Also, carbon can be lost from the ecosystem through harvesting and forest fires. After subtracting the autotrophic respiration of plants from GPP , what remains is called **net primary productivity**, NPP , and it is a measure of carbon stored in biomass within the ecosystem in a given time. NPP includes the production of below- and aboveground wood biomass (NPP_{WB}), litter biomass (NPP_L) and fruit biomass (NPP_{FR}).

$$NPP = R_h - NEE = GPP - R_a = NPP_{WB} + NPP_L + NPP_{FR} \quad (1.3)$$

By subtracting R_{ECO} from GPP we obtain **net ecosystem productivity**, NEP . NEP is the measure of the amount of carbon that is accumulating in (positive NEP) or is lost from (negative NEP) the ecosystem if in the observed period there was no loss of carbon from the ecosystem due to e.g. harvesting, carbon leaching or fire. NEP is equal to negative of **net ecosystem exchange**, NEE , of carbon between the atmosphere and the ecosystem.

$$NEP = GPP - R_{ECO} = -NEE \quad (1.4)$$

An ecosystem is a sink of carbon if the amount of carbon which has left the atmosphere is greater than the amount of carbon which has been released from the ecosystem to the atmosphere. Otherwise, the ecosystem is a source of carbon. NEE of forest ecosystem can be measured directly with the EC technique.

1.3 Eddy covariance technique

EC technique is a micrometeorological method for direct measurement of momentum, heat and mass exchange between a flat horizontally homogeneous surface and the overlying atmosphere [e.g. Baldocchi *et al.* 2001, 2003, Aubinet *et al.* 2000, 2012]. Under this kind of conditions, net transport between the surface and atmosphere is one-dimensional and the vertical flux density can be calculated by the covariance between turbulent fluctuations of the vertical wind speed component and the quantity of interest [e.g. Aubinet *et al.* 2012]. It has been proposed by Montgomery [1948], Swinbank [1951] and Obukhov [1951]. The airflow can be imagined as a horizontal flow of many rotating, 3D different-size eddies (Fig. 1.5) which transport molecules of trace gases.

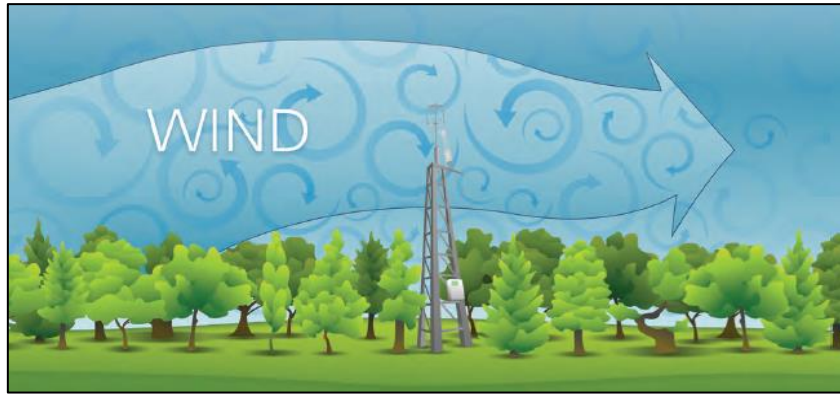


Figure 1.5: Horizontal flow (from [Burba 2013])

Smaller eddies are usually located closer to the ground. They rotate faster, so more transport is done by higher frequency movements of air near the ground. Larger eddies can be found further away from the ground. They rotate slower, so more transport is done by lower frequency movements of air away from the ground. In nature some transport is done at lower frequencies and some at higher ones because there is always a mixture of different eddy sizes [e.g. Burba 2013].

Each turbulent eddy has three dimensions. Each component can be measured at the EC tower. EC measurements are based on determining the correlation between changes in vertical wind velocity component and deviations in a mixing ratio of a trace gas. They are typically made in the surface layer [e.g. Aubinet *et al.* 2012]. The measurement system consists of three-dimensional sonic anemometer and infrared gas analyzer. Sonic anemometers measure three-dimensional wind speed and sonic temperature and they are well suited for turbulence measurements because they can take measurements with a very fine temporal resolution of 10 Hz or more. They measure the difference in transit time for an ultrasound pulse between pairs of transducers arranged at a known distance apart. Infrared gas analyzers are used to measure CO₂ and H₂O concentration in the air.

To derive the equation for vertical flux density we will start from the conservation equation of a scalar quantity:

$$\frac{\partial c}{\partial t} + u \frac{\partial c}{\partial x} + v \frac{\partial c}{\partial y} + w \frac{\partial c}{\partial z} = S + D \quad (1.5)$$

where c denotes scalar density, u , v and w mark components of wind velocity in the direction of the mean wind (x), the lateral wind (y) and normal to the surface (z) respectively, S term represents the source or sink and D is the molecular diffusion. On (1.5) will be first applied

Reynolds averaging where every variable will be decomposed into its mean value and fluctuations around average ($a = \bar{a} + a'$). After applying Reynolds averaging and integration along the z axis and assuming no horizontal eddy flux divergence, (1.5) becomes:

$$\int_0^{h_m} S dz = \overline{w'c'} + \int_0^{h_m} \frac{\partial \bar{c}}{\partial t} dz + \int_0^{h_m} \bar{u} \frac{\partial \bar{c}}{\partial x} dz + \int_0^{h_m} \bar{w} \frac{\partial \bar{c}}{\partial z} dz \quad (1.6)$$

The term on the left side of (1.6) represents *NEE* if the scalar quantity in question is CO₂. The first term on the right side of the (1.6) represents vertical turbulent flux of particular scalar variable at measurement height (h_m) while the third, fourth and fifth term on the right side of (1.6) represent respectively storage of scalar quantity below measurement height, horizontal and vertical advection of scalar quantity. Horizontal advection is significant over complex and heterogeneous terrain or at night over sloping terrain when respired CO₂ can escape the measurements by down-slope drainage. Under these conditions horizontal advection term cannot be neglected. EC technique demands atmospheric stationarity and horizontal homogeneity. Under those conditions second, third and fourth term on the right side of (1.6) decay, so flux of the quantity of interest is equal to the product of the mean air density, and the mean covariance between instantaneous deviations in vertical wind speed and mixing ratio of gas of interest [e.g. Aubinet *et al.* 2000]:

$$NEE = \overline{w'c'} \quad (1.7)$$

Implementation of the EC technique is very complex. Measurements are not perfect, and thus all measurements are subject to errors or uncertainties. High frequency raw data often contain spikes, constant and non-physical values, dropouts and noise. Sources of that bad data are instrumental problems, electrical power failure, animal influence, and rain or snowfall. Such data must be detected and removed before flux calculation. Fluxes of the gas of interest (here CO₂) can be computed after raw data quality check. When the stratification of the atmosphere is stable and turbulence is weak, material diffusing from leaves and the forest soil may not reach the measurement height resulting with violation of the assumption of steady-state conditions and a constant flux layer. Under such conditions the CO₂ storage term becomes nonzero and must be added to measured flux to obtain *NEE*. CO₂ storage term is small during the day and on windy nights, while the greatest values of CO₂ storage term are reached around sunrise and sunset when there is a transition between the daytime mixed layer and the stable nocturnal ABL and between respiration and photosynthesis [Baldocchi *et al.* 2001]. Ignoring it over the long term is acceptable because the daily mean of CO₂ storage is

zero, but, in short term, it may be a significant measure of ecosystem response [Aubinet *et al.* 2000]. Further processing of EC data requires the application of numerous corrections if one wants to obtain high quality fluxes. In Table 1.1 are listed common errors during the EC experiment and their impact on calculated fluxes.

Filtering procedures and measuring system malfunctions are leading to gaps in time series. The biggest issues are occurring during the calm nights when the stable nocturnal layer is fully developed. In such case, the EC technique underestimates the CO₂ flux what could lead to a strong overestimation of NEE at an annual scale because the ecosystem is a source of carbon during the night [e.g. Aubinet *et al.* 2012]. This error is called night flux error and it significantly affects almost every EC measurement site. Such fluxes must be detected and discarded from further processing. Numerous corrections and filtering procedures will result in many gaps in the time series which need to be filled with one of the gap-filling techniques [Falge *et al.* 2001, Reichstein *et al.* 2005]. The final result of EC measurement and data processing is *NEE* of CO₂ between the ecosystem and the atmosphere. Estimated *NEE* can be partitioned into *GPP* and *RECO* with some developed flux partitioning methods [Reichstein *et al.* 2005, Lasslop *et al.* 2010].

Table 1.1: Errors and their impact on calculated flux (from [Burba 2013])

Procedure	Affected fluxes	Effect	Range
Spike removal	all	depends	0-15%
Coordinate rotation	all	depends	0-25%
Angle of attack correction	all	depends	0-25%
Time delay adjustment	mostly closed path	increases flux	0-50%
Frequency response corrections	all	increases flux	0-50%
Sonic heat flux correction	sensible heat flux	depends	0-10%
Webb-Pearman-Leuning terms	any gas	depends	0-50%
Spectroscopic effects for LASERs	any gas	depends	0-25%
Band-broadening correction for NDIR	mostly CO ₂	depends	0-5%
Oxygen correction	some H ₂ O	depends	0-10%
Gas flux storage term	any gas	increases flux	0-5%

For the purpose of this work, EC technique has been chosen for CO₂ flux calculation because it is a scale-appropriate method and it provides measurements of net CO₂ exchange of a whole ecosystem across a spectrum of times scales, ranging from hours to years with minimal disturbance to the underlying vegetation. Also, it enables direct measurement of net CO₂ exchange between ecosystem and overlying atmosphere. EC technique is not perfect and

has some weaknesses. It is applicable over a flat terrain when the environmental conditions are steady and when the underlying vegetation extends upwind for an extended distance [Baldocchi 2003]. Despite that, its strengths far outweigh its weaknesses and today EC technique is one of the most defensible ways to measure trace gas fluxes [Burba 2013].

1.4 Review of previous research

From the 1950s to 1970s micrometeorological experiments were designed to investigate fundamental aspects of atmospheric turbulence over the homogeneous terrain. Later, in the 1980s, turbulent fluxes of momentum, sensible and latent heat over heterogeneous surfaces have been investigated in numerous studies. With the development of new generation of fast response sonic anemometers, rapid-responding infrared gas analyzers for water vapour and CO₂ measurement and computer software packages in the 1990s emerged possibility of continuous flux measurement [e.g. Aubinet *et al.* 2012]. With these technological advances EC technique has reached full potential and replaced flux-gradient method which has been previously used for flux calculation. Flux-gradient method is an indirect technique that evaluates flux densities as the product of a turbulent diffusivity (K) and the vertical gradient of scalar concentration (dc/dz) [e.g. Baldocchi 2003]. It has showed as inappropriate for CO₂ flux calculations over tall forests where vertical gradients of CO₂ are small and difficult to resolve because turbulent mixing is efficient. Besides that, turbulent transport is enhanced by the presences of a roughness layer so evaluation of eddy exchange coefficients using Monin-Obukhov similarity theory is invalid above forests [Raupach 1979]. Across the globe in the middle 1990s many EC towers had been set up and many estimations of *NEE* of CO₂ between the atmosphere and diverse ecosystems had been performed until today. Most sites are net sinks of CO₂ on an annual basis and the largest values of carbon uptake are associated with deciduous and coniferous temperate forests. Table 1.2 shows review of several studies which were performed in temperate broadleaved deciduous forests.

NEE of CO₂ in broadleaved deciduous forests depends on the length of growing season and the availability of nutrients, water and sunlight [Baldocchi *et al.* 2001]. During the winter broadleaved forests lose carbon because they are leafless and dormant. During the summer growing season, they are gaining carbon. The timing of the transition between uptake and carbon release along with the length of growing season is one of reasons for differences among broadleaved deciduous forests sites shown in Table 1.2. The situation is different in

the conifer forests. Differences of annual sums of *NEE* between EC sites in the coniferous forests are caused by latitudinal differences, continental positions (boreal, temperate, semiarid and humid conifers) and different physiological reasons [Baldocchi *et al.* 2001]. The estimated annual *NEE* at Hyytiälä site (southern Finland, 61°51'N, 24°17'E) in boreal Scots pine (*Pinus sylvestris* L.) forest were -234, -262 and -191 gC m⁻² yr⁻¹ in 1997, 1998 and 1999, respectively [Markkanen *et al.* 2001].

Table 1.2: EC measurements in temperate broadleaved deciduous forests

LOCATION	LATITUDE	VEGETATION	MEASUREMENT YEARS	NEE [gC m ⁻² yr ⁻¹]	CITATION
USA Massachusetts	42.53°N	Maple (<i>Acer</i>) Oak (<i>Quercus</i>)	1991	-280	Goulden <i>et al.</i> [1996a,b]
			1992	-220	
			1993	-140	
			1994	-210	
			1995	-270	
USA Massachusetts	42.53°N	Maple (<i>Acer</i>) Oak (<i>Quercus</i>)	1992	-220	Urbanski <i>et al.</i> [2007]
			1993	-150	
			1994	-170	
			1995	-280	
			1996	-200	
			1997	-210	
			1998	-100	
			1999	-230	
			2000	-220	
			2001	-470	
Indiana, USA	39°19'N	Deciduous forest	1998	-240	Schmid <i>et al.</i> [2000]
France	48°40'N	Beech (<i>Fagus</i>)	1996	-218	Granier <i>et al.</i> [2001]
			1997	-257	
England	51°46'N	Broadleaf deciduous forest	2008	-265	Thomas <i>et al.</i> [2011]
Denmark	55°29'N	Beech (<i>Fagus</i>)	1997	-169	Pilegaard <i>et al.</i> [2001]
			1998	-124	

Recently, with the improvement of infrared gas analyzers, researchers have started to use the EC technique also for measurements of fluxes of other trace gases. For example, Felber *et al.* [2015] showed that EC technique is sufficiently accurate to estimate mean methane (CH₄) emissions of animals (mostly cows) on the pasture. Also, numerous researchers have implemented the EC technique for measurement of energy exchange, water vapour and other trace gases, pollutants and aerosols between urban surface and atmosphere. Liu *et al.* [2012] carried out a four year EC experiment in the city of Beijing. The results showed that diurnal courses of CO₂ largely depend on the volume of traffic. Also, they showed that analysed urban area was a net source of CO₂ to the atmosphere. Some researchers started to use EC measurements in bioenergetics. Bioenergy crops have the potential to become economically important. Some of the energy crops can even grow in very extreme conditions and can still act as a significant sink of carbon. One such example is blue agave cactus (*Agave tequilana*, F.A.C. Weber) which has little water demand but significant productivity. Owen *et al.* [2016] showed that plantation of blue agave in Mexico was a significant sink of carbon with the amount of -333 gC m⁻² yr⁻¹, greater than some temperate and boreal forests.

In Croatia, the first open-path EC system was set up in 2007 for monitoring CO₂, H₂O, latent and sensible heat fluxes in young lowland pedunculate oak (*Quercus robur* L.) forest located near the town of Jastrebarsko [Marjanović *et al.* 2011], west of Zagreb. The second EC system has been set up recently in the City of Zagreb in Maksimir by Meteorological and Hydrological Service. In the neighbouring countries, the longest EC monitoring system is located in Hegyhátsál (46°57' N, 16°39' E), Hungary operated by the Eötvös Loránd University (Budapest) and the Hungarian Meteorological Service, Budapest [Haszpra *et al.* 2001]. Bárcza [2001] has estimated that small grassland area in Hegyhátsál sequestered 134, 146 and 92 gC m⁻² yr⁻¹ in 1997, 1998 and 1999, respectively.

There are over 650 EC towers in the world mounted today which are connected to the global network of micrometeorological flux measurement sites called the FLUXNET network [Baldocchi *et al.* 2001]. Unfortunately, the complexity and high maintenance cost of EC systems have limited the number of sites with measurements spanning a decade or longer [FLUXNET2015 Dataset].

1.5 Research objectives

The forested area in Croatia amounts to 2.493 million Ha what makes 47.5% of its total land area. Lowland forests of pedunculate oak (*Quercus robur* L.) are making 32% of growing stock in Croatia [Croatian Forests Ltd. 2017] and they are the most valuable forests in Croatia. They appear to be the most productive ecosystems in Croatia and represent an important economic resource for the state and local community [Marjanović *et al.* 2011], thus monitoring of their productivity and response to climate changes is very important. Pedunculate oak forests in Croatia can be found mostly in lowlands of rivers Drava, Kupa and Sava. Outside of these areas, pedunculate oak forests develop in flooding parts of *Ličko*, *Imotsko* and *Vrličko polje* as well as in basin of river Mirna in Istria (Fig. 1.6, [Trinajstić 1996]).

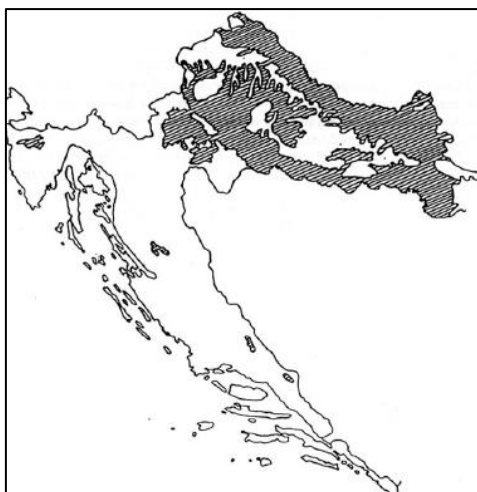


Figure 1.6: Prevalence of pedunculate oak in Croatia (from [Trinajstić 1996], page 100)

Main objectives of this dissertation are to: (1) estimate *NEE* of CO₂ between pedunculate oak forest and the atmosphere from long term EC measurements (2008-2017), (2) to understand the cause of inter-annual and short term variability of the carbon fluxes, (3) to investigate impact of weather extremes (droughts and flooding) on carbon fluxes and productivity of oak forest and (4) to estimate *NPP* with biometric method and assess the agreement in *NPP* estimates from EC and biometric measurements.

2. RESEARCH AREA AND MATERIALS

2.1. Research area

The research was carried out in Jastrebarsko forest which is a part of the forest complex of Kupa River basin, located approximately 35 km SW from Zagreb, near the town of Jastrebarsko (Fig. 2.1).

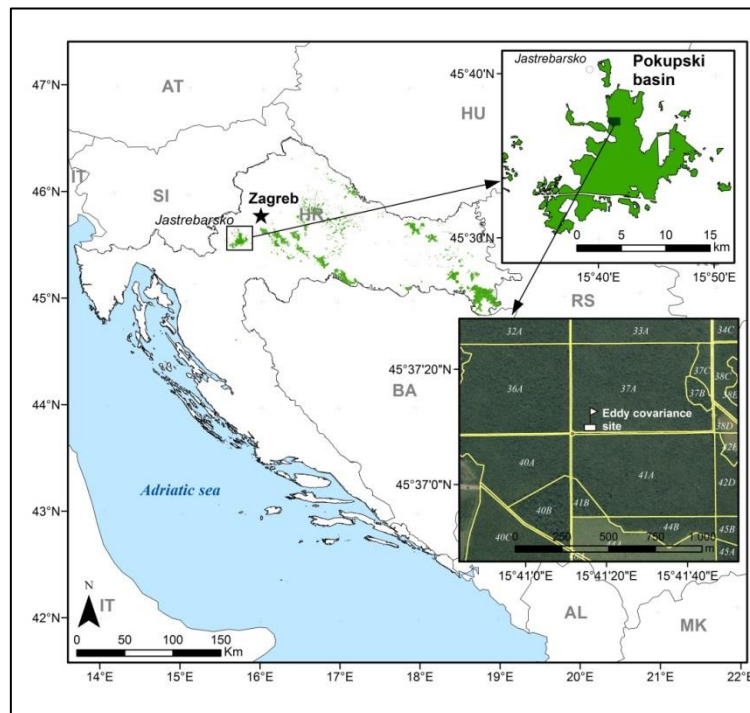


Figure 2.1: Location of the river Kupa basin within which Jastrebarsko forest is located

Lowland forests of Kupa River basin cover an area of approximately 13 600 ha which makes them the second largest complex of lowland oak forests in Croatia (*Spačva* in the east, spanning over 40 000 ha, is the largest one in Croatia and in Europe [Klepac 1996]). The area of state forests is divided into four Forest Management Units: *Draganički lugovi*, *Jastrebarski lugovi*, *Pisarovinski lugovi* and *Rečički lugovi*. Fig. 2.2 shows the location of the Kupa River basin with an aerial view. Kupa River basin is surrounded by *Samoborsko gorje* on NW side, *Vukomeričke gorice* on NE side and by river Kupa on S side. At the centre of the basin lay fish ponds *Crna Mlaka*, which were made after logging 650 ha of the forest at the beginning of 20th century. Human habitations around the research area are small villages (100-500 inhabitants) and the town of Jastrebarsko (approximately 10 000 inhabitants) with

medium industrial activity. Zagreb-Rijeka highway with very dense traffic separates the inhabited area from Kupa River basin on the north side.

The dominant tree species in the basin is Pedunculate oak (*Quercus robur* L.), with a significant share of other species, namely Common hornbeam (*Carpinus betulus* L.), Black alder (*Alnus Glutinosa* (L.) Geartn.), and Narrow-leaved ash (*Fraxinus angustifolia* Vahl.). There is also an understory of hazel (*Corylus avellane* L.) and Common hawthorn (*Crataegus monogyna* Jacq.). Oak forests in this area are managed in 140 year-long rotations, ending with two or three regeneration cuts during the last ten years of the rotation, which secures a continuous cover of forest soil.

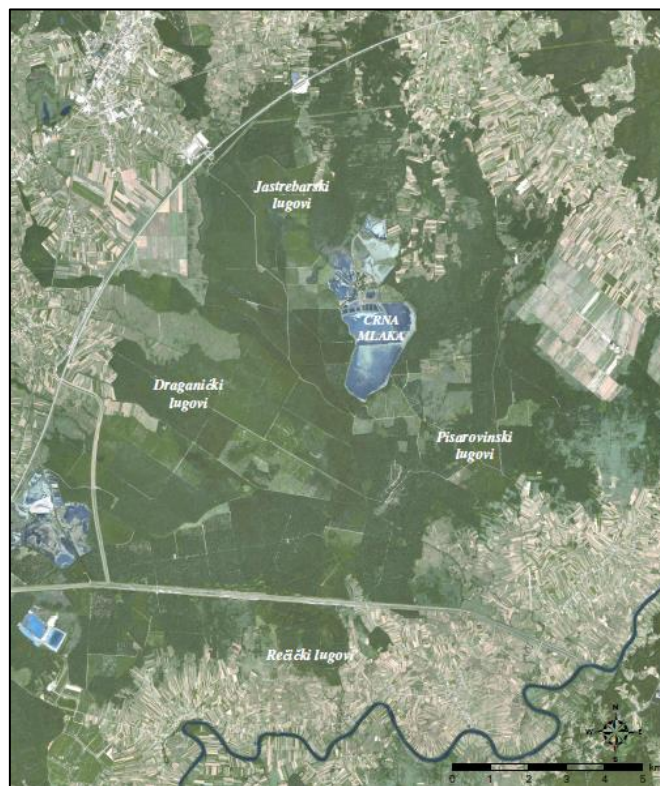


Figure 2.2: View on Kupa River basin from the air with marked economical units [Google Earth]

The terrain of the Kupa River basin is mainly flat, with altitudes ranging from 106 m above sea level at the central part of the basin up to 120 m and 130 m above sea level in the SW and N parts, respectively. The soil is mainly gleysol with low vertical water conductivity, and according to the World Reference Base for Soil Resources [WRB 2015] it is classified as luvic stagnosol. Parts of forest are waterlogged or flooded with stagnating water during winter and early spring, while during the summer the soil dries out. Basin is intersected with many

natural watercourses and man-made drench canals, and the average groundwater table depth ranged from 60 to 200 cm [Mayer 1996].

According to the Köppen classification, the climate of the area is maritime temperate climate (Csa) with a mean annual air temperature of 10.6°C for period 1981-2010 (data from the National and Hydrological Service for nearest meteorological station Jastrebarsko). Fog is frequent in autumn, while the occurrence of late frost in May is possible. Average annual precipitation is around 900 mm y^{-1} , out of which around 500 mm falls during the vegetation season (April-September).

2.2. Experimental site and measurements

Experimental station, EC tower (Fig. 2.3), is located (45°37'10''N and 15°41'16''E) in young (35-44 years old), managed stands dominated by pedunculate oak which are the result of regeneration cuts of old (~140 years) pedunculate oak stands in the early 1970s. Tower has been erected in 2007 as a part of project Carbon-Pro [Marjanović *et al.* 2011] and since then it provides meteorological and EC measurements. At the time of installation, measurement height was 23 m (3-5 m above canopy). Since forest stand has grown, in April of 2011 measurement height was elevated to 27 m (4-5 m above canopy).



Figure 2.3: Measurement station – EC tower, near Jastrebarsko, Croatia

The EC measurement system (Fig. 2.4) is made up of a three-dimensional sonic anemometer SAT (81000V, Young, USA) and an open path infrared gas analyser IRGA (LI-7500, Licor Inc., Lincoln, NE, USA). SAT measures three-dimensional wind velocity and speed of sound based on the transit time of ultrasonic acoustic signals. Sonic temperature is derived from the speed of sound which is corrected for crosswind effects. High speed, high precision and non-dispersive LI-7500 IRGA was used for accurate measurements of densities of CO₂ and water vapour in turbulent air structures. In the first measurement configuration, IRGA has been placed 30 cm southward from SAT. After April of 2011, when measurement height has been elevated, IRGA has been placed 30 cm eastward from the sonic anemometer. Both instruments operate at a sampling frequency of 20 Hz and data is recorded by a small hand computer (HP iPAQ, Palo Alto, CA, USA).

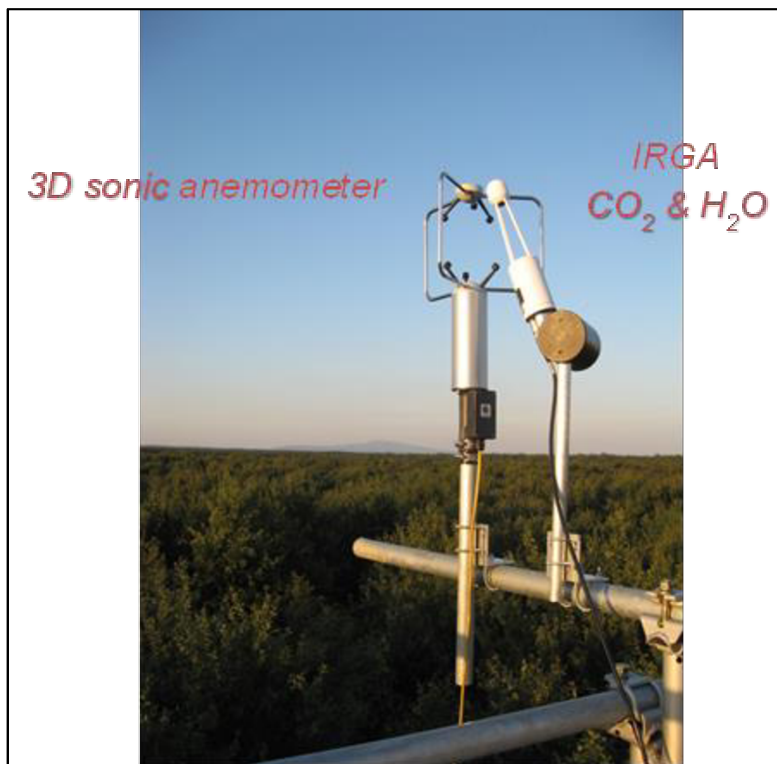


Figure 2.4: EC measurement system (first configuration): 3D sonic anemometer + infrared gas analyser (IRGA), near Jastrebarsko, Croatia

Meteorological elements are measured at 30 s intervals and then half-hourly averaged by the CR1000 data-logger (Campbell Sci. Inc., Logan, Utah, USA). Air temperature and humidity are measured with humidity and temperature probe (HMP45A, Vaisala Oyj, Finland), incoming and outgoing photosynthetic photon flux density – PPFD and net radiation are measured with net radiometer (NR Lite, Kipp&Zonen, Delft, Netherlands) while incoming

shortwave radiation is measured with pyranometer (CMP 3, Kipp&Zonen, Delft, Netherlands). Soil temperature was measured at three depths (5, 15 and 25 cm) with thermocouple probe (TCAV-L, Campbell Sci. Inc., Logan, UT, USA). For measurement of soil water content water content reflectometers (CS616, Campbell Sci. Inc., Logan, UT, USA) has been used. CO₂ storage term was measured with a profiler system for the CO₂ concentration measurement at six levels: 1, 2, 4, 8, 16 and 23 m (27 m from 1st April 2011). The profiler consisted of six tubes, pump, set of valves, 16 channel relay multiplexer (AM16/32B, Campbell Scientific, Inc., Logan, Utah, USA), the CO₂ analyser (SBA4, PP System, Amesbury, Massachusetts, USA) and was controlled by the CR1000 data-logger. However, due to, occasionally compromised data from the profiler (due to ants invading the filters of the tubes) and a final general failure of the profiler system in 2014, from 2014 until 2017 we decided to compute the storage term using only the CO₂ concentration measured at the top of the tower as suggested by in Wilkinson *et al.* [2012]. Continuous half-hourly meteorological data (air temperature, global radiation, relative humidity and precipitation) were measured from the auxiliary meteorological station (WatchDog 2900ET, Spectrum Technologies, Aurora, IL, USA) which is located approximately 2 km SW from EC tower. These measurements were used for gap-filling of meteorological data measured at EC tower. Small differences in measurements between these two stations were probably caused by the difference between the vegetation surrounding EC tower and auxiliary meteorological station. Auxiliary meteorological station is surrounded by saplings of pedunculate oak which were planted in 2008.

A network of 65 permanent circular plots has been set up in a 100 x 100 m² grid in management unit “Jastrebarski lugovi” around EC tower during the year 2007 and winter months of 2008 (Fig. 2.5). Their radius and size had been determined by age of the stands according to the methodology developed by Indir [2004]. The radius of 24 “dendrometer” plots (marked with red colour on Fig. 2.5) in subcompartments 37a, 37c, 40a and 41a is 8 m with the area of 201 m² per plot, which is equivalent to sampling intensity of 2% area. The radius of plots in subcompartment 36a is 10 m. The remaining plots (marked with yellow colour on Fig. 2.5) were designated to be measured every 10 years. All trees within plots were permanently marked with numbers and measured.

After preliminary footprint analysis of EC flux measurements, 24 plots which had the highest probability to be in the footprint area were selected for installation of dendrometer bands. Every aluminium dendrometer band has been made in the laboratory according to the

method described by Keeland and Young [2004]. A total of 643 dendrometer bands were installed on all trees with *DBH* (diameter at breast height) > 7.5 cm. Fig. 2.6 shows a tree with installed dendrometer band. During the vegetation season cumulative stem circumference increment was measured with a precision of 0.01 mm using small callipers with an electronic display. The frequency of measurements varied from weekly to monthly during the vegetation season, with lower frequency in the most recent year due to a limitation in resources.

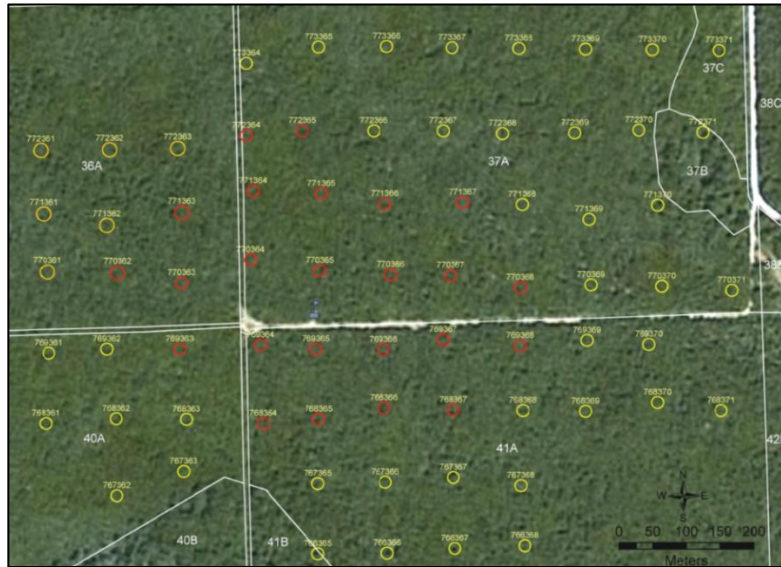


Figure 2.5: Air view on management unit *Jastrebarski lugovi* where circular plots had been set up. Plots with dendrometer bands are marked with red colour. The flag shows the location of EC tower. (Google Earth)

Alongside stem increment measurements, *DBH* and tree height measurements (*h*) using Vertex III hypsometers (Haglöf Sweden AD, Långsele, Sweden) at the end of every growing season has been performed to enable estimation of aboveground NPP. A total of 16 baskets (45 cm in diameter) were placed at centres of randomly selected plots with dendrometer bands for the assessment of leaf and litter production. Litterfall was collected from baskets several times a year.



Figure 2.6: Tree with installed dendrometer band

3. METHODOLOGY

3.1 Raw data description and treatment

EC raw data were stored in one-hourly binary files. Each binary file consists of nine rows header and six records: u, v and w wind component, sonic temperature, CO₂ and H₂O molar/mass density. Measurements were recorded every 0.05 s (20 Hz) and saved by a small hand computer in volts as an input unit. Variables were later converted in physical units: 3D wind components into m/s, sonic temperature into °C and molar/mass density of CO₂ and H₂O into mmol m⁻³. In the ideal case every one-hourly binary file should have 72000 records, but there were bad data with much less or more records which had to be discarded. Also, in the ideal case without any malfunctions of the measurement system, every year should have 8760 one-hourly binary files, that is 8784 in the case of a leap year. How much raw one-hourly binary files were missing in the same beginning before processing and after discarding of bad data is summarized in Table 3.1.

Table 3.1: Number of missing one-hourly binary files per year

Year	Max number of binary files	Number of missing files	Share of missing data [%]
2008	8784	392	4.5
2009	8760	1033	11.8
2010	8760	708	8.1
2011	8760	498	5.7
2012	8784	1468	16.7
2013	8760	630	7.2
2014	8760	374	4.3
2015	8760	354	4.0
2016	8784	1427	16.2
2017	8760	1871	21

Loss of data is inevitable, especially if measurement lasts several years. The EC measurement system is very sensitive and requires a lot of care. Common problems in the data acquisition are damages to instruments due to animals or thunderstorms, power breaks, human actions like vandalism and robbery and incorrect system calibration. Therefore, the measurement system can fail and measure nothing or measure bad values. It is necessary to

detect bad data before the start of processing and remove it from further analysis if one wants to obtain high quality fluxes.

The remaining one-hourly binary files had been further quality checked and discarded if they did not pass following quality criteria. First of all, the daily concentration of CO₂ [ppm] has been drawn for every day in the year. After that, for every one-hourly binary file, the mean value and standard deviation of CO₂ concentration were calculated. Also, the difference between CO₂ concentration in the next and previous moment named *delta* was calculated. The one-hourly binary file was dismissed from further analysis if the standard deviation was greater than 30 ppm, or mean value was less than 340 ppm or greater than 600 ppm, or the number of events when $\text{delta} > 10$ ppm was larger than 10. Raw data were once more visually checked for non-physical shifts, sudden dropouts and discontinuities which were not recognized by quality control. These binary files were manually discarded if needed. Dropouts are defined as short periods in which the time series sticks to some value that is statistically different from the average value calculated over the whole period. Examples of dropouts and discontinuities in time series of temperature can be seen on Fig. 3.1 and 3.2 respectively [Vickers and Mahrt 1997].

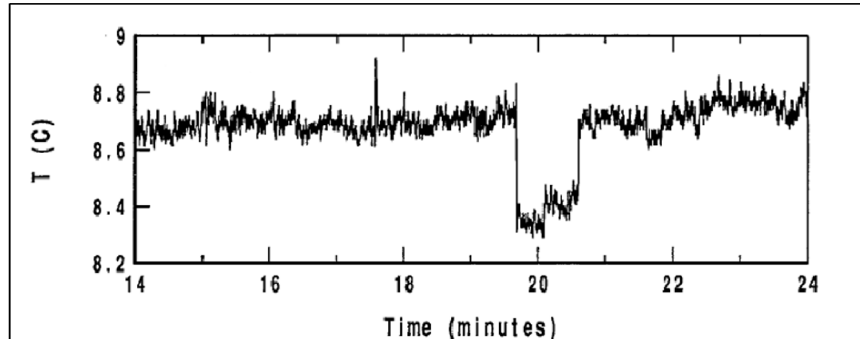


Figure 3.1: Example of dropout in time series of temperature [°C] [From Vickers and Mahrt 1997]

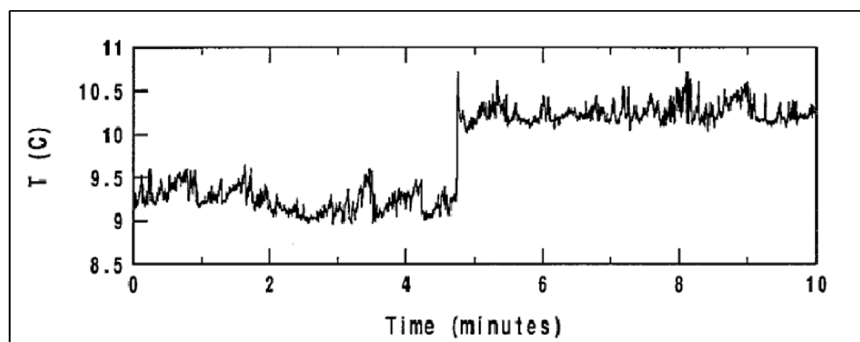


Figure 3.2: Example of discontinuity in time series of temperature [°C] [From Vickers and Mahrt, 1997]

This procedure removed bad data caused by rain and system malfunctions alongside non-physical shifts, dropouts and discontinuities. Needless to say, discarding of the one-hourly binary file created a gap of two half-hourly fluxes. The result of this procedure is summarized in Table 3.2.

Table 3.2: Percentage of missing one-hourly binary files per year after quality control

Year	Max number of binary files	Missing files after quality control	Percentage [%]
2008	8784	2671	30.4
2009	8760	3011	34.4
2010	8760	3005	34.3
2011	8760	1996	22.8
2012	8784	3114	35.5
2013	8760	2692	30.7
2014	8760	2629	30.0
2015	8760	2316	26.4
2016	8784	3444	39.2
2017	8760	3414	39.0

Quality control has greatly increased the number of missing one-hourly binary files. Most of the issues were related to instrumental problems during the bad weather. Our measurement instrument for CO₂ concentration is an open-path IRGA. Open path sensors, such as LI-7500, have known issues during rain, snow and fog. Water in optical path of the IRGA sensor causes an increased absorbance of the IRGA's infrared beam which is used for CO₂ measurements, resulted in false readings.

3.2 Flux calculation

Fluxes of CO₂ were calculated according to EuroFlux standards (Aubinet *et al.* 2000, 2012). Binary files were initially processed using the software tool EdiRe developed by Edinburgh University [<http://www.geos.ed.ac.uk/homes/jbm/micromet/EdiRe>]. EdiRe is open source software which includes all of the standard corrections needed for obtaining high-quality flux data.

3.2.1 Data quality control

High-frequency data often contain noise and impulse noise, i.e. spikes, dropouts, constant values and discontinuities. Spikes in time series can be caused by random electronic spikes or by instrumental problems such as insufficient electric power supply, as well as sonic transducer blockage during precipitation, bird droppings and fly-through insects. In contrast to noise, which is indistinguishable in a time series view of a signal, spikes are localized in time and usually can be detected because of their amplitude and duration. This characteristic allows us to identify spikes and to remove them from the time series. It is considered that electronic spikes have maximum width of three consecutive points in the time series with the amplitude of several standard deviations away from the the mean [Vickers and Mahrt 1997]. Despiking routine in EdiRe is based on procedure suggested by Højstrup [1993]. Spikes were detected using the absolute values of the differences in subsequent points in time series. The first step of the procedure was the calculation of standard deviations of these absolute values. Values which were greater than 3.5 standard deviations were then chosen to identify spikes. After that, the largest value from the absolute value data set was selected, and if that value was larger than the specified number of standard deviations a search routine which identifies spike was initiated. Detected spikes were flagged and replaced by linear interpolation of neighbouring values.

3.2.2 Time lag compensation

The physical distance between scalar concentration and wind speed sensors causes a time lag between those time series. Due to the inability of sampling at the same time some of the flux will be lost. If one wants to obtain high-quality flux data, it is necessary to determine time lag and perform the correction. This step in eddy covariance data processing is important because the incorrect determination of time lag will lead to flux underestimation. In closed-path eddy covariance systems gas concentrations are measured always with a certain delay because of the presence of the intake tube which can be several meters long. This delay depends on the inner volume of filters, tubes and valves, on the mass flow through the system, and on considered gas. The residence time of some compounds, such as water vapour is, in the tube is a function of temperature and relative humidity. If gas interacts with tube walls, larger time lag will be observed [Aubinet *et al.* 2012]. The situation is different in our case because we used an open-path IRGA for CO₂ and H₂O concentration measurement. In the

open-path eddy covariance systems, gas analyzer and anemometer are usually placed several decimetres or less apart so the time lag, in comparison with the closed-path systems, is significantly smaller due to the smaller physical distance between sensors. In this work the covariance maximization method has been performed for time lag removal. According to Taylor's hypothesis of frozen turbulence, a physical separation (x) can be translated into temporal separation (t) if the transition velocity (U) is known:

$$x = U \cdot t \quad (3.1)$$

Minimum and maximum thresholds of time lag were calculated as a ratio between separation of sensors and average wind speed which was fixed to 0.5 m s^{-1} [EddyPro manual]:

$$\tau_{min} = \frac{-\text{sensorseparation}}{0.5 \text{ m s}^{-1}} = \frac{-0.3 \text{ m}}{0.5 \text{ m s}^{-1}} = -0.6 \text{ s} \quad (3.2)$$

$$\tau_{max} = \frac{\text{sensorseparation}}{0.5 \text{ m s}^{-1}} = \frac{0.3 \text{ m}}{0.5 \text{ m s}^{-1}} = 0.6 \text{ s} \quad (3.3)$$

The lag time between gas concentration and vertical wind component was estimated by performing a cross correlation analysis between those variables [Lee *et al.* 1994]. Maximum (or minimum) of the cross correlation between those two signals will correspond to lag time. The time lag removal procedure has been performed before coordinate system rotation.

3.2.3 Coordinate rotation

It is impossible to level sonic anemometer perfectly, such that its w -axis is always perpendicular to the mean flow, i.e. mean wind streamlines. As a consequence of the misalignment of the sonic anemometer, w component of the wind will be contaminated by other two wind components. Such-cross contamination of velocities is the source of large errors in flux measurements [Wilczak *et al.* 2001]. There are several ways to correct situations of that kind, commonly called tilt corrections. Three types of tilt corrections, which are usually used, are: double rotation, triple rotation and planar fit rotation. Currently, the planar fit method is the most often used because it is less susceptible to run-to-run variations resulting from low-frequency variations in velocity means [Finnigan *et al.* 2003].

a) Double and triple rotation

In the first rotation measured wind components (subscript m) are rotated around z axis into mean wind using a rotation angle θ . This rotation forces average crosswind wind component ($\overline{v_1}$) to vanish while vertical components is unaffected. The new velocity components are given by [Kaimal and Finnigan 1994]:

$$u_1 = u_m \cos\theta + v_m \sin\theta \quad (3.4)$$

$$v_1 = -u_m \sin\theta + v_m \cos\theta \quad (3.5)$$

$$w_1 = w_m \quad (3.6)$$

where θ is rotation angle:

$$\theta = \tan^{-1} \left(\frac{\overline{v_m}}{\overline{u_m}} \right) \quad (3.7)$$

The second rotation is performed around new y -axis to nullify mean vertical wind velocity ($\overline{w_1}$). Now, rotation equations are [Kaimal and Finnigan 1994]:

$$u_2 = u_1 \cos\phi + v_1 \sin\phi \quad (3.8)$$

$$v_2 = v_1 \quad (3.9)$$

$$w_2 = -u_1 \sin\phi + v_1 \cos\phi \quad (3.10)$$

where ϕ denotes rotation angle:

$$\phi = \tan^{-1} \left(\frac{\overline{w_1}}{\overline{u_1}} \right) \quad (3.11)$$

After these rotations, the coordinate system of sonic anemometer is aligned with the wind streamlines. Rotated wind vector $\mathbf{u}_{\text{rot}}(u_2, v_2, w_2)$ has zero mean v and w wind components, while the value of the mean wind speed is contained in its u component.

Triple rotation involves first two rotations described above and a third rotation around the new x axis which is performed to eliminate the cross-stream stress component ($\overline{v_2 w_2}$). The new components are [Kaimal and Finnigan 1994]:

$$u_3 = u_2 \quad (3.12)$$

$$v_3 = v_2 \cos\psi + w_2 \sin\psi \quad (3.13)$$

$$w_3 = -v_2 \sin\psi + w_2 \cos\psi \quad (3.14)$$

where

$$\psi = \tan^{-1} \left(\frac{\overline{v_2 w_2}}{\overline{v_2^2 - w_2^2}} \right) \quad (3.15)$$

Triple rotation is not recommended anymore because it does not significantly influence fluxes, and often results in unphysical orientation of the vector basis [Aubinet *et al.* 2012].

b) Planar fit method

In this work planar fit method has been performed for coordinate rotation. Regression coefficients have been calculated separately and placed into appropriate fields in EdiRe. During computation of the regression coefficients low wind speed conditions (generally below 1 m s^{-1}) have been rejected [Aubinet *et al.* 2012].

The planar fit method proposed by Wilczak *et al.* [2001] assumes that the vertical wind component is equal to zero only over longer averaging periods (days or weeks). Here, the tilting is assessed by fitting a plane to the actual measurements of the average vertical wind component $\overline{w_m}$ as a function of horizontal components, $\overline{u_m}$ and $\overline{v_m}$. If the anemometer is tilted we can write:

$$\vec{u}_p = P(\vec{u}_m - \vec{c}) \quad (3.16)$$

where \vec{u}_p is the vector of the planar-fit rotated wind velocities, \vec{u}_m is the vector of the measured wind velocities, \vec{c} is a mean offset error in the measured wind and P is a partial rotation matrix that places the z axis perpendicular to the plane of the mean streamlines. The equations of rotations are:

$$\overline{u}_p = p_{11}(\overline{u}_m - c_1) + p_{12}(\overline{v}_m - c_2) + p_{13}(\overline{w}_m - c_3) \quad (3.17)$$

$$\overline{v}_p = p_{21}(\overline{u}_m - c_1) + p_{22}(\overline{v}_m - c_2) + p_{23}(\overline{w}_m - c_3) \quad (3.18)$$

$$\overline{w}_p = p_{31}(\overline{u}_m - c_1) + p_{32}(\overline{v}_m - c_2) + p_{33}(\overline{w}_m - c_3) \quad (3.19)$$

The planar fit coordinate system is defined to be aligned so that $\overline{w}_p = 0$. The tilt angles can be calculated according to equations (3.17)-(3.19) with multiple linear regressions:

$$\overline{w}_m = c_3 - \frac{p_{31}}{p_{33}} \overline{u}_m - \frac{p_{32}}{p_{33}} \overline{v}_m = b_0 + b_1 \overline{u}_m + b_2 \overline{v}_m \quad (3.20)$$

where $p_{31} = \sin\alpha$, $p_{32} = -\cos\alpha \sin\alpha$ and $p_{33} = \cos\alpha \cos\beta$. The coordinate system rotation can be performed after calculation of angles α and β . When the matrix P is known,

multiplying the horizontal velocities and stress tensor by P places them in the plane of the mean streamlines. After that, each single measurement must be rotated into the mean wind direction through multiplication by the matrix M :

$$M = \begin{pmatrix} \cos\gamma & \sin\gamma & 0 \\ -\sin\gamma & \cos\gamma & 0 \\ 0 & 0 & 1 \end{pmatrix} \quad (3.21)$$

where

$$\gamma = \arctan\left(\frac{\bar{v}_p}{\bar{u}_p}\right). \quad (3.22)$$

3.2.4 Flux determination

As it was mentioned in chapter 1.3, vertical turbulent fluxes of CO₂, sensible and latent heat have been deduced from the covariance between fluctuations of vertical wind speed w' and gas concentration fluctuations c' . Flux values were stored as half-hourly means. Positive flux values denote energy and mass flow away from the surface while negative flux values represent reverse. Carbon dioxide flux, F_c [$\mu\text{mol m}^{-2} \text{s}^{-1}$], was determined from fluctuations of vertical wind component (w') and CO₂ concentration fluctuations (c'):

$$F_c = \overline{w'c'} \quad (3.23)$$

Sensible heat flux, H [W m^{-2}] was determined from fluctuations of vertical wind component (w') and sonic temperature fluctuations (θ'_s). Flux value was obtained by multiplying calculated covariance by sensible heat flux coefficient ($\bar{\rho}C_p$):

$$H_s = \bar{\rho}C_p \cdot \overline{w'\theta'_s} \quad (3.24)$$

Latent heat (F_l), or water vapour, flux [W m^{-2}] has been calculated as a product of the latent heat of evaporation (L) and the covariance between fluctuations of vertical wind component (w') and H₂O concentration fluctuations (q'):

$$F_l = \lambda \cdot \overline{w'q'} \quad (3.25)$$

Also, the momentum flux τ was determined from fluctuations of vertical (w') and horizontal (u') wind components:

$$\tau = \bar{\rho}_d \cdot \overline{w'u'} \quad (3.26)$$

where $\bar{\rho}_d$ marks density of dry air.

3.2.5 Spectral corrections

Another important step in EC data processing is frequency response corrections. EC measurement systems remove both low- and high-frequency components of the signal. Low-frequency losses result from instrument and setup limitations that do not allow sampling the full turbulence fluctuations so averaging period can be too short to include all relevant low frequencies. On the other hand, high-frequency losses are connected with sensor separation, inadequate instrument frequency response, line averaging and, in closed path systems, tube attenuation [Aubinet *et al.* 2012]. In open path-systems frequency loss is usually small, on the order of 5-10% of flux [Burba 2013]. These flux losses are compensated by frequency response corrections which are applied to a cospectrum via transfer functions that describe losses at each frequency [Aubinet *et al.* 2012].

Measuring instruments are limited and cannot respond fast enough to small fluctuations contributing to the flux. This loss is compensated with a time response correction. The time response transfer function (G_w – wind measurements, G_s – scalar concentration measurements) is defined by:

$$G_{w,s} = \frac{1}{\sqrt{1+(2\pi n\tau_{w,s})^2}} \quad (3.27)$$

where $\tau_{w,s}$ are time constants specific to the sensors (e.g. Moore 1986) and n is natural frequency:

$$n = f \cdot \frac{U}{z-d} \quad (3.28)$$

Wind speed and scalar concentration sensors cannot measure the same volume of air exactly at the same time. This loss is compensated by sensor separation correction which was applied to cospectrum via sensor separation transfer function (T_{ss}) [Moore 1986]:

$$T_{ss} = e^{-9.9(n \cdot l / \bar{u})^{1.5}} \quad (3.29)$$

where \bar{u} is average wind speed, and l is physical distance between two sensors.

Path averaging correction compensates the loss of the flux due to the fact that the flux transport by small eddies is missed when averaged over a path, not a point. The transfer function for the wind vector component path averaging (T_{pw}) is given by [Moore 1986]:

$$T_{pw} = \sqrt{\frac{2}{2\pi n \frac{d_{pl}}{\bar{u}}} \left(2 + e^{-\frac{2\pi n d_{pl}}{\bar{u}}} - 3 \frac{1 - e^{-\frac{2\pi n d_{pl}}{\bar{u}}}}{\frac{2\pi n d_{pl}}{\bar{u}}} \right)} \quad (3.30)$$

where d_{pl} is sonic anemometer path length and transfer function for the scalar path averaging (T_{ps}) by [Moore 1986]:

$$T_{ps} = \sqrt{\frac{1}{2\pi n \frac{d_{s,w}}{\bar{u}_{pl}}} \left(3 + e^{-2\pi n \frac{d_{s,w}}{\bar{u}_{pl}}} - 4 \frac{1 - e^{-2\pi n \frac{d_{s,w}}{\bar{u}_{pl}}}}{2\pi n \frac{d_{s,w}}{\bar{u}_{pl}}} \right)} \quad (3.31)$$

where d represents the infrared gas analyser path length (index s) or path length of the sonic anemometer (index w) in the case of temperature measurements, while \bar{u}_{pl} is average air speed inside the sensor path length.

To compensate the loss of flux in the low frequency part of cospectrum recursive high-pass filter (T_{hp}) has been used:

$$T_{hp} = \frac{2\pi n \tau}{\sqrt{\frac{1 + (2\pi n \tau)^2}{\left(1 + \frac{1}{\tau n_c}\right)}}} \quad (3.32)$$

where τ is high pass filter constant and n_c cut-off frequency (1/2 of the sampling frequency) (Burba 2013).

The total transfer function is the convolution of above described individual transfer functions. For CO₂ and H₂O flux total transfer function was defined by:

$$T_{c,le} = G_w \cdot G_s \cdot T_{pw} \cdot T_{ps} \cdot T_{ss} \cdot T_{hp} \quad (3.33)$$

Total transfer function applied to fluxes of momentum was:

$$T_{uw} = T_{hp} \cdot T_{pw}^2 \cdot G_w \quad (3.34)$$

and total transfer function for sensible heat flux:

$$T_h = T_{hp} \cdot T_{pw} \cdot T_{ps} \cdot G_w \quad (3.35)$$

Required parameter values were entered in appropriate fields in EdiRe and transfer functions were calculated according to the formulas described above. Ideal model cospectra was calculated [Kaimal *et al.* 1972] and divided by attenuated cospectra which was calculated as a product of ideal cospectra and total transfer function for every flux separately. That ratio represents the frequency response correction factor which was multiplied with calculated fluxes to obtain frequency response corrected fluxes.

3.2.6 WPL correction

The final correction applied to the calculated CO₂ and latent heat fluxes was WPL correction by Webb, Pearman and Leuning [Webb *et al.* 1980]. This correction was performed to compensate for fluctuations in the density of CO₂ and water vapour resulting from fluctuations of temperature (thermal expansion) and water vapour (dilution) which are not representatives of measured flux. Corrections of latent heat and CO₂ flux for open-path systems [Webb *et al.* 1980] are:

$$E = (1 + \mu\sigma) \left(E_{raw} + \left(\frac{\bar{\rho}_v}{\rho} \right) \left(\frac{H}{c_p T} \right) \right) \quad (3.36)$$

$$F_c = F_{raw} + \left(\frac{\bar{\rho}_c}{\rho_a} \right) \left(\frac{\mu}{1 + \mu\sigma} \right) E + \frac{\bar{\rho}_c^2}{\rho_a \bar{\rho}} \left(\frac{H}{c_p T} \right) \quad (3.37)$$

where E labels latent heat flux, H sensible heat flux, F_c carbon dioxide flux, $\bar{\rho}_c$ mean CO₂ density, $\bar{\rho}_a$ mean dry air density, $\bar{\rho}_v$ mean water vapor density, μ ratio of molar masses of air to water ($\mu=1.6077$) and σ water to dry air density ratio. The first term on the right-hand side of (3.37) represents raw flux and other two terms are WPL terms. The first of them is water dilution term and second thermal expansion term. Impact of WPL correction varies from 0% to 50% of raw CO₂ flux [Burba 2013].

3.2.7 Self-heating correction (Burba correction)

When CO₂ and H₂O molar densities are measured with an LI-7500 open-path IRGA in cold environments (air temperatures below -10°C) the air in the analyser sensing volume may be warmer than ambient air because of heat release by the instruments electronics and instrument surface heating. To correct CO₂ flux, WPL correction uses sensible heat flux

which is measured outside the sensing volume of LI-7500 so WPL correction cannot fully remove the effects of temperature fluctuation on CO₂ density. Thus, correction called self-heating or Burba correction should be applied alongside WPL correction to obtain fully corrected CO₂ flux [Burba *et al.* 2008]. Self-heating correction has the largest impact in relatively cold climates so there was no need to apply this correction because there were only several occasions when air temperature was below -10°C in our measurements.

3.2.8 Stationarity test

Implementing the EC technique requires stationarity of the measuring process. This means that all statistical parameters are constant in time [Panofsky and Dutton 1984]. In-stationarity test was performed to check stationarity of the measurements in this work. Measured 30 min time series were divided into 6 intervals ($l=6$) whose duration was 5 min. Every interval consists of 6000 measured values ($m=6000$) because the frequency of measurement was 20 Hz, while the whole 30 min period has 36000 measured values ($M=36000$). For every 5 min interval covariances of specified signals ($\overline{w'c'}$, $\overline{w'q'}$, $\overline{w'T'}$, $\overline{w'u'}$) were calculated using equations:

$$\overline{x'_{il}x'_{jl}} = \frac{1}{m-1} \left[\sum_{k=1}^M x_{ikl} \cdot x_{jkl} - (\overline{x_{il}} \cdot \overline{x_{jl}}) \right] \quad (3.38)$$

After that, mean covariance of 6 segments was calculated for purposes of the test:

$$\overline{x'_{il}x'_{jl}}_{seg} = \frac{\sum x'_{il}x'_{jl}}{6} \quad (3.39)$$

For comparison of the calculated segment and full period covariances the stationarity statistics were calculated:

$$S = 100\% \cdot \left| \frac{\overline{x'_{il}x'_{jl}}_{full} - \overline{x'_{il}x'_{jl}}_{seg}}{\overline{x'_{il}x'_{jl}}_{full}} \right| \quad (3.41)$$

The measurement was considered as stationary if the difference between covariances was less than 30%. These data were considered as data with the highest quality so quality flag 0 was linked with them. Measurements with a difference smaller than 100% were accepted and linked with quality flag 1. Fluxes with quality flag 1 are suitable for general analysis such as annual budgets [Muader and Foken 2004]. Data for which difference between a segment and

full period covariances was more than 100% were linked with quality flag 2 and discarded from further calculations. This quality flag system was taken from Mauder and Foken [2004].

3.2.9 CO₂ flux storage computation

CO₂ flux storage term was calculated from CO₂ profile measurements. In the year 2015 profiler system sustained malfunction so profiler measurements were available until 2015. Measurements were quality checked, so all low-quality measurements related to ants or other insects or animal activity were discarded. In situations of that kind and in the period when the profiler system was not working CO₂, storage term was calculated using the CO₂ concentration measured at 23 and later at 27 m above the surface [Wilkinson *et al.* 2012]:

$$S_c = \int_0^{z_m} \rho_d \frac{\partial c}{\partial t} dz \quad (3.42)$$

CO₂ storage term was also stored as half hourly value.

3.3 Secondary flux data treatment

This step in data processing involved removal of low quality data. Flux data which did not pass stationarity test from section 3.2.7 were removed. After filtering procedures which are described in next sections, missing and bad quality data were gap-filled with more plausible estimates and *NEE* of carbon dioxide was partitioned into *GPP* and *R_{ECO}*.

3.3.1 Absolute limits

Calculated flux data were initially checked for absolute limits. All data which were out of defined range were removed from further processing. Limits for flagging CO₂, latent and sensible heat flux and CO₂ storage as unacceptable were:

$$F_c < -50 \mu\text{mol m}^{-2} \text{s}^{-1} \text{ or } F_c > 30 \mu\text{mol m}^{-2} \text{s}^{-1}$$

$$LE < -150 \text{ W m}^{-2} \text{ or } LE > 800 \text{ W m}^{-2}$$

$$H < -150 \text{ W m}^{-2} \text{ or } H > 500 \text{ W m}^{-2}$$

$$S_c < -50 \mu\text{mol m}^{-2} \text{s}^{-1} \text{ or } S_c > 30 \mu\text{mol m}^{-2} \text{s}^{-1}$$

Measured CO₂ and H₂O concentrations were also checked and removed if their values were outside of range:

$$\text{CO}_2 < 300 \text{ ppm or CO}_2 > 600 \text{ ppm}$$

$$\text{H}_2\text{O} < 0.001 \text{ mmol mol}^{-1} \text{ or H}_2\text{O} > 40 \text{ mmol mol}^{-1}$$

3.3.2 Secondary CO₂ flux despiking

High-frequency spikes, i.e. spikes affecting the single instantaneous measurement were removed by EdiRe software. Despite that, spikes were still occurring in the final half-hourly fluxes. Under the assumption that the extreme spikes are not representatives of local CO₂ flux they were detected and removed by filtering procedure proposed by Papale *et al.* [2006]. CO₂ storage term was added to CO₂ flux F_c to obtain NEE of carbon dioxide. Half-hourly *NEE* values were then divided into night-time (solar radiation $R_g < 20 \text{ W m}^{-2}$) and day-time *NEE* and processed separately. The spike detection was based on the double-differenced time series, using the median of absolute deviation about the median (*MAD*):

$$MAD = \text{median}(|d_i - M_d|) \quad (3.43)$$

where M_d denotes the median of the differences and value d_i was calculated for each half-hourly *NEE* as:

$$d_i = (NEE_i - NEE_{i-1}) - (NEE_{i+1} - NEE_i) \quad (3.44)$$

Half-hourly *NEE* was flagged as spike and discarded from further processing if:

$$d_i < M_d - \left(\frac{z \cdot MAD}{0.6745} \right) \quad (3.45)$$

or:

$$d_i > M_d + \left(\frac{z \cdot MAD}{0.6745} \right) \quad (3.46)$$

where z is a threshold value. For night-time fluxes value z was set to 4, but to allow greater diurnal variability of CO₂ flux z value was increased to 5.5.

3.4 Night CO₂ flux error and u_* filtering

During the stable conditions when stratification is usually stable and the winds are low, turbulence might not be fully developed. In such situations the hypothesis underlying EC technique theory cannot be met. Due to the strongly stable static conditions the footprint can increase significantly and instruments can measure flux which is not representative of the underlying surface. High wind velocity and gas concentration changes can appear and flow become non-stationary. In the absence of homogeneity and stationarity, storage and advection terms gain importance and can no longer be neglected. Surface air enriched by respired CO₂ can be flushed away by advection and pass unnoticed by the gas analyser. This error appears much more often during the night when the ecosystem acts as a source of carbon than during the day and can result with a carbon sequestration overestimation at annual scale. Because it occurs during the night, the error is named night flux error. It acts as a selective systematic error [Moncrieff *et al.* 1996] and fluxes affected with night flux error must be detected and corrected. To detect situations of such kind and to remove bad quality fluxes, Goulden *et al.* [1996a] proposed to use a criterion based on the friction velocity u_* . It says that data measured when u_* is below calculated u_* threshold (u_{*crit}) should be discarded from further processing. To check what is happening with fluxes at Jastrebarsko site, night-time flux data was divided into 20 u_* classes (from 0 to 1 m s⁻¹, increment 0.05 m s⁻¹). For each u_* class, average and median of *NEE* were calculated. The procedure has been performed for every year separately (Fig. 3.3) and for all years together (Fig. 3.4). Neither the average, nor the median of night-time *NEE* showed significant trend with u_* . Hence, it was not possible to determine a fixed value of u_{*crit} . Hence, the u_{*crit} values were calculated by the gap-filling online tool [Jena online tool]. Online tool derives u_* threshold using 95% threshold criterion described by Reichstein *et al.* [2005]. Data set was divided according to quantiles into 6 temperature classes of the same sample size and further subdivided into 20 u_* classes. The threshold for each temperature class is defined as the u_* class where the night-time flux reaches more than 95% of the average flux at the higher u_* classes. The final u_{*crit} was estimated as the median of all of the six temperature classes. Calculated values ranged from lowest of 0.04 m s⁻¹ in the year 2010 to highest of 0.10 m s⁻¹ in 2015 (Table 3.3). Except in 2017, u_{*crit} values were smaller than minimal theoretical defined u_* threshold value of 0.1 m s⁻¹ for tall forests [Aubinet *et al.* 2012]. It was possible to manually discard all night time half-hourly *NEE* for which u_* was lower than 0.1 m s⁻¹. However, this procedure would discard almost 10% of yearly *NEE* data and validity of this step has not been proved because there

was no significant trend of declining night-time NEE with declining u_* after u_{*crit} value of 0.1 m s^{-1} (Fig. 3.3 and 3.4).

Table 3.3: Values of $u_{*,crit}$ calculated by Jena online tool

Year	$u_{*,crit} \text{ [m s}^{-1}\text{]}$
2008	0.08
2009	0.08
2010	0.04
2011	0.08
2012	0.08
2013	0.06
2014	0.06
2015	0.10
2016	0.06
2017	0.09

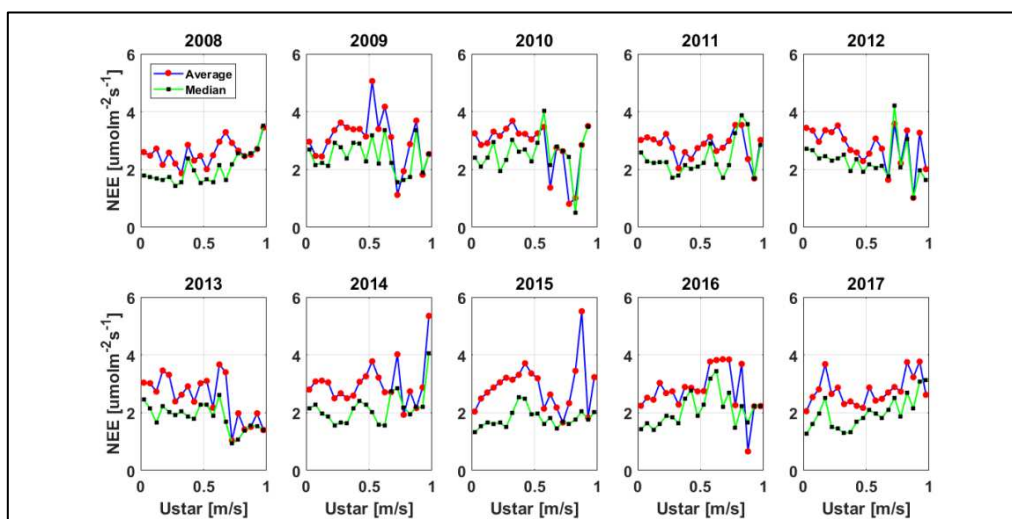


Figure 3.3: u_* block averaged nocturnal NEE vs u_* for years 2008-2017

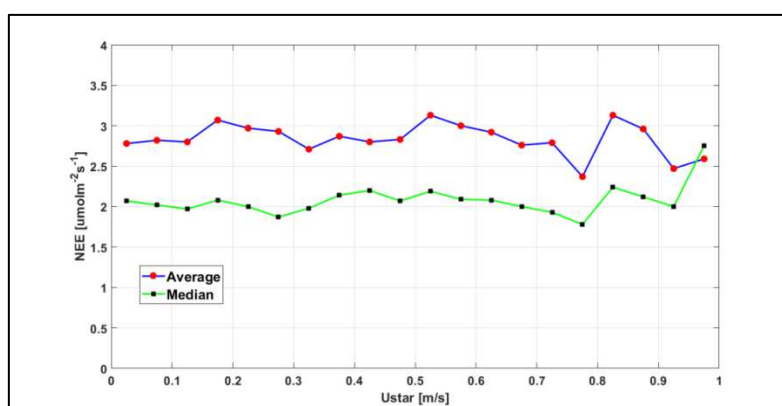


Figure 3.4: u_* block averaged nocturnal NEE vs u_* across whole 10 years of measurement

U_* filtering procedure dismissed, on average 6% of total half-hourly NEE values per year. For comparison, NEE was also calculated without performing u_* filtering.

3.5 Data gap-filling

Measurement system failures alongside with numerous filtering procedures lead to significant amount of gaps in time series. Majority of gaps are occurring during the night. It is necessary to replace these gaps with plausible values to estimate long-term ecosystem carbon budgets. The average data coverage within a year is between 65% and 75% [Falge *et al.* 2001]. At Jastrebarsko site average data coverage per year was even smaller than that value, especially after performing u_* filtering as a step in EC data processing. Table 3.4 shows the final percentage of missing half-hourly CO_2 fluxes in time series per year with and without performing u_* filtering.

Table 3.4: Percentage of NEE data coverage per year before gap-filling with and without u_* filtering

Year	Data coverage before u_* filtering [%]	Data coverage after u_* filtering [%]
2008	46.6	39.4
2009	46.8	42.1
2010	47.0	45.4
2011	56.5	47.7
2012	49.8	42.7
2013	53.0	48.4
2014	51.4	47.3
2015	52.9	43.2
2016	45.1	41.6
2017	45.0	38.0

Several methods were developed for estimating the flux values for the missing data, e.g. methods based on the look-up tables, interpolation, non-linear regression, probabilistic filling and neural networks. It was shown that biases associated with different gap-filling procedures are generally small and the performance of the gap-filling method depends on the site, gap length and time of the day [Moffat *et al.* 2007]. In this work missing flux values were replaced with estimates using standardized Marginal Distribution Sampling (MDS) technique employed by FLUXNET, which is available as an online tool mentioned in the previous chapter [Jena online tool]. MDS showed consistently good gap-filling performance

and low annual sum bias in comparison with other techniques [Moffat *et al.* 2007]. Another advantage of MDS technique is its ability to deal with the missing meteorological data. This is important because available meteorological data helps in improving of the accuracy of gap-filled values [Moffat *et al.* 2007]. MDS method developed by Reichstein *et al.* [2005] is an enhancement of the basic look-up table. It considers temporal auto-correlation of fluxes and replaces missing value with the average value under the same meteorological conditions which are present when air temperature, global radiation and vapor pressure deficit do not deviate more than 2.5 °C, 50 W m⁻² and 5.0 hPa respectively. The algorithm considers three different cases. In the first one, only data of interest is missing while all meteorological variables are known. Missing values are then replaced with average values under similar meteorological conditions within the 7-day window. If there are no such conditions, averaging time-window is increased to 14 days. In the second case, only global radiation is available, while air temperature, vapour pressure deficit and data of interest are missing. To gap-fill missing values, the algorithm performs the same procedure as in the first case, but similar meteorological conditions can only be defined via global radiation deviation while averaging window length is not increased. In the third case when global radiation data is also missing, alongside air temperature, vapour pressure deficit and data of interest, algorithm replaces missing value with the average value at the same time of the day (mean diurnal course). If after all of these three steps, the value still could not be filled, the procedure was repeated with increased time-window size until value can be filled. Gap-filled data have lower accuracy for larger gaps of several consecutive days.

3.6 Flux partitioning

After gap-filling of missing values, *NEE* was partitioned into *GPP* and *R_{ECO}*. This was also done by using online tool [Jena online tool]. In the first step, algorithm estimates the short-term temperature sensitivity parameter (*E₀*) using the exponential regression model [Lloyd and Taylor 1994]:

$$R_{ECO}(T) = R_{ECO,ref} e^{E_0 \left(\frac{1}{T_{ref}-T_0} - \frac{1}{T-T_0} \right)} \quad (3.47)$$

where *R_{ECO}(T)* marks ecosystem respiration at given air temperature, *R_{ECO,ref}* denotes ecosystem respiration at reference temperature (*T_{ref}*) which was set to 15°C while *T₀* is a constant temperature of -46.02 °C as proposed by Lloyd and Taylor [1994]. Night-time data

was divided into short subperiods of 14 days and the latter regression was performed for each subperiod separately. Also, the relative standard error of the estimates of parameter E_0 was calculated for each subperiod. Only three estimates of E_0 with the smallest standard error, and which were within an accepted range of 0-450K [Reichstein *et al.* 2005] were accepted and averaged to obtain the value of E_0 for the whole dataset. In the second step, the algorithm calculates $R_{ECO,ref}$ using the same non-linear regression model with a seven-day moving window in steps of four days. All parameters are fixed except $R_{ECO,ref}$. Missing values of $R_{ECO,ref}$ for the periods in which $R_{ECO,ref}$ could not be estimated were linearly interpolated. With known $R_{ECO,ref}$ and E_0 ecosystem respiration R_{ECO} can be estimated as the function of temperature T using the exponential regression model. In this work for estimating respiration rate, air temperature was used because air temperature varies more than soil temperature so more variance in R_{ECO} can be explained with air temperature [Van Dijk and Dolman 2004]. GPP was calculated as the difference between R_{ECO} and NEE [Reichstein *et al.* 2005]:

$$NEE = GPP - R_{ECO} \Rightarrow GPP = NEE + R_{ECO} \quad (3.48)$$

In order to estimate NPP from EC measurements (NPP_{EC}), R_{ECO} was partitioned to heterotrophic (R_h) and autotrophic (R_a) part. Heterotrophic part of R_{ECO} was estimated in 2008 and 2009 from soil respiration measurements [Marjanović *et al.* 2011]. Using data for R_h from Marjanović *et al.* [2011] and R_{ECO} obtained from NEE flux partitioning for 2008 and 2009, R_a and the ratio R_h/R_{ECO} were calculated. The average ratio of 39.19% was then used for the partitioning of R_{ECO} into R_h and R_a for the remaining years. NPP_{EC} was calculated by subtracting R_a from GPP :

$$NPP_{EC} = R_h - NEE = 0.3919 \cdot R_{ECO} - NEE \quad (3.49)$$

3.7 Estimation of NPP based on biometric measurements (NPP_{BM})

Estimation of forest stand NPP with biometric method requires assessment of different components, namely the production of: stems and branches, leaves, flowers and fruits, coarse and fine roots, ground vegetation and non-woody plants, herbivory losses, pollen, volatile organic compounds (VOCs) and non-structural carbohydrates (NSC). Some of these components of NPP like VOCs, NSC and herbivory are very difficult and/or costly to measure while some, like pollen, have a fairly insignificant contribution to the total NPP and could be disregarded. Within this research, production of total woody biomass (NPP_{WBt}) was

estimated by components: stem and branches (NPP_{S+B}), twigs (NPP_T) and roots (NPP_R). Furthermore, NPP of leaves and fruits (NPP_{LF}) was estimated from litterfall measurements. The sum of NPP_{LF} and NPP_{WBi} is denoted as NPP_{BM} . Net primary production of a given component is expressed in units of gC m^{-2} , while net primary productivity is expressed in units of $\text{gC m}^{-2} \text{yr}^{-1}$.

3.7.1 NPP of total woody biomass (NPP_{WBi})

Stem production was estimated using stem diameter at breast height (d) increment measurements during the vegetation season with dendrometer bands on selected trees, as well as d and tree height measurements on all trees at the end of the vegetation season. This provided sample data for construction of species-specific, age-dependent height curves. All measured data have been manually quality checked for errors before further analysis. At the beginning of vegetation season small notch next to the number marked on the band has been made on every dendrometer. The band was stretching with tree growth and this stem increment was measured using small calliper with an electronic display (red line on Fig. 3.5). In Fig. 3.5 r_p denotes tree radius at breast height before the beginning of growing season, r marks radius at the moment of measurement, α is the angle between two radii, L marks length of arc and t tendon. It is not possible to directly recalculate measured tendon into the tree diameter at breast height; therefore, a method based on iterations has been used (Marjanović 2009).

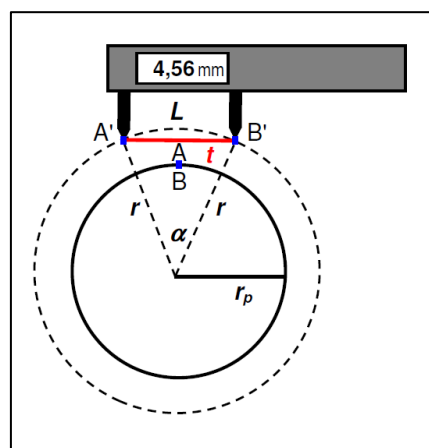


Figure 3.5: Measurement of stem increment on dendrometer band with a small calliper (Marjanović, 2009); r_p denotes tree radius at breast height, r is radius at the moment of measurement, α is the angle between two radii, L marks length of arc and t tendon

Equations for the arc and corresponding angle are:

$$L = r \cdot \alpha = \left(\frac{d}{2}\right) \cdot \alpha \quad (3.50)$$

$$\alpha = 2 \arcsin \left[\frac{t}{2r} \right] = 2 \arcsin \left[\frac{t}{d} \right] \quad (3.51)$$

Inserting (3.51) into (3.50) gives:

$$L = d \cdot \arcsin \left[\frac{t}{d} \right] \quad (3.52)$$

The equation for tree circumference is:

$$O_P = d_P \pi \quad (3.53)$$

$$O_M = d_M \pi = d_P \pi + L \quad (3.54)$$

Diameter at the moment of measurement can be estimated as:

$$d_M = d_P + L/\pi \quad (3.55)$$

Now, inserting (3.53) into (3.52) gives:

$$L = \left(d_P + \frac{L}{\pi}\right) \cdot \arcsin \left[\frac{t}{d_M} \right] \quad (3.56)$$

Finally, diameter at the moment of measurement can be estimated as:

$$d_M = d_P + \pi^{-1} \cdot d_M \cdot \arcsin \left[\frac{t}{d_M} \right] \quad (3.57)$$

Equation (3.57) can be solved by an approximation method. With known t and d_P , diameter at breast height can be obtained by an iterative procedure:

$$d_{n+1} = d_P + \pi^{-1} \cdot d_n \cdot \arcsin \left[\frac{t}{d_n} \right], n = 0, 1, 2, 3, \dots, \infty \quad (3.58)$$

In this work the diameter at breast height d_M was calculated using only the first iteration:

$$d_M = d_P + \pi^{-1} \cdot \left(d_P + \frac{t}{\pi}\right) \cdot \arcsin \left[t / \left(d_P + \frac{t}{\pi}\right) \right] \quad (3.59)$$

The measurement error of d was around 1% [Marjanović 2009]. The increment in d , until a given day of the year, of trees without dendrometer bands was calculated using their measured annual increment and the average percentage of the realization of total increment

estimated from trees with dendrometers. Furthermore, height curves were constructed, separately for each species and year, using Michailoff function [Michailoff 1943]:

$$h = a \cdot e^{\frac{-b}{d_M}} + 1.30 \quad (3.60)$$

Parameters a and b were calculated using linear regression on ln-transformed variables d_M and h' ($h'=h-1.30$). Thus obtained parameters a and b were then regressed again stand age (Age) using linear regression ($a = \alpha_0 + \alpha_1 \cdot Age$; $b = \beta_0 + \beta_1 \cdot Age$) with the aim of obtaining age-dependant and species specific height curves that have following form:

$$h = (\alpha_0 + \alpha_1 \cdot Age) \cdot e^{\frac{-(\beta_0 + \beta_1 \cdot Age)}{d_M}} + 1.30 \quad (3.61)$$

where α_0 , α_1 , β_0 and β_1 are parameters listed in Table 3.5.

Table 3.5: Parameters for species specific, age-dependent tree height curves; *Based on 36-45 years old stands; **For all other tree species the parameters for *Carpinus betulus* were used

Species**	Parameters*			
	α_0	α_1	β_0	β_1
<i>Alnus glutinosa</i>	10.31	0.37	0.59	0.1385
<i>Carpinus betulus</i>	6.60	0.59	-2.31	0.2863
<i>Fraxinus angustifolia</i>	6.25	0.58	-3.89	0.3275
<i>Quercus robur</i>	3.86	0.63	-1.61	0.2496

Volume ($V_{\geq 3cm}$) over bark, of tree stem and branches ($d \geq 3cm$) was assessed with the allometric equation of Schumacher and Hall [Schumacher and Hall 1933] using local, species specific parameters:

$$V_{\geq 3cm} = b_0 \cdot d_M^{b_1} \cdot h^{b_2} \quad (3.62)$$

where b_0 , b_1 and b_2 are parameters listed in Table 3.6.

Taking into account (3.61) and (3.62) the total aboveground tree volume ($V_{\geq 3cm}$) was calculated as:

$$V_{\geq 3cm} = b_0 \cdot d_M^{b_1} \cdot \left((\alpha_0 + \alpha_1 \cdot Age) \cdot e^{\frac{\beta_0 + \beta_1 \cdot Age}{d_M}} + 1.30 \right)^{b_2} \quad (3.63)$$

Table 3.6: Parameters of Schumacher and Hall function (eq. 3.62) for the wood volume (including bark) of tree stem and branches; *For all other tree species the parameters for *Carpinus betulus* were used

Species*	Parameter			Source
	b ₀	b ₁	b ₂	
<i>Alnus glutinosa</i>	4.23243·10 ⁻⁰⁵	2.002354	1.001300	[Cestar and Kovačić 1982]
<i>Carpinus betulus</i>	2.96400·10 ⁻⁰⁵	2.022705	1.102119	[Špiranec 1975]
<i>Fraxinus angustifolia</i>	3.95282·10 ⁻⁰⁵	1.974875	1.001444	[Cestar and Kovačić 1984]
<i>Quercus robur</i>	4.96820·10 ⁻⁰⁵	2.048384	0.892124	[Špiranec 1975]

Volume of thin branches and twigs (< 3cm in diameter) was assumed to be 5% of total aboveground tree volume [Balboa-Murias *et al.* 2006].

$$V_{<3cm} = V_{\geq 3cm} \cdot 1.05 \quad (3.64)$$

Volume of below ground coarse roots (>2 mm) was calculated assuming a constant, species-invariant, root-to-shoot (*RS*) ratio of 0.257. The value of *RS* ratio was obtained as the average of the *RS* ratios for stands with pedunculate oak published in Cairns *et al.* [1997]. Total tree volume was converted to biomass using species specific basic wood densities (*BWD*), namely 450, 630, 570 and 580 kg m⁻³ for *Alnus glutinosa*, *Carpinus betulus*, *Fraxinus angustifolia* and *Quercus robur*, respectively [Šumarska enciklopedija 1959] and converted to carbon using a carbon fraction (*CF*) of 0.5 [IPCC 2003, 2006]. Carbon stock (*C*) at the time of measurement (*t_m*) was calculated for each tree component (*C_{S+B}*(*t_m*) – stem and branches, *C_T*(*t_m*) – twigs and *C_R*(*t_m*) – roots) as:

$$C_{S+B,i}(t_m) = V_{\geq 3\text{ cm},i}(t_m) \cdot BWD \cdot CF \quad (3.65)$$

$$C_{T,i}(t_m) = 0.05 \cdot C_{S+B,i}(t_m) \quad (3.66)$$

$$C_{R,i}(t_m) = 0.257 \cdot (C_{S+B,i}(t_m) + C_{T,i}(t_m)) \quad (3.67)$$

Total tree woody biomass was calculated as a sum of all three components:

$$C_{Wbt,i}(t_m) = (C_{S+B,i} + C_{T,i}(t_m) + C_{R,i}(t_m)) \quad (3.68)$$

hence, the *NPP* was calculated from changes in *C_i* of each tree components on a given plot.

Total *NPP* of woody biomass was calculated as:

$$\begin{aligned}
NPP_{WBt} &= \overline{NPP_{WBt}(plot)} = \\
&= \frac{1}{N_{plots}} \sum_{plot} \frac{1}{A \cdot (t_2 - t_1)} \cdot \left[\sum_{i=1}^{N_{alive}} (C_{WBt,i}(t_2) - C_{WBt,i}(t_1)) + \sum_{j=1}^{N_{dead\ or\ removed}} (C_{WBt,j}(t_j) - \right. \\
&\quad \left. C_{WBt,j}(t_1)) \right] \tag{3.69}
\end{aligned}$$

Where N_{plots} denotes the number of circular plots, A is the plot area, t_1 and t_2 are times of the beginning and the end of the period of interest and $C_{WBt,j}(t_j)$ is estimated carbon stock of tree j at the time (t_j) of its deaths or removal ($t_1 < t_j < t_2$).

3.7.2 NPP of tree foliage and fruits (NPP_{LF})

Collected litterfall from litterfall baskets was sorted into three fractions: leaves, twigs ($d < 1\text{cm}$) and fruits. Samples were dried and weighed with precision of 0.01 g. Value of biomass (dry weight) was divided by the area of the sample and multiplied by the carbon fraction of 0.5 to obtain the production from leaves (NPP_L), fruits (NPP_F) and their sum (NPP_{LF}).

3.7.3 Modelling within-seasonal dynamics of NPP_{BM}

The stem increment of deciduous trees growing in the continental parts of Europe starts in the spring before the new leaves develop. Part of that stem increment is due to tree re-hydration and it should not be considered as growth in terms of increase in carbon stock. Furthermore, although all of the carbon in leaf biomass is usually accounted as part of the current season's NPP , a part of that carbon actually comes from tree reserves of the previous season(s) and not from carbon fixed in the current season [Carbone *et al.* 2013]. On the other hand, stem increment almost ceases in summer, particularly after the mid of August [Granier *et al.* 2008]. However, from the CO_2 flux measurements we can observe that the forest continues to accumulate carbon; apparently more than the amount required for the growth of stems and branches (see Results). The fixed carbon is likely stored in tree reserves [Granier *et al.* 2008]. These facts should be addressed when comparing within-seasonal dynamics of NPP estimates from EC and biometric measurements.

Since measurement and assessment of changes in trees' reserves is very challenging, and was beyond the scope of this work, in order to account for the within seasonal NPP_{LF} we

assumed a simplistic model where the amount of carbon mobilised from trees' reserves and used in early spring for the formation of new tissues (primarily that of leaves), is approximately equal to NPP_{LF} . Consequently, NPP_{LF} of the current season should not be accounted for in the spring, but only later in the season, when reserves are being replenished. The actual mechanism of carbon reserve management in trees is significantly more complex and is currently still being researched [Dietze *et al.* 2014, Martinez-Vilalta 2014, Richardson *et al.* 2013].

In simple model, we assumed that the production of every tree component under the average growing conditions exhibits the pattern which can be described by the logistic curve of the form:

$$NPP_i(DOY) = \frac{NPP_{i_annual}}{1 + e^{-k(DOY - DOY_{max}(i))}} \quad (3.70)$$

where $NPP_i(DOY)$ is the cumulative net primary production of the i -th component (e.g. stem and branches, leaf, fruit) from the first until a given Day-Of-Year (DOY), NPP_{i_annual} is the annual NPP of the component i , $DOY_{max}(i)$ is the DOY when the rate-of-change of $NPP(i, DOY)$ is at its maximum (i.e. the inflexion point of the annual NPP curve), and k is a parameter related to the maximum rate-of-change of NPP (r_{max}) where r_{max} is the quotient of the maximum daily net primary production ($dNPP_{max}$) and the annual net primary production (NPP_{annual}):

$$r_{max} = \frac{dNPP_{max}}{NPP_{annual}}. \quad (3.71)$$

If r_{max} is known (or estimated) the parameter k can be calculated using:

$$k = 4 \cdot \operatorname{atanh}(r_{max}) = 2 \cdot \ln\left(\frac{1+r_{max}}{1-r_{max}}\right). \quad (3.72)$$

Inversely,

$$r_{max} = \tanh\left(\frac{k}{4}\right) = \frac{e^{k/4} - e^{-k/4}}{e^{k/4} + e^{-k/4}}. \quad (3.73)$$

Using the `nl` routine for nonlinear least-squares estimation in STATA 14 statistical software [StataCorp LP, College Station, Texas, USA] we fitted the NPP_{WBt} with (3.70) for each year separately and obtained estimates for the parameters $NPP_{WBt, annual}$, DOY_{max_WBt} and k (Table 3.7). Seasonal dynamics of NPP_{LF} was estimated assuming that the shape parameter k for NPP_{LF} is the same as for NPP_{WBt} . Parameter $NPP_{LF, annual}$ equals the measured NPP_{LF} . Looking into the characteristics of the logistic curve, we propose that the DOY_{max_LF} occurs on DOY at which the time derivative of NPP_{WBt} has the second inflexion point (Fig. 3.6 A), resulting with the general behaviour of NPP_{BM} analogous to that shown in Fig. 3.6 B. In that

case, DOY_{max_LF} must be the value in which the second derivative of the logistic function has its minimum and the third derivative is zero.

An analytical solution for DOY_{max_LF} in this case exists and it is:

$$DOY_{max_LF} = DOY_{max_WBt} - \frac{\ln(2-\sqrt{3})}{k}. \quad (3.74)$$

Finally,

$$NPP_{BM}(t) = NPP_{WBt}(t) + NPP_{LF}(t). \quad (3.75)$$

Table 3.7: Parameters of the NPP_{WBt} fit with equation (3.70)

Parameter	Year	Estimate	Std. Err.	t	P> t	CI95 _{lower}	CI95 _{upper}
DOY_{max_WBt}	2008	151.6	0.5	317.43	0.000	150.7	152.6
	2009	154.1	0.7	227.61	0.000	152.7	155.5
	2010	158.3	1.1	138.99	0.000	155.9	160.7
	2011	144.7	1.6	91.91	0.000	141.3	148.0
	2012	143.2	1.3	108.31	0.000	140.3	146.1
	2013	152.0	2.0	75.94	0.000	147.6	156.4
	2014	156.3	1.2	126.73	0.000	153.5	159.0
	2015	155.3	1.7	93.04	0.000	151.5	159.1
	2016	154.4	2.7	57.64	0.000	146.9	161.8
	2017	163.5	0.3	590.49	0.001	160.0	167.0
k	2008	0.0476	0.0011	42.77	0.000	0.0453	0.0499
	2009	0.0426	0.0012	36.81	0.000	0.0402	0.0450
	2010	0.0397	0.0015	26.67	0.000	0.0365	0.0428
	2011	0.0431	0.0027	15.83	0.000	0.0373	0.0490
	2012	0.0356	0.0015	23.36	0.000	0.0323	0.0389
	2013	0.0287	0.0017	16.5	0.000	0.0249	0.0325
	2014	0.0322	0.0010	31.4	0.000	0.0299	0.0345
	2015	0.0404	0.0026	15.63	0.000	0.0346	0.0463
	2016	0.0293	0.0019	15.24	0.000	0.0240	0.0346
	2017	0.0307	0.0001	248.18	0.003	0.0291	0.0322
NPP_{WBt} annual	2008	504.9	2.3	216.26	0.000	500.1	509.8
	2009	550.9	3.7	150.55	0.000	543.3	558.6
	2010	571.5	7.5	76.41	0.000	555.7	587.3
	2011	513.1	9.7	52.89	0.000	492.3	533.9
	2012	457.0	5.3	85.69	0.000	445.3	468.6
	2013	540.4	9.1	59.64	0.000	520.5	560.4
	2014	486.5	4.8	102.17	0.000	475.9	497.1
	2015	409.9	6.3	65.16	0.000	395.7	424.1
	2016	526.9	11.6	45.46	0.000	494.8	559.1
	2017	302.0	0.3	900.4	0.001	297.7	306.2

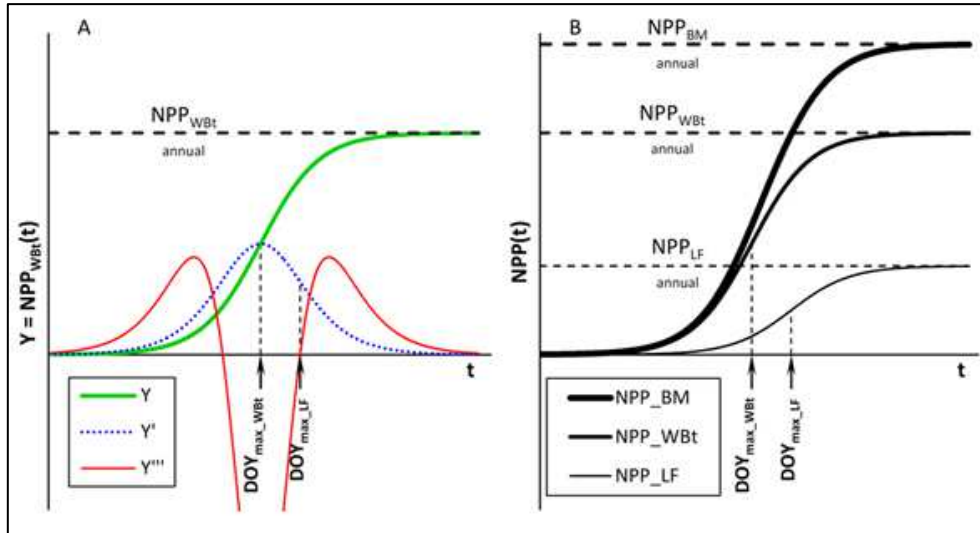


Figure 3.6: Proposed theoretical framework for calculation of NPP_{BM} . Logistic curve model of NPP_{WBt} (Y) has an upper asymptote at $NPP_{WBt, annual}$ and the inflexion point and the maximum of Y' in DOY_{max_WBt} . DOY_{max_LF} is assumed to occur at the second inflexion point of Y' i.e. the point where third derivative $Y'''=0$ (panel A); annual dynamics of NPP_{WBt} and NPP_{LF} modelled using the same parameter k (see text), and their sum NPP_{BM} (panel B)

3.8 Meteorological data treatment

Meteorological data measured at EC tower were checked for outliers and non-physical values. Absolute limits for global radiation (R_g), air temperature (T_a), soil temperature (T_s), relative humidity (rH) and precipitation (P) were respectively:

$$0 > R_g > 1200 \text{ W m}^{-2}$$

$$-50 > T_a > 50 \text{ }^\circ\text{C}$$

$$-20 > T_s > 50 \text{ }^\circ\text{C}$$

$$0 > rH > 100 \%$$

$$0 > P > 200 \text{ mm (30min)}^{-1}$$

All data which were out of defined range were removed from further processing. Shorter gaps in time series of the latter meteorological variables were linearly interpolated. Longer gaps in time series of air temperature were gap-filled using the data measured at the auxiliary meteorological station. A linear model has been assumed between air and soil temperature data measured at EC tower and at the auxiliary meteorological station.

3.9 Flux footprint

Flux footprint analysis was carried out to describe the position and spatial extent of the source area that contributes to a carbon flux measurement. Source area represents a fraction of the surface that contains sources and sinks which contribute to a measurement point [Kljun *et al.* 2002] and depends on measurement height, wind speed and wind direction. According to such flux, the footprint is defined by the relative contribution from each element of the surface area source or sink to the measured vertical flux. Functions that describe the relationship between the spatial distribution of sources or sinks and a signal are called footprint functions. They are commonly defined by an integral equation of diffusion:

$$\eta(\vec{x}) = \int \phi(\vec{x}, \vec{x}') Q(\vec{x}') d\vec{x}' \quad (3.76)$$

where η represents quantity which is measured at a location \vec{x} while $Q(\vec{x}')$ represents the strength of the surface source or sink [e.g. Aubinet *et al.* 2012]. To determine flux footprint function 3D Lagrangian stochastic particle dispersion model was used in this study. In a Lagrangian formulation diffusion of scalar released from the surface is assumed to be statistically equivalent to the dispersion of an ensemble of particles that impact the ground within the surface area source and thereafter transport the scalar [Kljun *et al.* 2002]. Generalised Langevin equation describes the diffusion of scalar:

$$du_i = a_i(\vec{x}, \vec{u}, t) dt + b_{ij}(\vec{x}, \vec{u}, t) d\xi_j \quad (3.77)$$

$$d\vec{x} = \vec{u} dt \quad (3.78)$$

where $\vec{x}(t)$ and $\vec{u}(t)$ represent trajectory coordinates and velocity as function of time, while a and b are functions of trajectory coordinates, velocity and time. Here $d\xi_j$ are the increments of a vector-valued Wiener process. Equation (3.77) determines the evolution of a particle in space and time by combining functions a_i that determine correlated part depending on turbulent velocity components and b_{ij} that determine uncorrelated random contribution [Thomson 1987].

Lagrangian footprint model was 2D scaled and parameterised [Kljun *et al.* 2015]. 2D parameterisation describes flux footprint function's upwind extent and the crosswind spread of the footprint. Before calculation of flux footprint function, the data was quality checked for stationarity and horizontal homogeneity of the flux. Criteria for data rejection were following:

$$u_* < 0.1 \text{ m s}^{-1}$$

$$-15.5 \leq \frac{z_m}{L}$$

where z_m measurement height, while L is Monin-Obukhov length. All half-hourly data outside of defined range were dismissed before footprint calculation. Model is available as an online tool [FFP online tool].

4. RESULTS AND DISCUSSION

4.1 Meteorological conditions during the study period 2008-2017

During the study period, average air temperature was 11.23 °C, while average precipitation was 1058 mm. Annual averages of air temperature (T_a), soil temperature at 5 cm depth (T_s), global radiation (R_g), vapour pressure deficit (VPD), soil water content (SWC) and annual sums of precipitation (P) are summarized in Table 4.1.

Table 4.1: Annual averages of T_a , T_s , R_g , VPD , SWC and total annual sums of P

Year	$\overline{T_a}$ [°C]	$\overline{T_s}$ [°C]	$\overline{R_g}$ [W m ⁻²]	\overline{VPD} [hPa]	\overline{SWC} [%]	ΣP [mm]
2008	11.34	11.12	153	4.1	45	899
2009	11.25	11.23	155	4.7	42	940
2010	10.22	10.26	143	4.2	52	1255
2011	11.05	10.63	160	5.7	40	576
2012	11.49	11.06	162	6.3	42	987
2013	10.92	10.52	148	5.2	49	1238
2014	12.11	11.82	140	4.4	59	1755
2015	11.47	11.10	152	5.3	50	1260
2016	11.05	11.01	147	4.5	51	744
2017	11.39	10.76	164	6.0	49	927
2008-2017	11.23	10.95	152	5.0	47.9	1058

Lowest $\overline{T_a}$ of 10.22 °C was recorded in the year 2010, which was the only year with lower $\overline{T_a}$ than the 30-years (1981-2010) average T_a of 10.62 °C for Jastrebarsko (data from National Meteorological and Hydrological service) (Fig. 4.1). The year 2014 had the highest $\overline{T_a}$ and $\overline{T_s}$ of 12.11 °C and 11.82 respectively. In the same year, highest annual P of 1755 mm has been recorded which is for 793 mm greater than the 30 year average P of 962 mm (data from National Meteorological and Hydrological service). With annual P of 576 mm, year 2010 was the driest year over the study period. The highest rate of radiated energy was recorded in the year 2017, while the lowest was recorded in 2014.

Maximum half-hourly average T_a of 38.92 °C was recorded in August 2013. August and July were hottest months with the average daily T_a over 25°C. Coldest months were December, January and February with minimal half-hourly T_a of -20.68 °C recorded in February 2012. Daily averages of T_a and T_s are shown in Fig. 4.2.

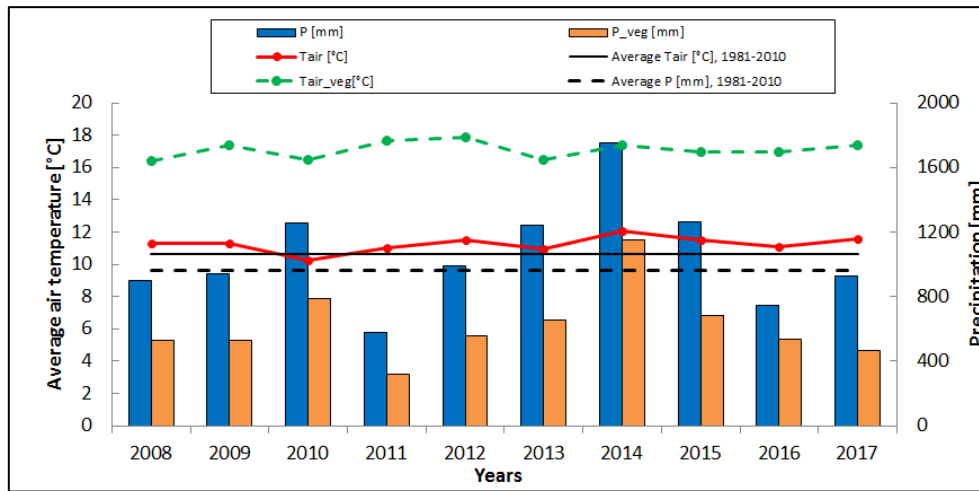


Figure 4.1: Average annual air temperature and total annual precipitation from 2008-2017. Black lines mark average air temperature and average precipitation for period 1981-2010 (Data from Meteorological and Hydrological Service)

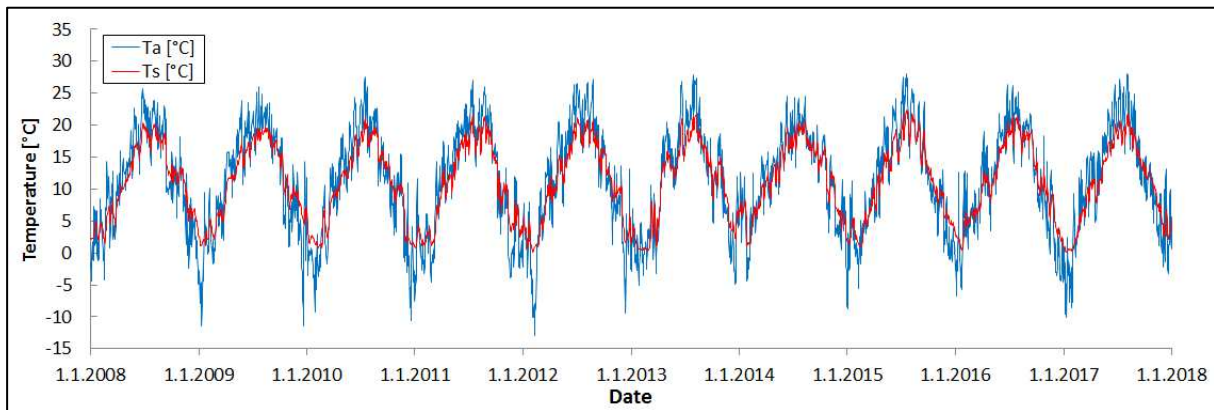


Figure 4.2: The average daily values of air and soil temperature [°C] over the study period

Most of the precipitation falls in summer and early autumn. In the wettest year of 2014, total rainfall during the summer months was 727 mm which made 44% of the total annual precipitation in that year. Lowest total rainfall during the summer months of 143 mm was recorded in the year 2011. *SWC* in the top 30 cm of soil is closely related to *P*. Due to the geography and soil texture at the site, the *SWC* during wintertime was always high (at, or close to, the saturation point) with the beginning of gradual soil drying as the vegetation season progresses. The exception was year 2014 when, because of heavy rainfall during the summer, soil has not dried as it did during the summer months in other years and over almost the whole 2014 *SWC* was between field capacity (F_c , 53% by volume) and saturation point (SWC_{SP} , 61% by the volume), (Fig. 4.3). During warmer and dryer summers of the other years in the study period, the soil dried out, especially in 2011, 2012 and 2017 when *SWC* in the top

30 cm has dropped almost to the wilting point (SWC_{WP} , 20% of volume). A similar situation had occurred in 2017, but in that year drought had started during the spring months, extending throughout the summer, and ending in late August with a sudden transition into relatively cold and wet September.

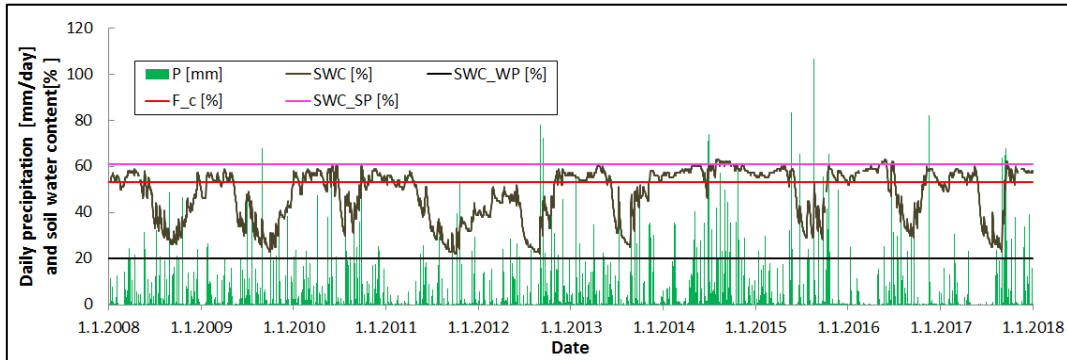


Figure 4.3: The daily sum of precipitation [mm/day] and the average daily soil water content [%] over the study period

The daily averages of R_g [$W\ m^{-2}$] and VPD [hPa] are shown in Fig. 4.4 and 4.5. Both meteorological variables had highest values during summer months. VPD was especially high during the hot and dry summer of 2012.

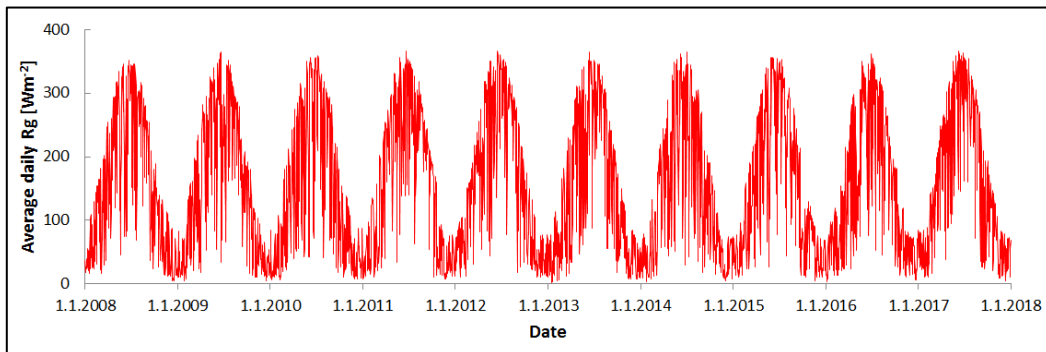


Figure 4.4: The average daily global radiation [$W\ m^{-2}$] over the study period

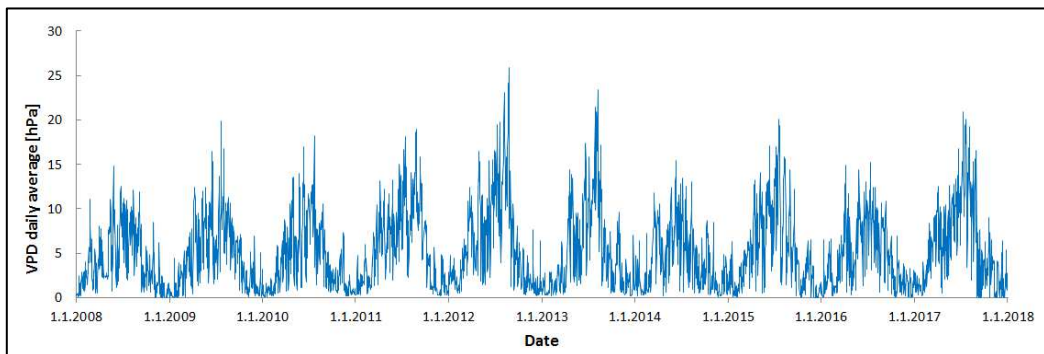


Figure 4.5: The average daily vapor pressure deficit [hPa] over the study period

The highest average T_a during vegetation season of 17.68 °C and 17.87 °C were recorded in the years 2011 and 2012 respectively, while the lowest average T_a of 16.49 °C and 16.46 °C occurred in 2010 and 2013, respectively (Fig. 4.1). Highest total rainfall of 1154 mm was achieved in vegetation season of 2014 what is even more than total annual rainfall in the years 2008, 2009, 2011, 2012, 2016 and 2017. With total rainfall of 322 mm the vegetation season of 2011 was driest vegetation season during the study period. The lowest average T_a , R_g and VPD during the summer of 2014 are the result of many rainy days. Total rainfall in the summer of 2014 reached 777 mm and resulted with the saturation of soil with water ($SWC \approx 60\%$). Spring of 2014, with 368 mm of rainfall was also the rainiest. Because of mild winter with highest average T_a of 5.94 °C and warm autumn with the highest average autumn T_a of 9.56 °C the year 2014 was the warmest year among years in the study period. With only 144 mm of total rainfall, the year 2011 had the driest summer. As a result of drought, SWC dropped to 29 % during summer months of 2011. The same situation occurred in the following year. In those two years the highest average summer VPD values of 10.3 and 11.8 hPa and highest average summer air temperatures of 20.60 and 20.96 °C, respectively, were measured. Also, the years 2011 and 2012 had driest winters among the investigated years with only 32 and 78 mm of precipitation during winter months. The third instance of severe drought occurred in spring of 2017 when total rainfall was only 41 mm. It seems that 416 mm of total rainfall during the summer of 2017 were enough to increase SWC to the maximum of 33 %. According to this, four years can be singled out as extreme years: warm and wet 2014, and warm and dry 2011, 2012 and 2017. Anomalies of air temperature and precipitation during the vegetation season are shown in Fig. 4.6. Average seasonal values of T_a , T_s , R_g , VPD , SWC and total sums of P are summarized in Table 4.2.

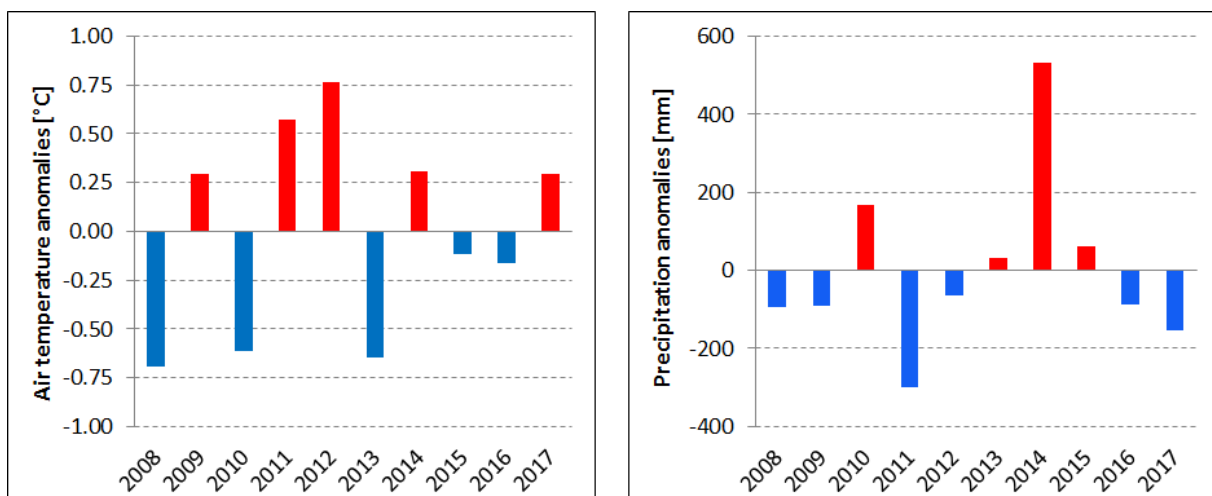


Figure 4.6: Air temperature [°C] and precipitation anomalies [mm] during vegetation season

Table 4.2: Average values of T_a , T_s , R_g , VPD , SWC and total sums of P by season

Winter						
Year	T_a [°C]	T_s [°C]	R_g [W m ⁻²]	VPD [hPa]	P [mm]	SWC [%]
2008	4.02	4.2	82	2.6	131	54
2009	1.77	3.53	74	1.9	149	53
2010	0.96	2.88	67	1.7	225	55
2011	2.11	2.81	71	2.4	32	53
2012	1.45	3.02	95	3.2	78	42
2013	1.78	2.14	65	1.5	313	55
2014	5.94	5.91	72	3.0	232	57
2015	3.31	3.39	77	2.4	161	56
2016	4.23	4.30	66	2.3	96	56
2017	2.08	3.41	61	2.2	304	54
Spring						
2008	13.93	12.11	214	4.8	231	53
2009	15.11	12.77	226	6.9	202	47
2010	14.36	12.27	202	6.2	349	56
2011	14.96	12.82	245	7.5	178	48
2012	14.96	12.78	234	7.9	252	46
2013	13.77	12.37	217	6.7	144	55
2014	14.55	13.24	215	6.5	368	58
2015	14.88	12.99	234	7.6	226	55
2016	14.05	12.38	203	6.1	214	58
2017	15.17	12.81	246	7.9	41	51
Summer						
2008	19.53	17.96	245	7.1	267	33
2009	19.92	17.98	242	7.4	301	34
2010	19.01	17.43	235	7.0	359	42
2011	20.6	18.35	249	10.3	144	29
2012	20.96	18.44	253	11.8	288	29
2013	19.6	17.66	242	9.6	292	35
2014	18.71	17.79	203	5.5	777	60
2015	20.56	18.65	238	9.0	318	36
2016	20.28	18.81	242	7.6	319	41
2017	20.21	18.09	242	10.1	416	33
Autumn						
2008	8.27	10.10	74	2.0	268	39
2009	7.34	10.17	77	2.4	240	34
2010	6.52	8.40	66	1.9	316	55
2011	6.45	8.25	74	2.8	220	32
2012	8.15	9.79	69	2.3	346	50
2013	7.65	9.31	68	2.5	261	52
2014	9.56	10.40	68	2.3	360	59
2015	7.04	9.08	59	2.2	285	55
2016	6.4	8.72	75	2.2	109	51
2017	7.33	8.89	80	2.6	285	57

4.2 Length of growing season

Broadleaved deciduous forests release carbon during a state of dormancy and gain carbon during growing season. It is important to know when growing season has started and ended and how many days it lasted because *NEE* of carbon in this type of forest strongly depends on the length of the growing season [Baldocchi *et al.* 2001]. In this work, the length of growing season (*GSL*) was defined as a number of days between the first and the last day with a negative integrated 3-day *NEE* [Wilkinson *et al.* 2012]. *GSL* varied from year to year (Table 4.3). The longest *GSL* of 218 days during the research period was recorded in the year 2008 (Fig. 4.7) while the shortest of 180 days in 2013. Growing season in the year 2008 started (*SGS*) on 17th of March and ended (*EGS*) on 21st of October. The average *GSL* over the study period was 196 ± 8 days (95% confidence interval (CI)). On average, the *SGS* was around *DOY* 93 (2nd April) while *EGS* was around *DOY* 288 (14th of October).

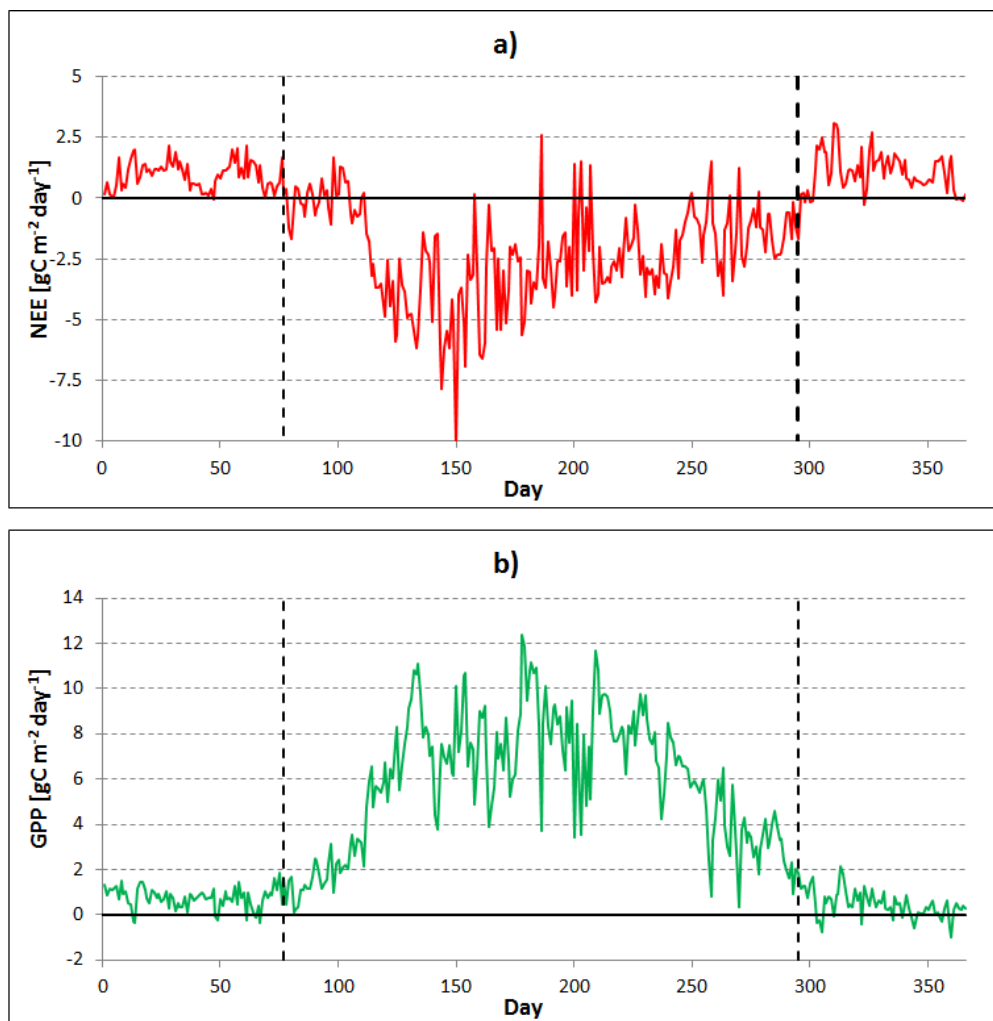


Figure 4.7: *GSL* in the year 2008 (vertical dashed black lines mark *SGS* and *EGS*); a) *NEE*; b) *GPP*

Table 4.3: *DOY* for the start of growing season (*SGS*), end of growing season (*EGS*) and growing season length (*GSL*) at Jastrebarsko forest

Year	<i>SGS</i> [<i>DOY</i>]	<i>EGS</i> [<i>DOY</i>]	<i>GSL</i> [days]
2008	77	295	218
2009	98	293	195
2010	86	287	201
2011	88	295	207
2012	90	296	206
2013	111	291	180
2014	90	272	182
2015	86	278	192
2016	101	282	181
2017	100	292	192
Mean	93	288	196
Std	9.8	8.2	12.7
SE	3.1	2.6	4.0
95% CI	6.1	5.1	7.9

4.3 Flux footprint analysis

Flux footprint analysis showed that the distance from the tower, which encircles the area encompassing 90% of the footprint, was approximately 400 m before the elevation of the tower and 600 m after the tower was elevated (Fig. 4.8).

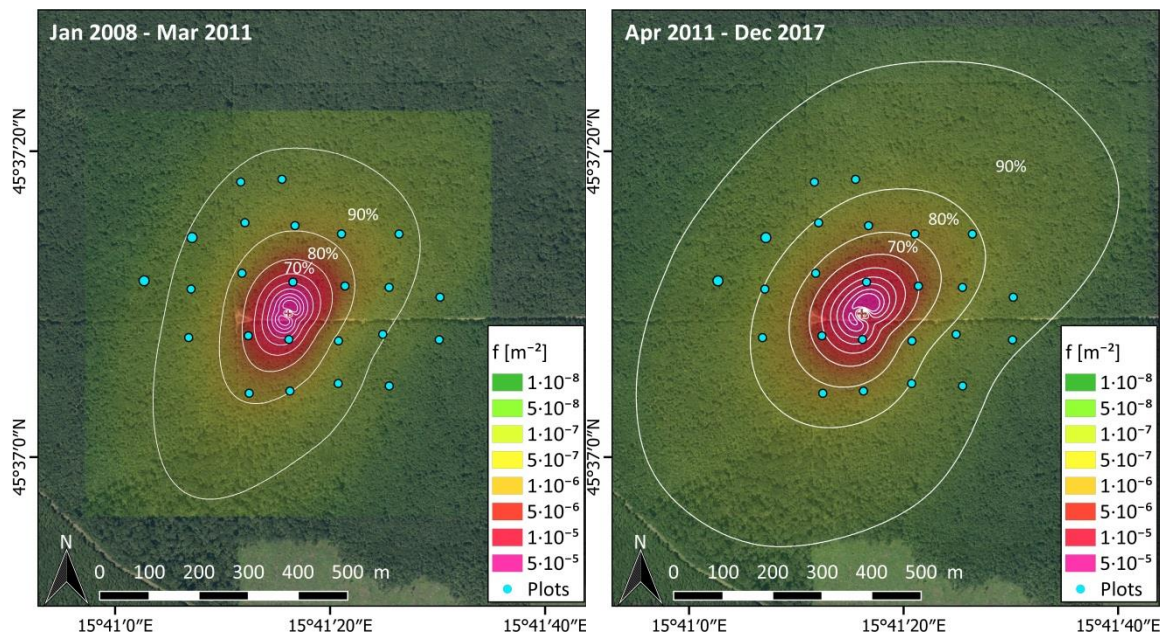


Figure 4.8: Flux footprint; a) before the elevation of EC tower (23 m); b) after the elevation of EC tower (27 m); little cyan circles mark the location of 24 circular plots

Wind rose for Jastrebarsko forest confirms that footprint area is spreading in direction of the dominant wind (Fig. 4.9).

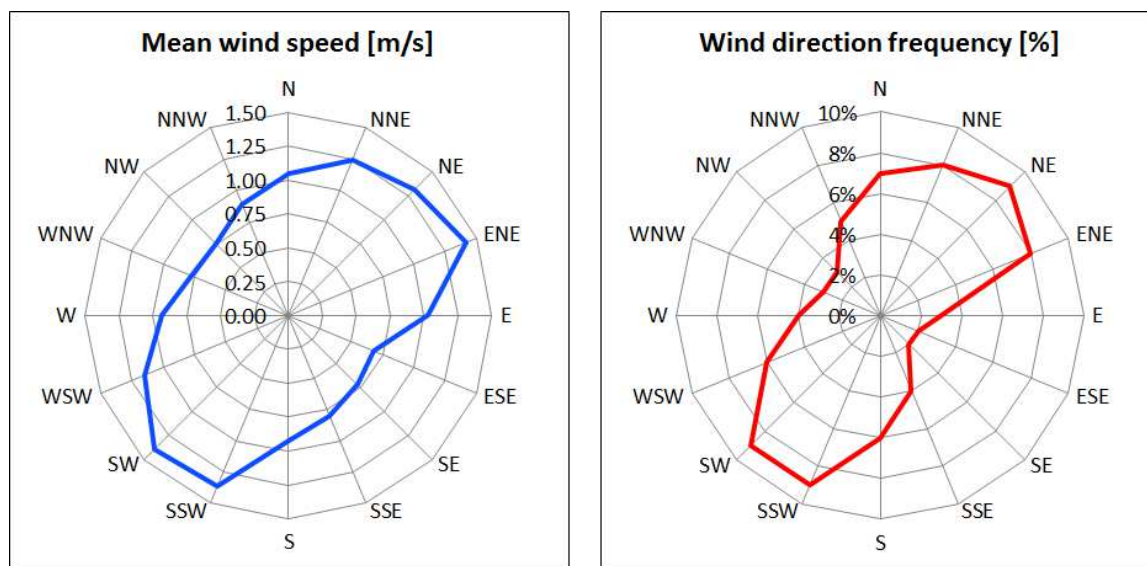


Figure 4.9: Wind rose for Jastrebarsko forest, 2008-2017

Jastrebarsko is a town with medium industrial activity. Industrial zones are located approximately 5 km from EC tower. Furthermore, Zagreb-Rijeka highway is approximately 2.4 km N from from the EC tower. Footprint analysis has excluded these anthropogenic emissions of CO₂ as a significant contributor to a measured carbon flux. Also, Fig. 4.8 shows that all of the 24 circular plots with the installed dendrometer bands on the trees lie in the fetch of EC tower what justifies the comparison of EC measurements with the biometric measurements.

4.4 Net ecosystem exchange of CO₂

Here the results of EC measurements of carbon *NEE* are described. First, in section 4.4.1, the diurnal cycle of *NEE* is presented. The annual cycle of *NEE* in Jastrebarsko forest is described in section 4.4.2. In the final section of chapter 4.4, the annual sums of *NEE* are summarized.

4.4.1 Diurnal cycle of *NEE*

Fig. 4.10 shows daily cycle of *NEE* for a random day during a growing part of the season when vegetation was fully developed and one random day during the dormant part of the season.

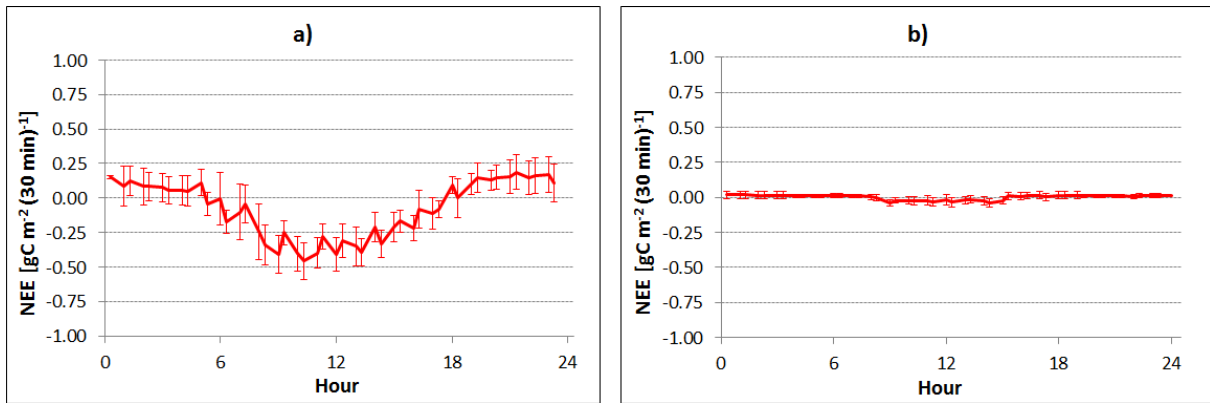


Figure 4.10: Diurnal cycle of NEE [gC m^{-2}] ($\pm 95\%$ CI) for a random day in a) growing season (1st of July 2008); b) dormant season (4th of January 2008); negative values of NEE indicate that the ecosystem is acting as a sink of carbon

Exchange of CO_2 showed a clear daily pattern. During the growing season the CO_2 uptake, i.e. negative values of NEE , took place with the onset of photosynthesis soon after a sunrise. Photosynthesis is the process in which light energy is captured and used by green plants to synthesize reduced carbon compounds from CO_2 and H_2O [e.g. Kozlowski and Pallardy 1997]. The peak of CO_2 uptake occurred usually around noon and that correlates well with the peak in global radiation R_g . On the other hand, positive values of NEE represent that the ecosystem respiration outgrew GPP , which typically occurs around 1 h prior to nightfall. During the dormant season NEE was small and had values around zero. The lowest NEE was observed in January. Because there are no evergreen species of trees in the footprint of the EC tower, negative NEE during dormant season is probably a result of CO_2 uptake by grasses and mosses. The highest half-hourly CO_2 uptake of $-1.00 \text{ gC m}^{-2} (30 \text{ min})^{-1}$ was measured on 13th July 2013, while the highest half-hourly CO_2 release of $0.63 \text{ gC m}^{-2} (30 \text{ min})^{-1}$ on 20th May 2011.

To get a closer into how daily cycle of NEE varies by months, half-hourly NEE values were averaged by time of day, month and year, so every point in Fig. 4.11 represents a mean of the half-hourly values of NEE in the specific month through ten years. On average, half-hourly values of NEE were lowest during the dormant part of the season which entirely includes months January, February, November and December. With the appearance of leaves at the end of March and the beginning of April, the NEE starts to become more negative, especially during May, and reached on average the highest absolute values during June when vegetation is fully developed. A daily period of CO_2 uptake was gets longer with the elongation of the daylight until the summer solstice. Half-hourly values of NEE remained high on average during July and August, while their lower values during September indicated

the beginning of leaf senescence. Leaf senescence is the final and important stage of leaf development during which nutrients are recycled to the other parts of the deciduous plants [Gan and Amasino 1997]. During November, after leaves are fully rejected, half-hourly values of *NEE* are small.

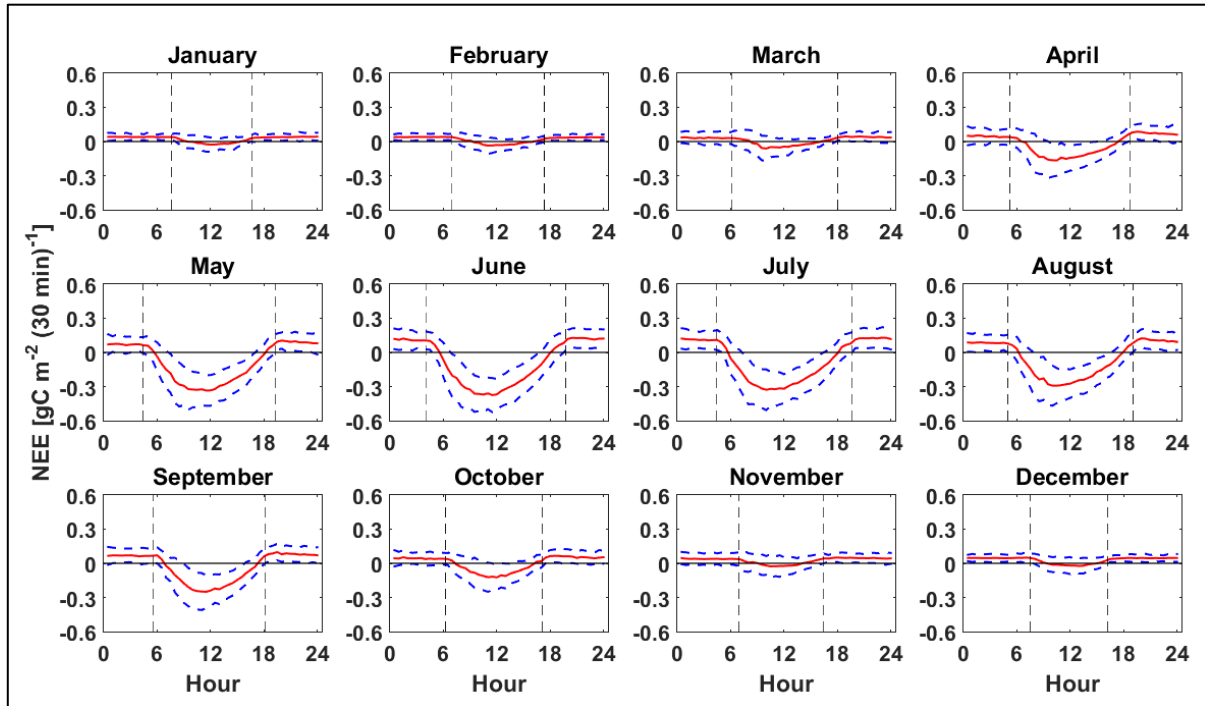


Figure 4.11: Mean diurnal variation of *NEE* by months during the years 2008 to 2017; blue dashed line marks 1 standard deviation; vertical dashed line marks the time of sunrise and sunset on the 15th day of the month

4.4.2 The annual cycle of *NEE*

To obtain daily *NEE* of CO₂, half-hourly values of *NEE* were summed by day so every daily *NEE* represents the sum of 48 half-hourly *NEE* values. Highest daily uptake of CO₂ of -10.2 gC m⁻² day⁻¹ was recorded on 29th May 2008 while the highest daily release of CO₂ of 5.01 gC m⁻² day⁻¹ was recorded on 10th December 2011. Exchange of CO₂ showed a clear seasonal pattern (Fig. 4.12). Uptake of CO₂ started in early spring with the development of leaves. During May, carbon CO₂ increased strongly and reached a peak in June. However, there were also days when ecosystem lost carbon to the atmosphere during the growing season which indicates that the respiration was stronger than the uptake due to unfavourable conditions. With the start of leaf senescence in early autumn, carbon uptake rapidly declined. During winter, when vegetation was in a state of dormancy, absolute values of *NEE* reached

their minimum values and ecosystem was a net source of carbon indicating active respiration even during the cold winter days.

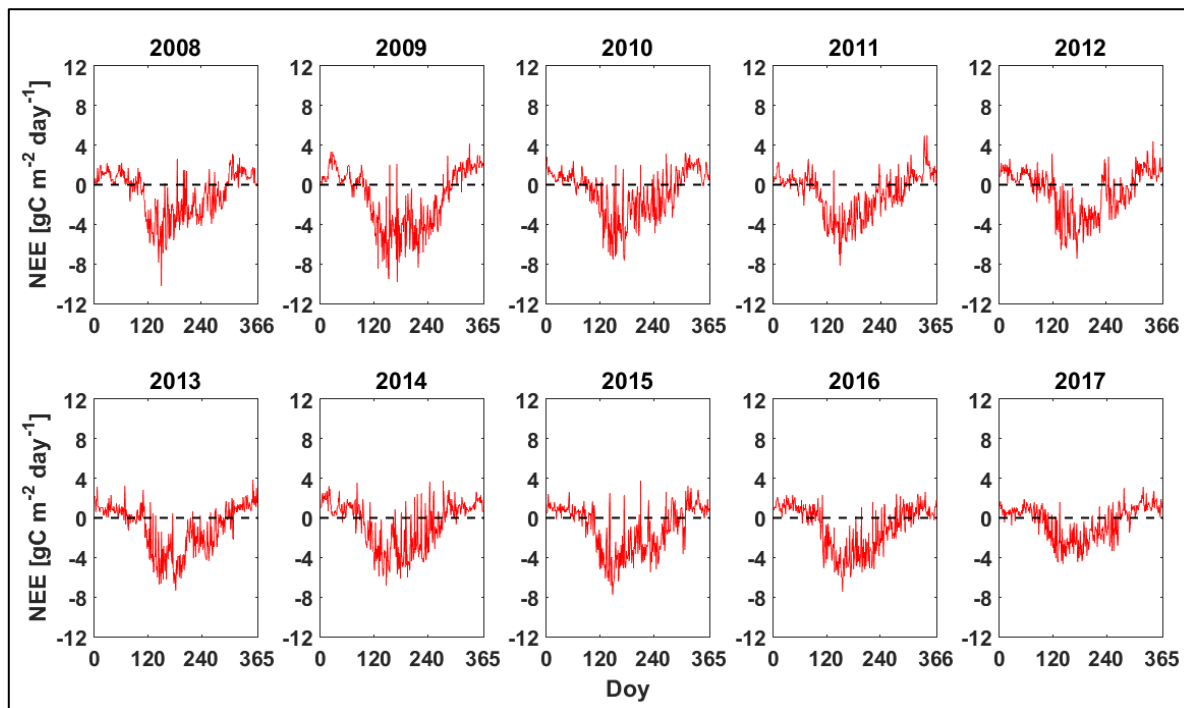


Figure 4.12: The daily sums of NEE [$\text{gC m}^{-2} \text{day}^{-1}$] in Jastrebarsko forest, 2008-2017

4.4.3 Total sums of NEE

Daily values of NEE were summed to obtain annual net carbon budgets. Annual sums of NEE ranged from $-147 \pm 13 \text{ gC m}^{-2} \text{yr}^{-1}$ in 2017 to $-496 \pm 15 \text{ gC m}^{-2} \text{yr}^{-1}$ in the year 2009. The average sink of carbon over the study period was $-319 \pm 30 \text{ gC m}^{-2} \text{yr}^{-1}$, while the overall net sink of carbon was $-3195 \text{ gC m}^{-2} (10 \text{ yr})^{-1}$. Annual values of NEE are summarized in Table 4.4.

Furthermore, the growing season NEE_{GS} was calculated as the sum of daily NEE values from the start to the end of the growing season (see Table 4.3). Growing season of 2009 achieved highest carbon sink of $-703 \pm 15 \text{ gC m}^{-2} \text{grs}^{-1}$ (Table 4.5). Growing seasons of 2017 and 2012 achieved the smallest sinks of carbon over the study period. The average sink of carbon during growing seasons was $-483 \pm 31 \text{ gC m}^{-2} \text{grs}^{-1}$. Causes of inter-annual variability of carbon fluxes will be discussed later.

Table 4.4: Annual sums of *NEE* [gC m⁻² yr⁻¹] for years 2008-2017

Year	<i>NEE</i> ± SE [gC m ⁻² yr ⁻¹]
2008	-352 ± 13
2009	-496 ± 15
2010	-286 ± 14
2011	-353 ± 14
2012	-261 ± 14
2013	-356 ± 13
2014	-232 ± 14
2015	-373 ± 13
2016	-339 ± 13
2017	-147 ± 13
Average	-319 ± 30
Overall sum	-3195 gC m ⁻² (10 grs) ⁻¹

Table 4.5: *NEE_{GS}* during the growing seasons [gC m⁻² grs⁻¹]*

Year	<i>NEE_{GS}</i> ± SE [gC m ⁻² grs ⁻¹]
2008	-501 ± 13
2009	-703 ± 15
2010	-453 ± 13
2011	-483 ± 13
2012	-439 ± 13
2013	-509 ± 12
2014	-441 ± 13
2015	-508 ± 12
2016	-493 ± 12
2017	-298 ± 12
Average	-483 ± 31
Overall sum	4828 gC m ⁻² (10 grs) ⁻¹

* grs – growing season

Estimation of *NEE* with EC technique possesses a high degree of uncertainty and probably largest uncertainties are related to CO₂ fluxes during calm periods when turbulent mixing is insufficient and thermal stratification is stable. Usually, calm periods appear during the night when ecosystem acts as a source of carbon, so underestimation of CO₂ fluxes during the night leads to overestimation of *NEE* at the annual scale. This underestimation of night-time CO₂ fluxes is an example of selective systematic error, i.e. an error that applies to one part of the daily cycle (Moncrieff *et al.* 1996). During calm nights, CO₂ can be either stored in the canopy air or removed by advection and this represents a big problem because CO₂ removed by advection from measurement area will be lost and measured flux will be underestimated. Advection occurs mainly in the presence of flows associated with terrain

slopes or with land use changes [Aubinet *et al.* 2010]. Since terrain around the EC tower is flat, significant advection fluxes due to sloping terrain could not occur, and the advection was not regarded as a problem. A common approach to night-time flux error is filtering of CO₂ fluxes for which u_* is lower than the estimated u_{*crit} . For comparison, EC fluxes were calculated with and without applying the u_* filtering. The NEE estimated with the application of u_* filtering during the flux calculation (NEE_{usf}) was more frequently larger in magnitude than NEE estimated without performing u_* filtering procedure (NEE_{no-usf}) (Table 4.6). Difference in NEE_{no-usf} and NEE_{usf} for years 2008, 2009, 2010, 2011, 2013, 2014 and 2016 was small and ranged from 1 gC m⁻² yr⁻¹ in 2013 to 12 gC m⁻² yr⁻¹ in 2009. Significantly larger difference between NEE_{no-usf} and NEE_{usf} of -73, -50 and 26 gC m⁻² yr⁻¹ was estimated in years 2012, 2015 and 2017, respectively. Overall sums of NEE and NEE_{usf} over the study period were almost identical (Table 4.6).

Table 4.6: Comparison of annual sums of NEE estimated by applying u_* filtering (NEE_{usf}) with annual sums of NEE estimated without performing u_* filtering (NEE_{no-usf})

Year	$NEE_{no-usf} \pm SE$ [gC m ⁻² yr ⁻¹]	$NEE_{usf} \pm SE$ [gC m ⁻² yr ⁻¹]
2008	-342 ± 12	-352 ± 13
2009	-482 ± 15	-496 ± 15
2010	-280 ± 14	-286 ± 14
2011	-347 ± 13	-353 ± 14
2012	-188 ± 13	-261 ± 14
2013	-357 ± 13	-356 ± 14
2014	-225 ± 14	-232 ± 14
2015	-423 ± 13	-373 ± 13
2016	-348 ± 13	-339 ± 13
2017	-173 ± 12	-147 ± 13
Average	-316 ± 29	-319 ± 30
Overall sum	3164 gC m ⁻² (10 yr) ⁻¹	-3195 gC m ⁻² (10 yr) ⁻¹

Furthermore, u_* filtering procedure removed approximately 5-10% of measured data per year, producing even more gaps in time series which should be filled. Thus additional uncertainty is induced. In this work, gaps were filled by using enhanced MDS technique. According to this method, a missing half-hourly NEE was replaced by the average value under the similar meteorological conditions (see chapter 3.5). In this way, missing NEE values under the calm periods discarded by u_* filtering procedure are replaced with average NEE values under the windy conditions which might be questionable. Implementing EC

experiment is very challenging, large errors are possible and the u_* filtering should be considered in data processing. However, the u_* filtering is to some degree subjective, site dependent procedure with some shortcomings. It is hard to say whether applying the u_* filtering is good decision or not at the Jastrebarsko site. In any case, the comparison showed that there were no big differences in NEE for majority of years. However, for three years the difference was considerable (Table 4.6). Since the u_* filtering is a standard step in the EC technique and in our case yields differences in the results, at least in some years, all EC-originating fluxes presented below are calculated by applying the u_* filtering procedure.

4.5 Partitioned fluxes of carbon: GPP , NPP and R_{ECO}

Net ecosystem exchange of CO_2 was partitioned into three carbon fluxes: gross primary productivity, GPP , ecosystem respiration R_{ECO} and net primary productivity, NPP . Respiration rates were extracted from air temperature using Lloyd-Taylor [Lloyd and Taylor 1994] regression model. Half-hourly values of R_{ECO} were summed by day to obtain daily values of R_{ECO} . Highest daily R_{ECO} values of $12.97 \text{ gC m}^{-2} \text{ day}^{-1}$ were achieved on 3th of July 2015. Fig. 4.13 shows the temporal variation of the daily R_{ECO} throughout the measurements period. Largest negative carbon flux, R_{ECO} , has followed yearly pattern of air and soil temperatures, as expected, because R_{ECO} was estimated using the air temperature. Highest daily values of R_{ECO} were achieved in the summer, while during dormant season daily values of R_{ECO} were significantly lower. Higher daily R_{ECO} values during some winter days are the consequence of higher air and soil temperatures in that period. Secondary peaks which occur during autumn are probably the result of decomposition of new litterfall. Daily sums of R_{ECO} were summed by year to obtain annual sums of R_{ECO} which are summarized in Table 4.7, alongside with yearly sums of autotrophic (R_a) and heterotrophic (R_h) respiration which were partitioned from R_{ECO} to obtain NPP (see chapter 3.6). Highest annual sums of R_{ECO} of $1402 \text{ gC m}^{-2} \text{ yr}^{-1}$ were obtained in 2015 which is in good agreement with the higher air temperatures in that year, while the lowest R_{ECO} of $1117 \text{ gC m}^{-2} \text{ yr}^{-1}$ was obtained in 2008. The average R_{ECO} over the ten years of measurement was $1275 \pm 94 \text{ gC m}^{-2} \text{ yr}^{-1}$. Cumulative curves of R_{ECO} show rapid increase during the spring and the summer months (Fig. 4.14).

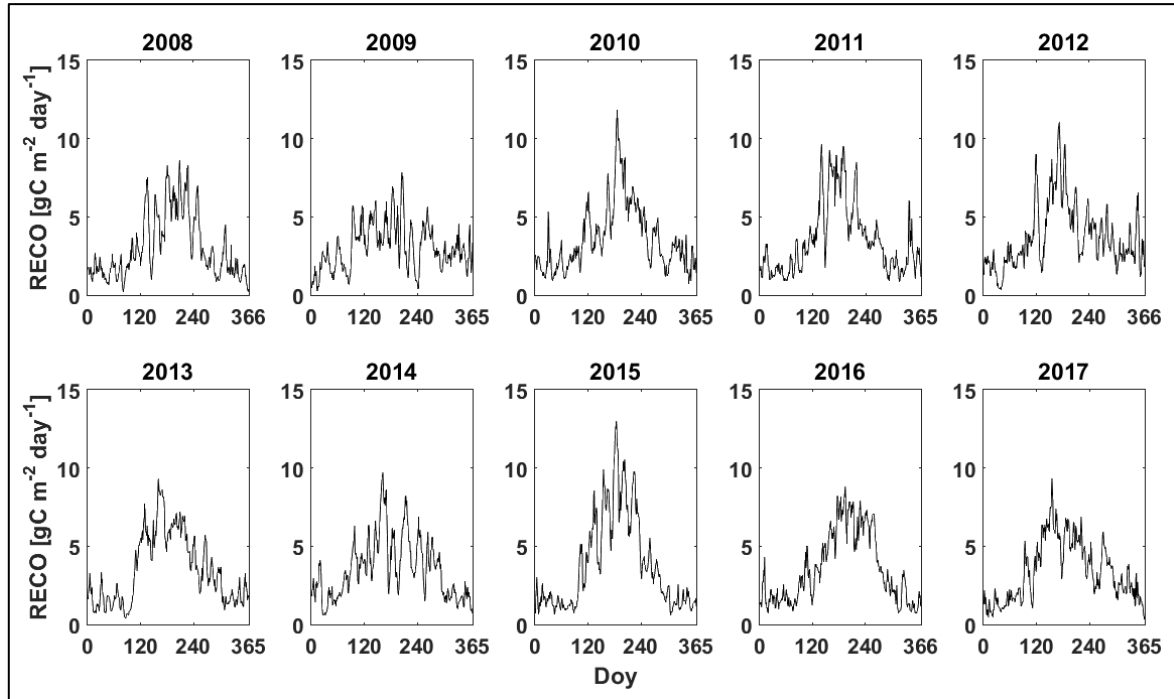


Figure 4.13: Annual variation of daily sums of R_{ECO} [$\text{gC m}^{-2} \text{day}^{-1}$] in Jastrebarsko forest, 2008-2017

Table 4.7: Annual sums of R_{ECO} , R_a and R_h [$\text{gC m}^{-2} \text{yr}^{-1}$], 2008-2017

Year	R_{ECO} [$\text{gC m}^{-2} \text{yr}^{-1}$]	R_a [$\text{gC m}^{-2} \text{yr}^{-1}$]	R_h [$\text{gC m}^{-2} \text{yr}^{-1}$]
2008	1117	679	438
2009	1126	685	441
2010	1329	808	521
2011	1289	784	505
2012	1382	840	541
2013	1275	775	500
2014	1290	785	506
2015	1402	852	549
2016	1305	794	512
2017	1236	752	484
Average	1275 ± 94	775 ± 57	500 ± 37
Overall sum	$12751 \text{ gC m}^{-2} (10\text{yr})^{-1}$	7754	4997

GPP , the amount of carbon fixed by photosynthesis, was calculated as a difference between NEE and R_{ECO} . Daily sums of GPP were calculated as a sum of 48 half-hourly values. The maximum rate of GPP of $16.83 \text{ gC m}^{-2} \text{day}^{-1}$ was measured on 4th of June 2015. Fig. 4.15 shows a clear seasonal pattern of GPP .

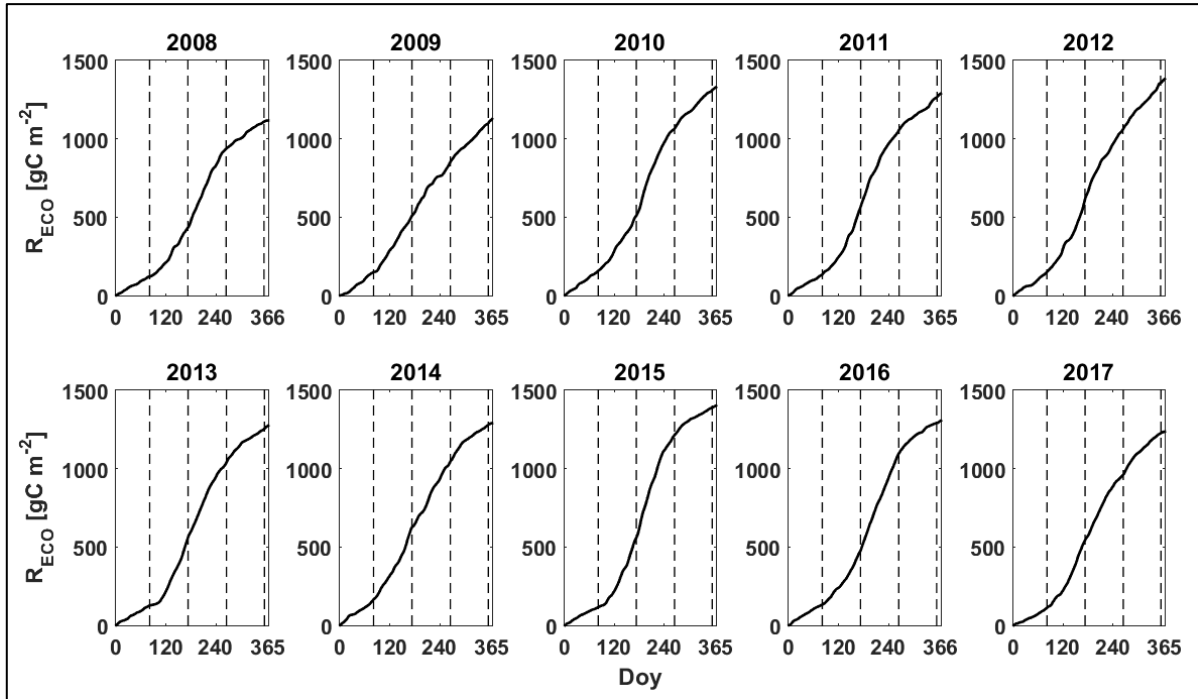


Figure 4.14: Cumulative curves of R_{ECO} [gC m^{-2}] in Jastrebarsko forest 2008-2017, black dashed lines mark beginnings of different seasons

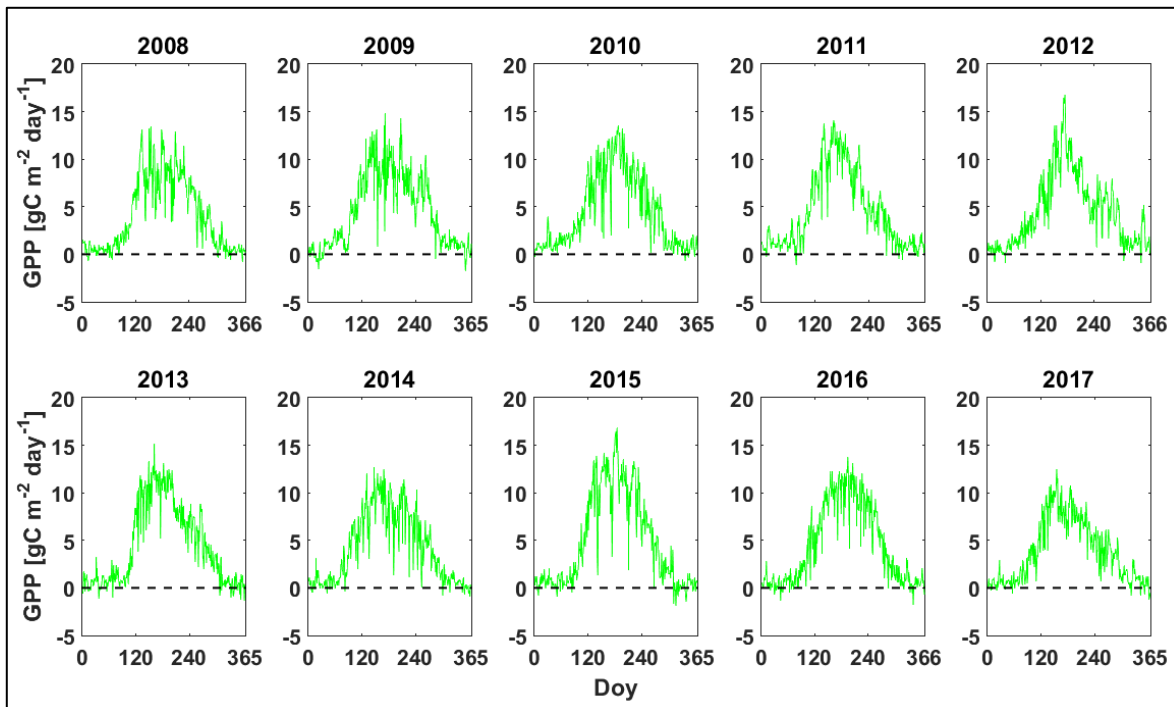


Figure 4.15: Annual variation of daily GPP [$\text{gC m}^{-2} \text{day}^{-1}$] in Jastrebarsko forest, 2008-2017

During dormant season daily values of GPP were small. Carbon sequestration started with development of leaves in early spring which is manifested with a high increase in daily values of GPP . Maximum rates of GPP were achieved during summer months. After a peak in early summer, GPP started to decline slowly and dropped again to near zero after the leaf fall.

There were several days over the study period with negative daily values of *GPP* which is impossible. Such situations resulted from gap-filling and were regarded as errors in measurements. An interesting situation occurred during the summer 2012 when *GPP* has rapidly dropped to small values. This can be explained by a severe drought which occurred in the middle of August 2012. After an episode of drought values of *GPP* grew to typical values for Jastrebarsko forest for that part of the year. Despite the drought, 2012 was the year with the third highest annual sums of *GPP* of $1642 \text{ gC m}^{-2} \text{ yr}^{-1}$. Rapid and strong growth in daily *GPP* values during spring and summer months can be also seen in Fig. 4.16 where cumulative curves of *GPP* are shown.

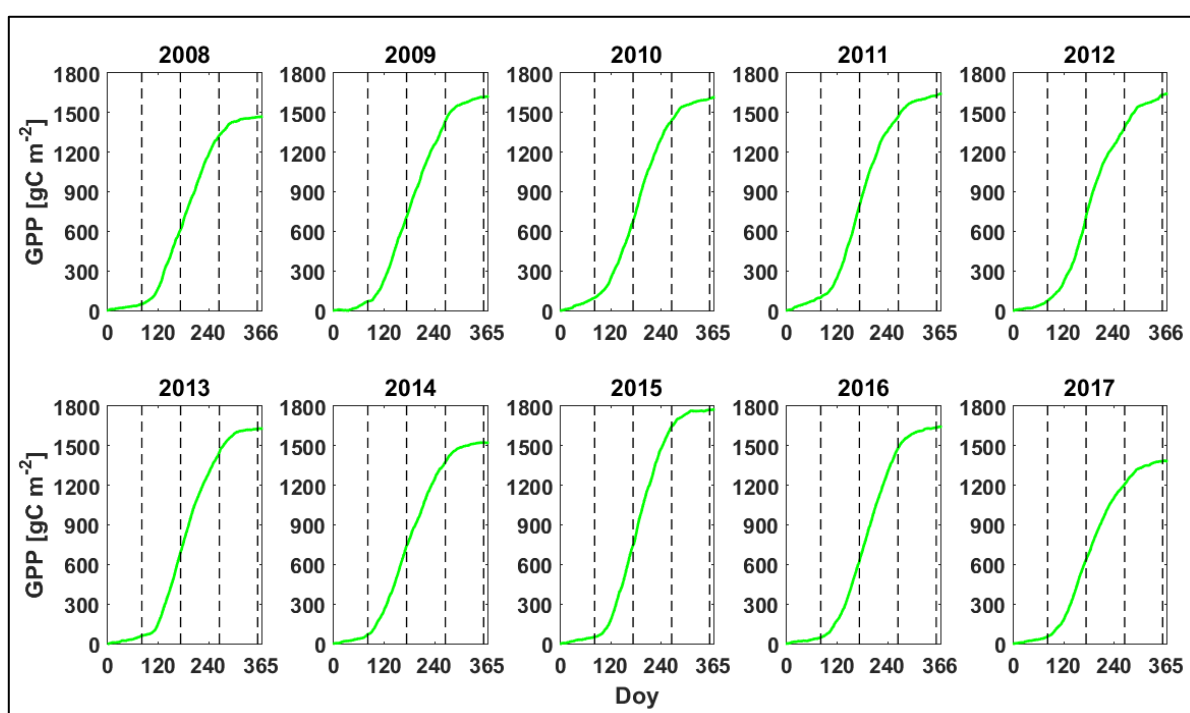


Figure 4.16: Cumulative curves of *GPP* [gC m^{-2}] in Jastrebarsko forest 2008-2017, black dashed lines mark beginnings of different seasons

Annual sums of *GPP* ranged from lowest of $1384 \text{ gC m}^{-2} \text{ yr}^{-1}$ in 2017 to highest of $1775 \text{ gC m}^{-2} \text{ yr}^{-1}$ in 2015 (Table 4.8). Average *GPP* during ten years of measurement was $1594 \pm 109 \text{ gC m}^{-2} \text{ yr}^{-1}$.

NPP was calculated as a difference between heterotrophic respiration (R_h) and *NEE*. The yearly cycle of *NPP* followed the yearly cycle of *GPP*. Highest daily values of *NPP* were also achieved in June and lowest during dormant season (Fig. 4.17). Negative *NPP* is possible. It indicates that autotrophic respiration was stronger than *GPP*. The situation of that

kind occurred mainly during the cold part of the year when vegetation was in the state of dormancy. Hasty drop in *NPP* during August 2012 is probably a consequence of drought.

Table 4.8: Annual sums of *GPP* [$\text{gC m}^{-2} \text{yr}^{-1}$], 2008-2017

Year	<i>GPP</i> [$\text{gC m}^{-2} \text{yr}^{-1}$]
2008	1469
2009	1622
2010	1615
2011	1642
2012	1642
2013	1630
2014	1522
2015	1775
2016	1644
2017	1384
Average	1594 ± 109
Overall	$15945 \text{ gC m}^{-2} (10\text{yr})^{-1}$

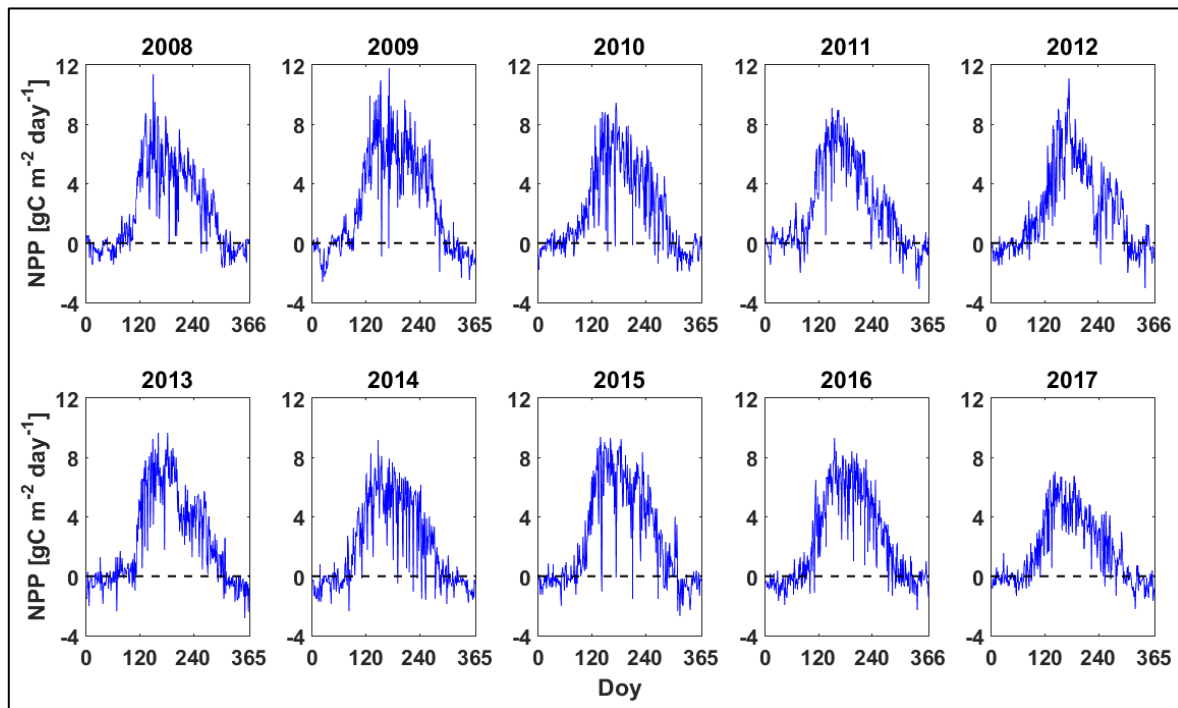


Figure 4.17: Annual variation of daily *NPP* [$\text{gC m}^{-2} \text{day}^{-1}$] in Jastrebarsko forest, 2008-2017

Cumulative curves of *NPP* are shown in Fig. 4.18. Effect of drought in August 2012 is visible from declining of *NPP* cumulative curve in the middle of the summer in that year. Despite that, the annual value of *NPP* of $802 \text{ gC m}^{-2} \text{yr}^{-1}$ in 2012 was not the lowest among investigated years. Highest daily *NPP* of $10.78 \text{ gC m}^{-2} \text{day}^{-1}$ was achieved on 21st of June

2011. Average NPP during ten years of measurements was $819 \pm 89 \text{ gC m}^{-2} \text{ yr}^{-1}$. Highest annual value of NPP of $937 \text{ gC m}^{-2} \text{ yr}^{-1}$ was achieved in 2009, while the lowest of $632 \text{ gC m}^{-2} \text{ yr}^{-1}$ in 2017 (Table 4.9). Overall sum of NPP over the ten years of measurements was $8192 \text{ gC m}^{-2} (10 \text{ yr})^{-1}$.

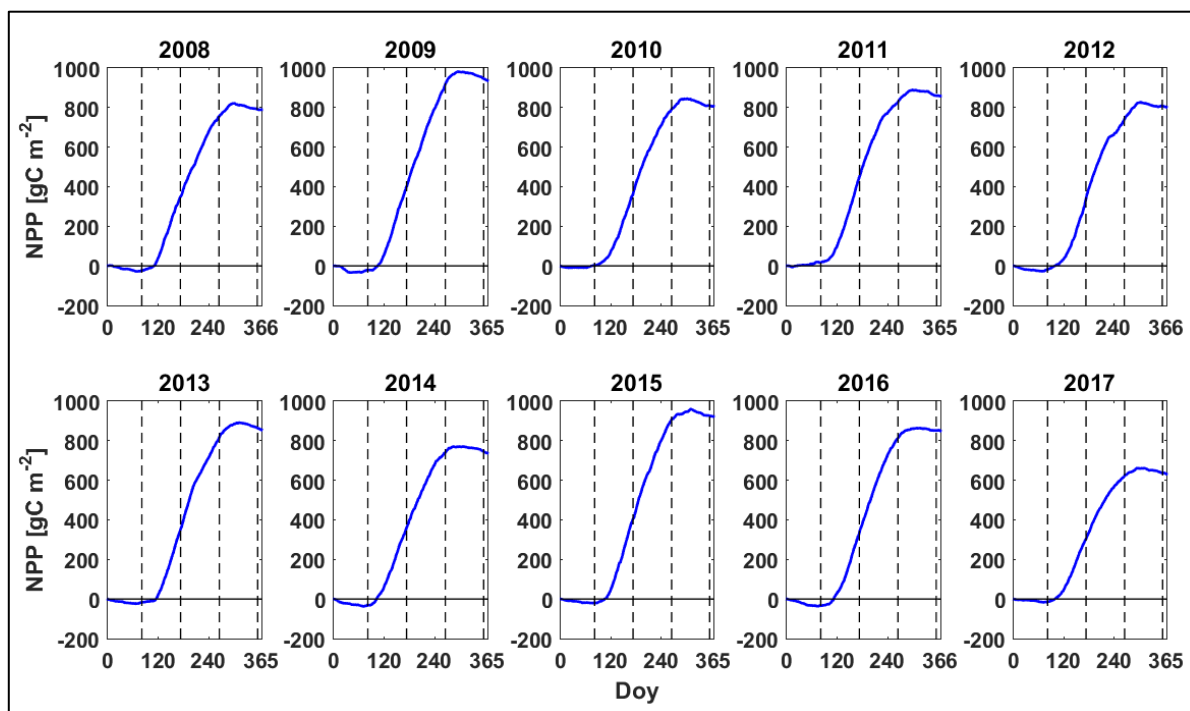


Figure 4.18: Cumulative curves of NPP [gC m^{-2}] in Jastrebarsko forest 2008-2017, black dashed lines mark beginnings of different seasons

Table 4.9: Annual sums of NPP [$\text{gC m}^{-2} \text{ yr}^{-1}$], 2008-2017

Year	NPP_{EC} [$\text{gC m}^{-2} \text{ yr}^{-1}$]
2008	790
2009	937
2010	807
2011	858
2012	802
2013	855
2014	738
2015	923
2016	850
2017	632
Average	819 ± 89
Overall sum	$8192 \text{ gC m}^{-2} (10 \text{ yr})^{-1}$

4.6 Inter-annual variability of carbon *NEE*

Except for the dependence on the length of a growing season, inter-annual variability of *NEE* is also driven by differences in the balance of *GPP* and *R_{ECO}* which is controlled by environmental variables [Malhi *et al.* 1999, Law *et al.* 2002]. Long-term measurements allow us to examine the response of the measured *NEE* to the environmental factors. The main variables that control the behavior of vegetation are global radiation, temperature, soil moisture and vapor pressure deficit. Availability of light controls photosynthesis and determines the maximum length of the growing season in spring and autumn in mid-latitudes [e.g. Malhi *et al.* 1999]. The major influence of temperature on net carbon balance is through its effects on rates of both autotrophic and heterotrophic respiration [Malhi *et al.* 1999]. Besides *R_{ECO}*, temperature, through the effect on vapour pressure deficit (*VPD*), affects stomatal opening and closure. At high *VPD* (e.g. in a hot summer afternoon during dry period) stomata close in order to reduce the transpiration and control the loss of water [Anthoni *et al.* 1999, Schulze 2005]. Stomas are openings (pores) which can be found in the epidermis of leaves, that facilitates gas exchange. If they are closed, plants cannot obtain CO₂ from the air and cannot perform the photosynthesis. Low soil moisture or *SWC* can restrict photosynthesis in the late summer and reduce carbon uptake by inducing stomatal closure and by this it has a direct effect on the rate of photosynthesis. Low *SWC* in Jastrebarsko forest rarely occurs in spring because *SWC* reserves are mainly replenished by autumn and winter precipitation, although spring 2012 was an exception when the drought of 2011 continued also during the winter. The low *SWC*, as a result of drought, can affect carbon and nutrient release through decomposition by restricting microbial activity [Malhi *et al.* 1999].

Ten years of EC measurements of carbon *NEE* showed high inter-annual variability. Difference between year with the highest (2009) and a year with the lowest sink of carbon (2017) was 349 gC m⁻² yr⁻¹. The year with the most pronounced *NEE* anomaly, when *NEE* deviated more than one standard deviation from the average *NEE* was 2009. To get a closer insight into causes of inter-annual variability of carbon *NEE* seasonal anomalies of *T_a*, *T_s*, precipitation *P*, *SWC*, *VPD* and *R_g* were calculated. Anomalies of stated environmental variables are shown in Fig. 4.19 – 4.24.

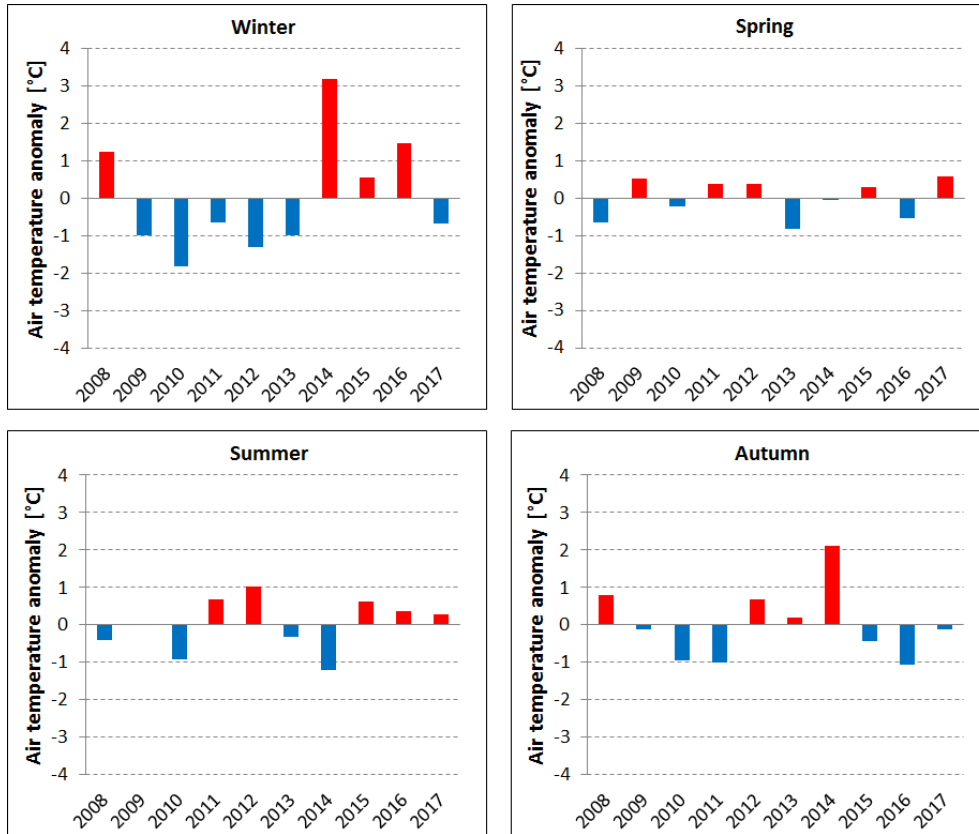


Figure 4.19: Seasonal anomalies of air temperature [°C], 2008-2017

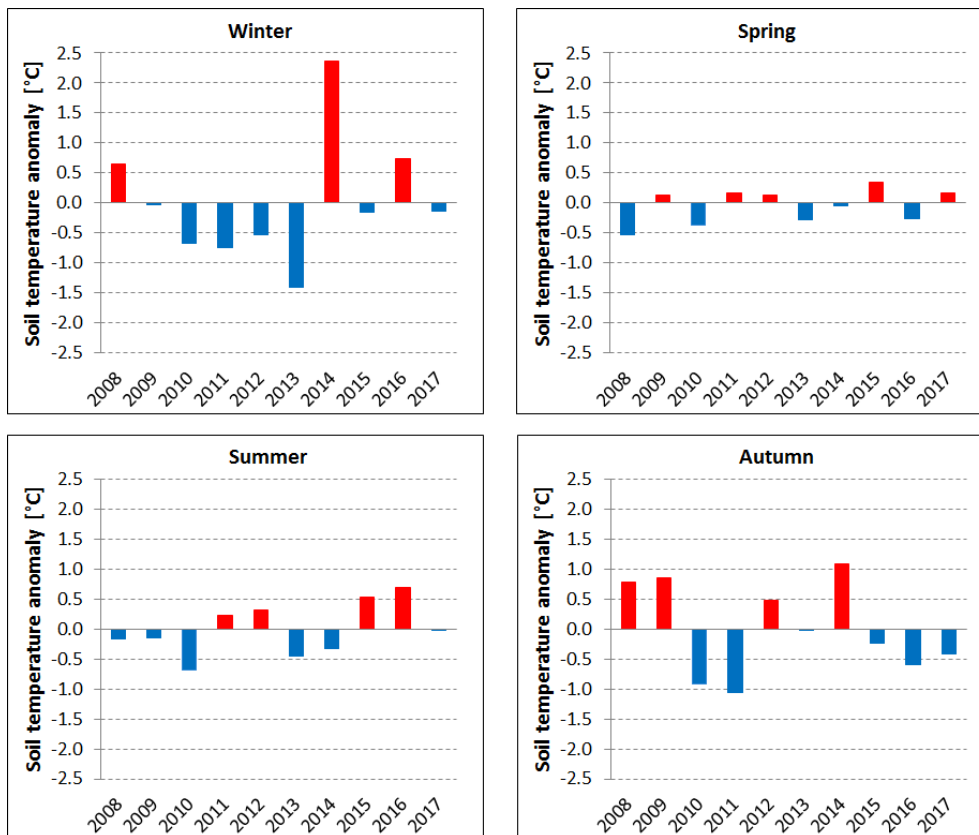


Figure 4.20: Seasonal anomalies of soil temperature [°C], 2008-2017

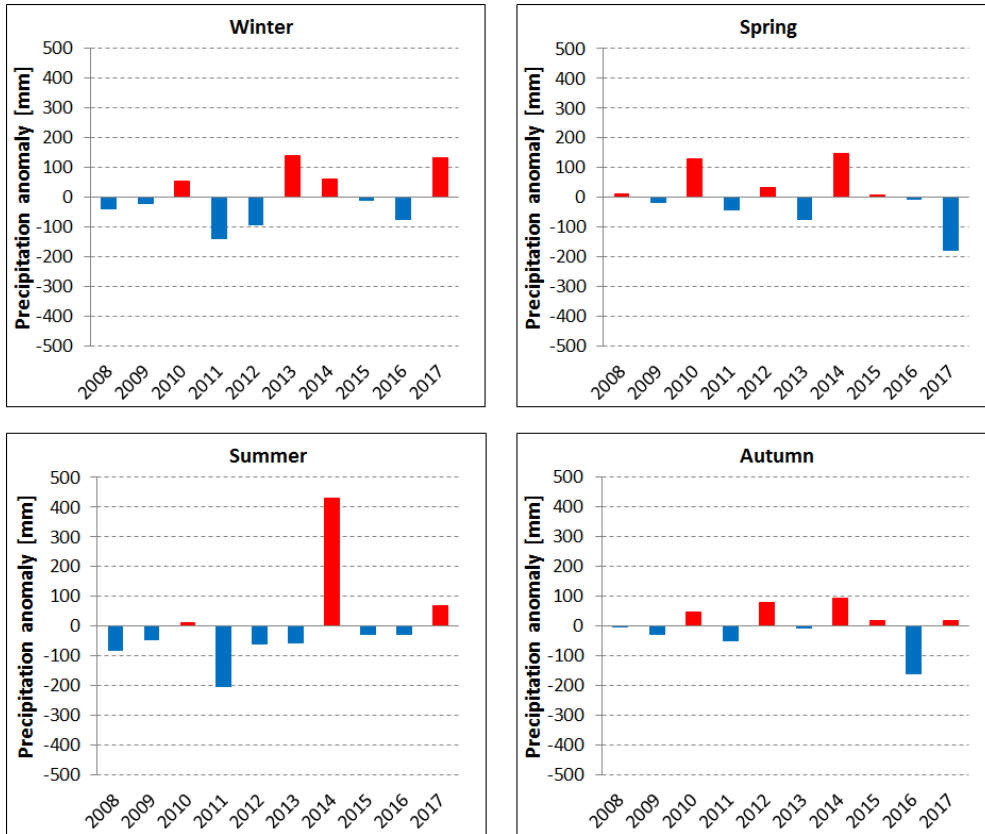


Figure 4.21: Seasonal anomalies of precipitation [mm], 2008-2017

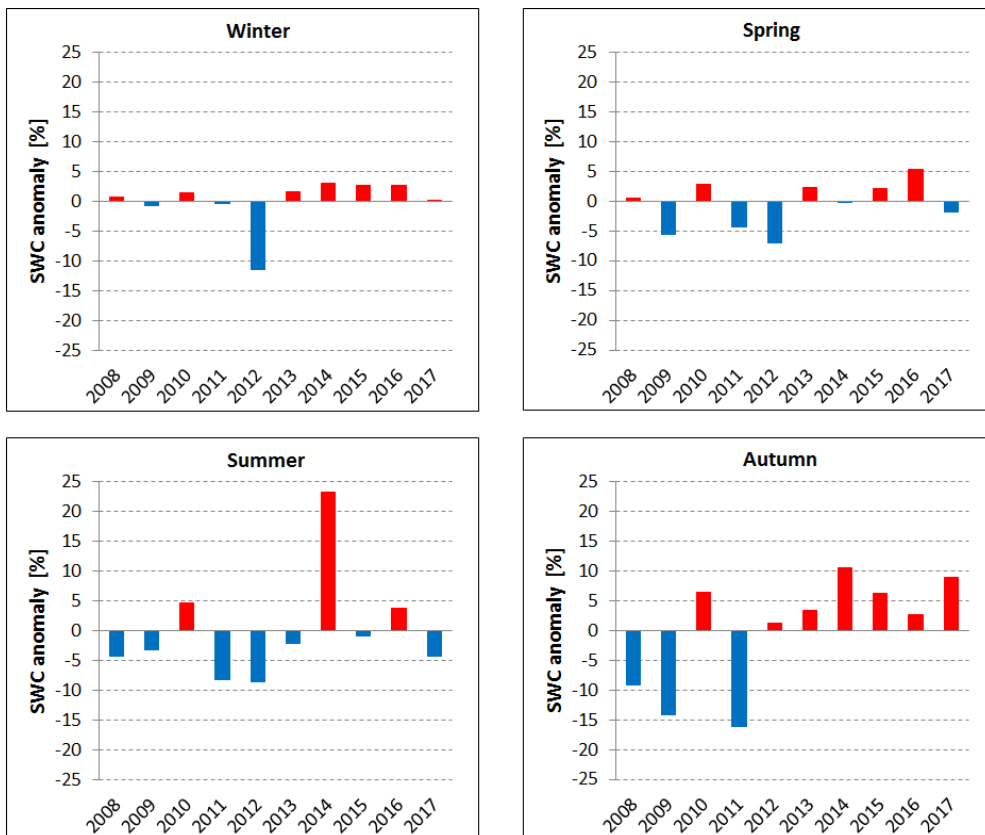


Figure 4.22: Seasonal anomalies of SWC [%], 2008-2017

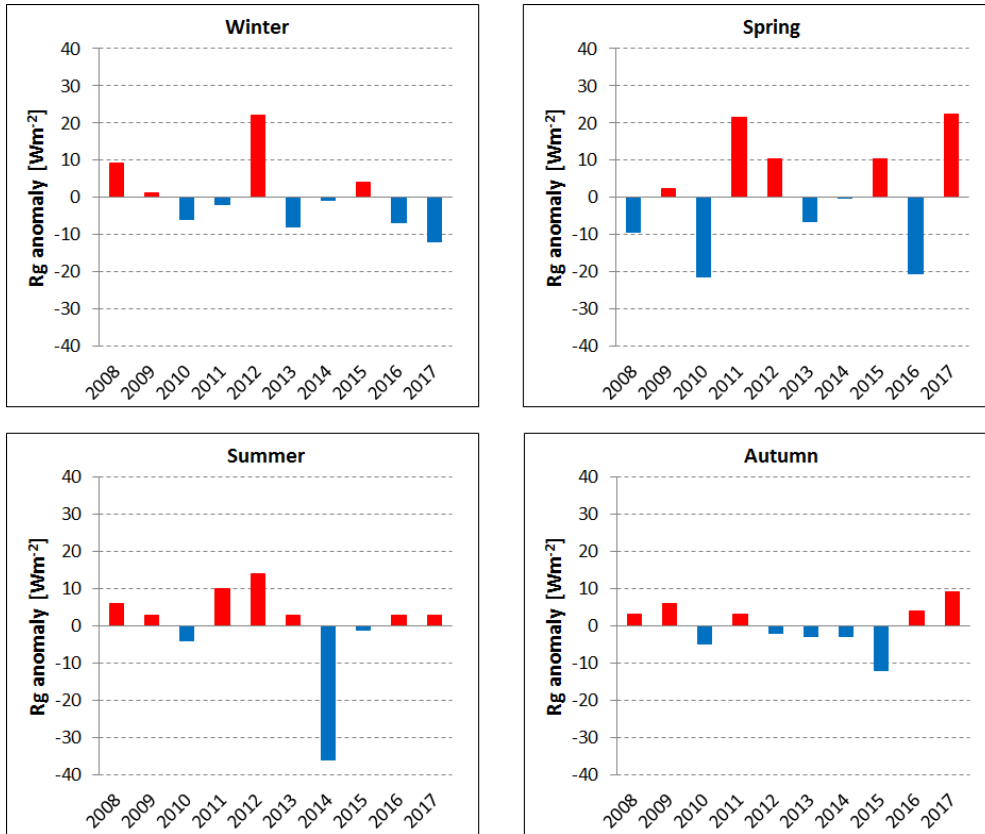


Figure 4.23: Seasonal anomalies of R_g [$W m^{-2}$], 2008-2017

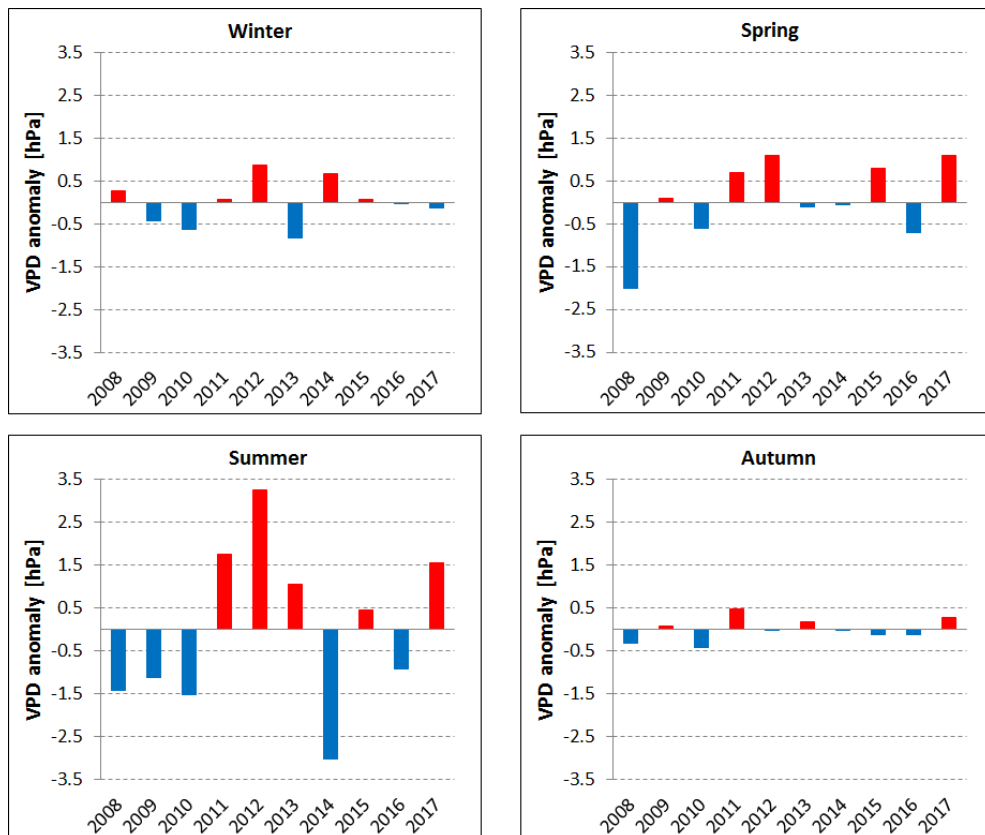


Figure 4.24: Seasonal anomalies of VPD [hPa], 2008-2017

Fig. 4.25 shows the cumulative curves of NEE per year while the vertical dashed black lines mark beginning of given seasons.

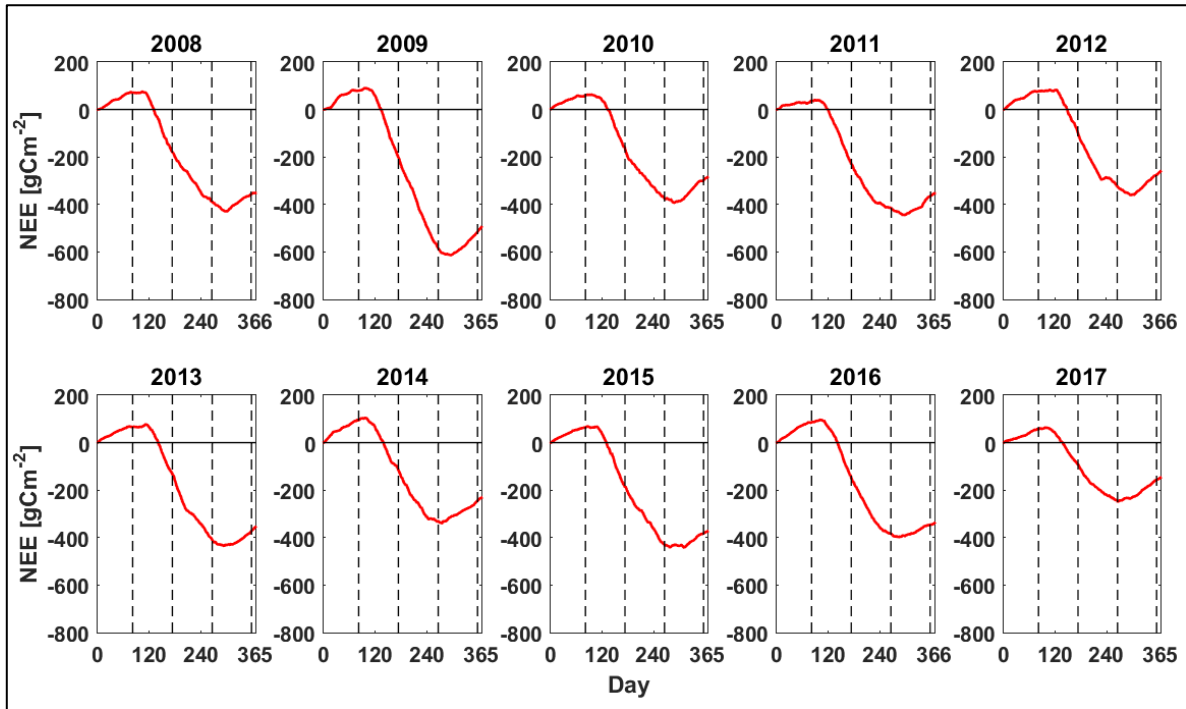


Figure 4.25: Cumulative curves of NEE for years 2008-2017; vertical black dashed lines mark beginnings of different seasons (winter, spring, summer and autumn)

The rapid increase of carbon uptake during spring of 2008 and 2010 was followed by the significantly slower evolution of carbon sink during summer of stated years (Fig. 4.25). The year 2008 had the longest growing season among investigated years that resulted with higher annual sums of NEE for that year. High summer GPP values in 2010 were balanced with high R_{ECO} values, resulting with lower summer NEE values in comparison to years 2009, 2013, 2015 and 2016 which also had high GPP during summer but lower R_{ECO} values. The result was that the summer values of NEE during those years were significantly higher than in 2010 (Fig. 4.26). Lower GPP values during the spring of 2008 and 2010 can be explained by the lower amount of radiated energy during the spring in those years (Fig. 4.23). Low R_{ECO} values during autumn and winter of 2008 resulted with lowest annual sums of R_{ECO} among investigated years. Due to favourable environmental conditions over almost the whole year, the year 2009 had the highest annual sums of NEE despite that the growing season of 2009 was for 14 days shorter than the growing season of 2008. Summer and spring values of GPP in 2009 were relatively high, while values of R_{ECO} during stated seasons were relatively low, especially during the summer of 2009 when R_{ECO} achieved lowest summer values among investigated years. Higher summer sums of GPP alongside with the lowest summer sums of

R_{ECO} in 2009 resulted with the largest magnitude of NEE summer sums among the investigated years. Pronounced drought occurred during the year 2011.

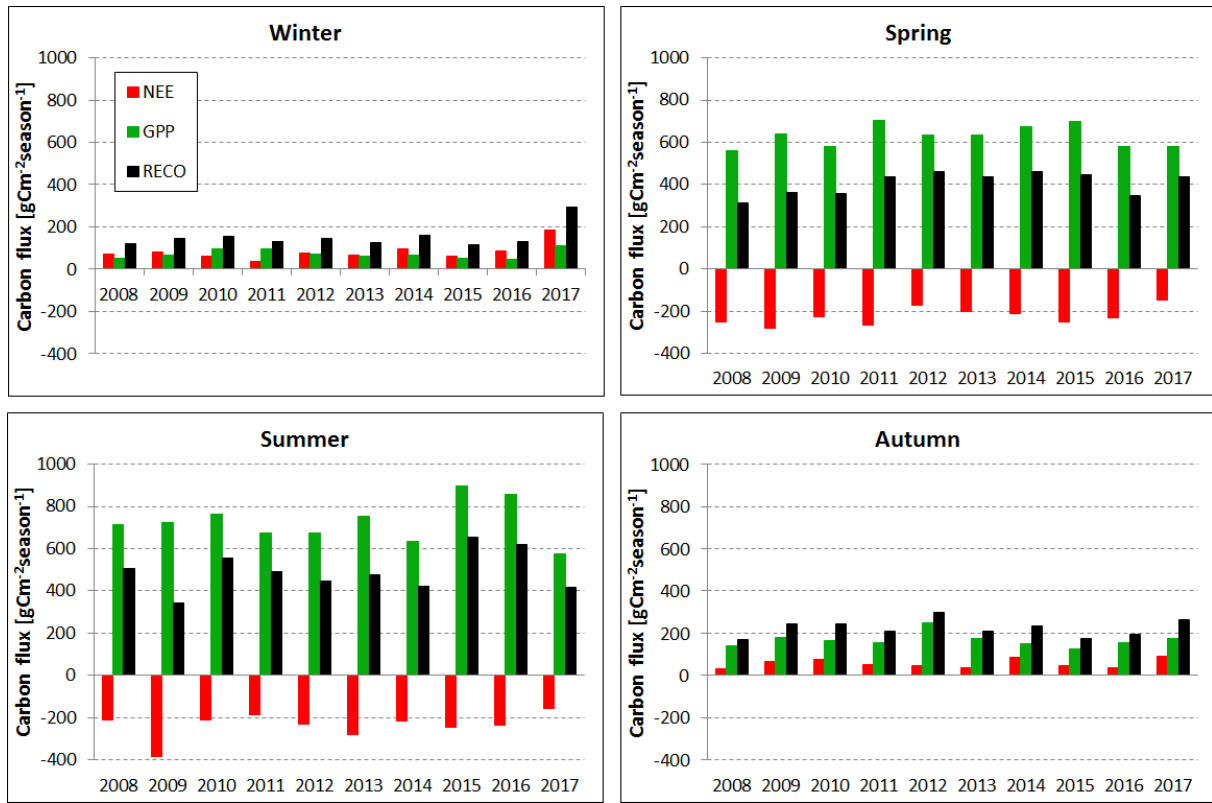


Figure 4.26: Seasonal sums of carbon fluxes NEE (red bars), GPP (green bars) and R_{ECO} (black bars)

Negative anomalies of precipitation were recorded in all four seasons of 2011 (Fig. 4.21). Significantly high negative anomalies of precipitation of -200 mm were recorded in summer of 2011. The low rate of precipitation continued during winter and summer of 2012 resulting with the drying of the soil. Anomalies of SWC were negative from winter of 2011 until autumn of 2012 (Fig. 4.22) confirming the existence of water stress (SWC close to wilting point value of ~20%). Despite large amount of radiated energy and higher temperatures, sums of GPP during summer of 2011 and 2012 were lower in comparison to summer of 2008, 2009, 2010, 2013, 2015 and 2016 which is probably due to higher values of VPD during summer months of 2011 and 2012 (Fig. 4.24), suggesting that the photosynthesis was probably restricted. Due to unfavourable conditions, carbon uptake in the year 2012 started significantly later than in other years in the investigation period. As a consequence, the 2012 had lowest spring sums of NEE among investigated years. Sums of R_{ECO} were high during the whole of vegetation season 2012, especially during spring and autumn, thus 2012 was a year with the highest annual sums of R_{ECO} . This can be probably explained with the higher air temperatures during spring and summer months of 2012. Due to the unfavourable conditions

in the second part of the summer of 2012, R_{ECO} was even larger than GPP resulting in the ecosystem starting to act as a source of carbon, as can be seen in Fig. 4.25. Similar situation but with lower magnitude occurred during the summer of 2011. The most likely reason for that was severe drought which occurred during the summer months of 2011 and 2012. High air and soil temperatures alongside with the lack of precipitation dried out the soil and restricted the photosynthesis thus reducing the carbon uptake. After the rainfall, carbon uptake continued until early autumn, but slower than in other investigated years. Soil water reserves were replenished during autumn of 2012 and winter of 2013. Warm winter of 2014 followed by early, warmer spring enabled the earlier start of carbon uptake. The situation changed in summer of 2014 which was the coldest summer during the measurement period. Comparatively low amount of radiated energy, along with heavy rainfall has negatively affected the rate of photosynthesis and resulted with a low summer sums of GPP in 2014. Also, because of heavy rainfall, the soil became saturated with water and as a result, the R_{ECO} was reduced. Due to unfavourable environmental conditions during summer, 2014 was a year with the shortest growing season and carbon uptake stopped earliest among the years in the investigated period resulting with a relatively small carbon sink in 2014. Due to the suitable environmental conditions, the carbon sink in 2015 was large. Lower spring sums of GPP in 2016 were probably caused by a lower amount of radiated energy during spring of that year. Despite that spring sums of NEE were high because spring sums of R_{ECO} were lower. Although 2016 was a year with the low rate of precipitation, the soil did not dry out as it did during 2011 and 2012. Lowest spring and summer sums of GPP were achieved during the year 2017. The most likely reason was high VPD values during the spring and summer of 2017. As a consequence spring and summer sums of NEE were small. So, weak carbon sink during vegetation season combined with relatively strong winter carbon source, which was caused by high R_{ECO} during winter months of 2017, resulted with low annual sums of NEE in 2017.

4.7 *NPP* estimated with biometric method (NPP_{BM})

Most important part of the stand production, at least from the perspective of timber production, comes from the formation of new xylem in tree stems and branches. In addition, coarse root increment, new foliage, fruits, fine root production as well as root exudates, volatile organic compounds and ground vegetation have to be taken into account when estimating *NPP* of a forest stand. While it is relatively easy to assess the contribution of a given tree species to the part of the *NPP* that is attributed to aboveground woody growth, the situation is much more complex for non-woody plant components. Therefore, we present only the results of the NPP_{WB} (total woody above- and below-ground biomass).

Results of NPP_{WB} measurements are presented in Table 4.10. Lowest annual NPP_{WB} of 299 gC m⁻² yr⁻¹, alongside with lowest annual values of NPP_{S+B} (Production of stem and branches) and NPP_{S+B+T} (production of stem, branches and twigs) of 227 gC m⁻² yr⁻¹ and 238 gC m⁻² yr⁻¹, respectively, were estimated in 2017. In 2010 highest annual values of NPP_{S+B} and NPP_{S+B+T} of 430 gC m⁻² yr⁻¹ and 451 gC m⁻² yr⁻¹ respectively were estimated. In the same year highest annual NPP_{WB} among investigated years of 567 gC m⁻² yr⁻¹ was recorded. Average NPP_{WB} over the study period was 484 ± 24 gC m⁻² yr⁻¹.

Table 4.10: Annual production of (mean \pm std.error): stem and branches (NPP_{S+B}), stem + branches + twigs (NPP_{S+B+T}), total woody above- and below-ground biomass – stem + branches + twigs + roots (NPP_{WB})

Year	NPP_{S+B} [gC m ⁻² yr ⁻¹]	NPP_{S+B+T} [gC m ⁻² yr ⁻¹]	NPP_{WB} [gC m ⁻² yr ⁻¹]
2008	387	406	511 \pm 20
2009	413	434	545 \pm 24
2010	430	451	567 \pm 24
2011	395	415	521 \pm 22
2012	351	368	463 \pm 28
2013	403	423	532 \pm 34
2014	359	377	474 \pm 25
2015	310	326	409 \pm 17
2016	393	413	519 \pm 26
2017	227	238	299 \pm 21
Average	367 \pm 18	385 \pm 19	484 \pm 24

Results of measurement of annual production of leaf litter (NPP_L) and tree fruits (NPP_F) in the stands which surround the EC tower are summarized in Table 4.11. A total number of installed littertraps in the period from 2008 to 2015 was 16. In 2016 a total of 23

new littertraps were added to existing 16, so in 2016 and 2017 total number of littertraps was 39. Data from littertraps that were damaged were discarded, hence a number of littertraps ($N_{littertraps}$) was always lower than 16 and 39. Littertraps were occasionally damaged by wild boars, presumably if acorns were present in them. For example, in 2015 which was rich with tree fruit, data from only 8 littertraps were taken for NPP_{LF} estimation.

Table 4.11: Annual production of leaf litter and tree fruits (mean \pm std. error) in the stands around the EC tower estimated using littertraps

Year	$N_{littertraps}$	NPP_L [gC m ⁻² yr ⁻¹]	NPP_F [gC m ⁻² yr ⁻¹]	NPP_{LF} [gC m ⁻² yr ⁻¹]
2008	14	163 \pm 20	1 \pm 0	164 \pm 20
2009	13	207 \pm 10	4 \pm 1	211 \pm 10
2010	13	206 \pm 15	9 \pm 4	215 \pm 16
2011	16	200 \pm 11	18 \pm 5	218 \pm 12
2012	13	166 \pm 8	1 \pm 0	167 \pm 8
2013	12	204 \pm 12	20 \pm 6	223 \pm 13
2014	11	174 \pm 8	6 \pm 2	180 \pm 9
2015	8	163 \pm 13	60 \pm 25	223 \pm 28
2016	35	166 \pm 5	4 \pm 1	170 \pm 5
2017	38	183 \pm 5	1 \pm 0	184 \pm 5
Average	15	183 \pm 23	12 \pm 17	195 \pm 20

Values of annual NPP_{LF} ranged from the lowest 164 \pm 20 gC m⁻² yr⁻¹ in 2008 to the highest 223 gC m⁻² yr⁻¹ recorded in both 2013 and 2015. Interestingly, the year 2015 was a year with the lowest annual production of leaves (163 \pm 13 gC m⁻² yr⁻¹), but because of very high annual production of tree fruit (60 \pm 25 gC m⁻² yr⁻¹), NPP_{LF} had the highest annual value among investigated years.

To obtain NPP_{BM} the NPP_{LF} was added to the NPP_{WB} . Total NPP_{BM} ranged from 483 \pm 34 gC m⁻² yr⁻¹ in year 2017 to 782 \pm 33 gC m⁻² yr⁻¹ in 2010 with the mean of 680 \pm 26 gC m⁻² yr⁻¹ during the period 2008-2017. Annual values of NPP_{BM} are presented in Table 4.12.

Table 4.12: Annual NPP_{BM} (mean \pm std. error) estimated in the stands around the EC tower using biometric method as a sum of NPP_{LF} and NPP_{WB}

Year	NPP_{LF} [gC m ⁻² yr ⁻¹]	NPP_{WB} [gC m ⁻² yr ⁻¹]	NPP_{BM} [gC m ⁻² yr ⁻¹]
2008	164 \pm 20	511 \pm 20	675 \pm 26
2009	211 \pm 10	545 \pm 24	756 \pm 33
2010	215 \pm 16	567 \pm 24	782 \pm 33
2011	218 \pm 12	521 \pm 22	739 \pm 32
2012	167 \pm 8	463 \pm 21	630 \pm 28
2013	223 \pm 13	532 \pm 34	755 \pm 49
2014	180 \pm 9	474 \pm 25	654 \pm 31
2015	223 \pm 28	409 \pm 17	632 \pm 26
2016	170 \pm 5	519 \pm 26	689 \pm 34
2017	184 \pm 5	299 \pm 21	483 \pm 34
Average	195 \pm 20	484 \pm 24	680 \pm 26

4.8 Comparison of NPP estimates from EC and BM measurements

To validate EC measurements, NPP estimated from EC measurement (NPP_{EC}) was compared with NPP estimated from biometric measurements (NPP_{BM}). Sums of NPP are shown in Table 4.13. Our results are in line with previous studies stating that only long-term monitoring of carbon fluxes can reveal correlation between biometric and EC estimates [Gough *et al.* 2008, Ohtsuka *et al.* 2009]. The comparison showed good overall agreement ($R^2=0.46$, Fig. 4.27), although EC estimates were higher in every year than the biometric one. There could be several plausible explanations. First of all, NPP_{EC} includes the production of whole ecosystem (trees, understory and ground vegetation) with all of its above- and belowground carbon pools, while NPP_{BM} (in our study) includes only the production of trees, excluding fine roots and grasses. Consequently, we can assume that higher NPP_{EC} is due to incomplete biometric estimate [Campioli *et al.* 2016] from which productions of fine roots and understory vegetation are missing. Production of fine roots and understory vegetation can be significant contributors to total NPP biometric estimate, ranging from 10% [Granier *et al.* 2008] and 28% [Ohtsuka *et al.* 2007] for fine roots or 45% for fine roots and understory vegetation together [Ohtsuka *et al.* 2007]. Furthermore, the fixed R_h/R_{ECO} ratio assumption is questionable, and probably not true [Subke *et al.* 2006, Bond-Lamberty *et al.* 2018], but we think that it is not fully unjustified. Namely, the forest in the footprint was thinned in 2006

and 2007 with average intensity of 8% by volume. Thinning residues constituted a one-time addition to the litter pool probably causing slight increase in R_h in several years following thinning. In addition, Bond-Lamberty *et al.* [2018] recently provided evidence that global R_h is rising due to shifts in soil organic carbon (SOC) forms and enhanced SOC mineralization driven by rising global temperatures. At the same time, according to Mori *et al.* [2010], continuous accumulation of living biomass during the study period should have resulted with an increase in R_a . Considering both studies [Bond-Lamberty *et al.* 2018, Mori *et al.* 2010], R_{ECO} should have exhibit an increase with time. At our site, R_{ECO} exhibited small, positive, but not statistically significant trend ($p=0.140$). All these facts do not point unanimously toward conclusion that there should be a significant trend in R_h/R_{ECO} during the study period. Therefore, in the absence of sufficient evidence, we considered that the use of the constant R_h/R_{ECO} ratio is the only justifiable approach. Nevertheless, further research at Jastrebarsko site is needed on the partitioning of the ecosystem respiration into autotrophic and heterotrophic in order to improve the estimates of NPP from eddy flux measurements.

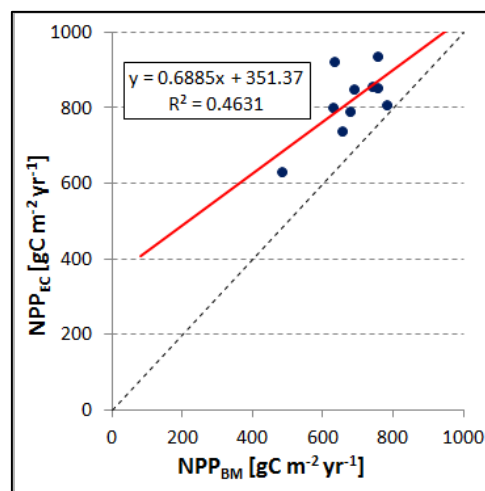
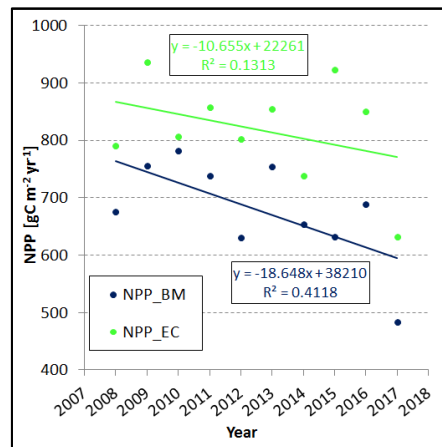


Figure 4.27: Comparison of NPP estimates from eddy covariance (NPP_{EC}) and biometric measurements (NPP_{BM}) at Jastrebarsko forest

When comparing trends of two NPP estimates, we can see that NPP_{BM} has a stronger negative trend ($-18.7\ gC\ m^{-2}\ yr^{-2}$) than NPP_{EC} ($-10.7\ gC\ m^{-2}\ yr^{-2}$) (Fig. 4.28). The probable cause of such trend in NPP could be the fact that the stands became denser and competition among trees for resources increased.

Table 4.13: Comparison of NPP_{EC} with NPP_{BM} for years 2008-2017

Year	NPP_{EC} [$gC\ m^{-2}\ yr^{-1}$]	NPP_{BM} [$gC\ m^{-2}\ yr^{-1}$]
2008	790	675 ± 26
2009	937	756 ± 33
2010	807	782 ± 33
2011	858	739 ± 32
2012	802	630 ± 28
2013	855	755 ± 49
2014	738	654 ± 31
2015	923	632 ± 26
2016	850	689 ± 34
2017	632	483 ± 34
Average	819 ± 23	680 ± 26
Overall sum	$8192\ gCm^{-2}\ (10\ yr)^{-1}$	$6795\ gCm^{-2}\ (10\ yr)^{-1}$

**Figure 4.28:** Negative trend of both NPP estimates (NPP_{EC} and NPP_{BM})

Analysis of seasonal dynamic of NPP (Fig. 4.29) reveals clear difference in seasonal NPP dynamics from two independent estimates, but before comparing seasonal dynamic of NPP it is important to recall processes which drive each estimate. NPP_{BM} estimate represents biomass growth which uses carbohydrates from current assimilation as well as previously stored NSC [Gaudinski *et al.* 2009, Delpierre *et al.* 2016, Palacio *et al.* 2018]. On the other hand, NPP_{EC} is primarily driven by canopy photosynthesis [Baldocchi 2003], therefore it reflects current accumulation of atmospheric carbon that can further be partitioned into structural growth and labile C storage [Gough *et al.* 2009]. This is visible on Fig. 4.29 during the spring when NPP_{BM} starts before NPP_{EC} on the account of carbon reserves stored in

previous years. Later in the vegetation season, stem growth slows down and even ceases, but forest ecosystem continued to absorb carbon, most likely in the NSC pool [Granier *et al.* 2008, Curtis *et al.* 2002]. NSC represent very important storage/reserve pool of carbon mostly used for spring growth [Delpierre *et al.* 2016, Palacio *et al.* 2018], but also important for overcoming unfavourable meteorological conditions, i.e. such as drought. To account for this carbon pool we used a simple modelling approach, assuming that this year NSC equals to this year leaf and fruit production and its seasonal dynamic is modelled with logistic function. NPP estimated in this way improved the agreement with NPP_{EC} (Fig. 4.29). Nevertheless, we are aware of the limitations of our approach due to the complexity of the NSC and wood formation dynamics [Delpierre *et al.* 2016, Begum *et al.* 2018]. Thus, further development of the used model is highly needed. Understanding and modelling of seasonal carbon allocation to reserve pool is still a matter of discussion [Dietze *et al.* 2014, Martínez-Vilalta 2014, Richardson *et al.* 2013].

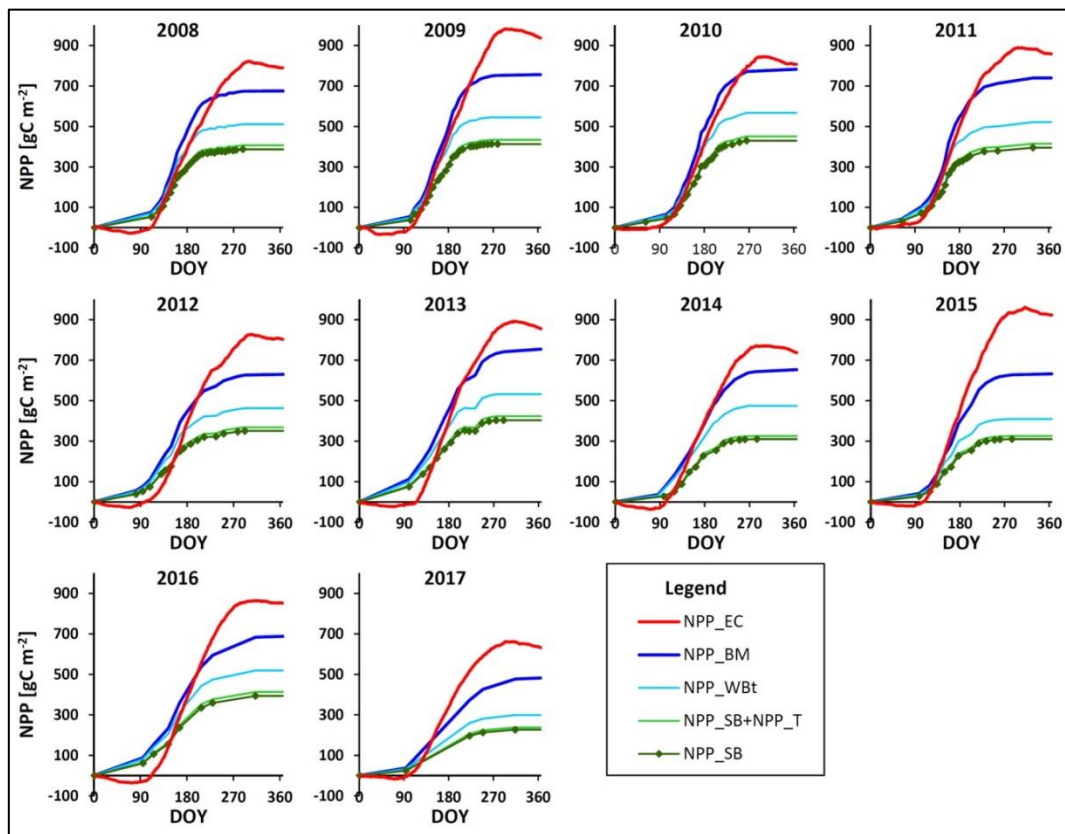


Figure 4.29: Comparison of cumulative NPP determined with EC technique and with biometric measurements in Jastrebarsko pedunculate oak forest for years 2008 until 2017 (NPP_{EC} – eddy covariance; NPP_{BM} – biometric method; NPP_{WBt} – total woody biomass including coarse roots; NPP_T – twigs; NPP_{SB} – stem and branches, points indicate DOY of dendrometer measurements)

Furthermore, it is hard to say which method is more accurate because both of them possess certain degree of uncertainty. Uncertainties related to the EC technique were described before. During early spring tree stems swell and grow, but the part corresponding to swelling should not be accounted for as increment. Opposite situation occurs during summer and droughts. In that case, trees tend to shrink so measured stem increment can be small and estimated *NPP* for these periods might be underestimated. All that, alongside with possible human error during stem and tree height measurements, are the main source of uncertainty for estimation of *NPP* with the biometric method.

Finally, comparison of models with field measurements has shown to be highly important as it quickly highlights the discrepancies in estimates and it serves as a good platform for productive discussion which can bring out a new understanding of underlying processes responsible for observed differences.

4.9 Comparison with other carbon flux estimates

The observed seasonal variability of carbon fluxes at Jastrebarsko forest shows a pattern typical for the temperate broadleaved forest in the northern hemisphere [Carrara *et al.* 2004, Wilkinson *et al.* 2012]. Annual sums of carbon fluxes are within the range of values for temperate deciduous broadleaved forests published in a recent review by Baldocchi *et al.* [2018] (Table 4.14). It should be also noted that *NPP* estimates are rather rare, as can be seen in Table 4.14, where only *NPP* for Hesse forest in France has been provided. One of the limiting factors in assessing *NPP_{EC}* is the need for the assessment of R_h . Such assessments are rare at the year-to-year scale, and R_h is usually calculated as a share in R_{ECO} which is modelled [Stoy *et al.* 2006]. The use of a fixed proportion of R_h in R_{ECO} enables the estimation of *NPP*, but at the same time implies that the ratio R_a/R_{ECO} is also fixed. In the case of Jastrebarsko forest it is 0.6081, which is smaller than the older forest at Hesse for which Granier *et al.* [2008] have reported the R_a/R_{ECO} of 0.722. Significantly higher *NEE* at Hainich site [Herbst *et al.* 2015], in comparison to Jastrebarsko site, might be related to the difference in forest structure. Hainich forest is characterised as an old-growth forest (up to 250 years), with highly diverse horizontal and vertical structure. Also, while average *GPPs* are similar, higher *NEE* at Hainich might be due to lower R_{ECO} as a result of significantly lower average air temperature at Hainich site (8°C) compared to Jastrebarsko (11.2°C). There are two sites (the UK and Duke Forests) where all fluxes are significantly higher than the ones observed at

Jastrebarsko site. The UK Straits Inclosure site [Wilkinson *et al.* 2012] is an 80-years old oak plantation in a climate that typically does not exhibit summer drought, which can contribute to the higher annual carbon accumulation than Jastrebarsko natural forest in a climate with hot and, comparatively, dry summers. Nevertheless, relatively large fluxes observed at the UK site are still interesting and more detailed comparison would be needed. On the other hand, higher fluxes observed at Duke Forest might not be directly comparable due to some differences in methodology, namely gap-filling and partitioning [Novick *et al.* 2015, Sulman *et al.* 2016]. The aim of this simple comparison with other sites is not to explain the reported differences in fluxes but to emphasize the multitude of possible issues and the very limited number of sites with long time-series that might help in explaining the observed differences.

Table 4.14: Carbon fluxes [$\text{gC m}^{-2} \text{yr}^{-1}$] in temperate deciduous broadleaved forests (average \pm standard deviation)

Country, Site	Genus	Meas. year	NEE	GPP	R_{ECO}	NPP	Reference
Denmark, Soroe	<i>Fagus</i>	1996-2009	-156 \pm 103	1727 \pm 136	1570 \pm 97		Pilegaard <i>et al.</i> [2011]
France, Hesse	<i>Fagus</i>	1995-2005	-386 \pm 171	1397 \pm 192	1011 \pm 138	674 \pm 84	Granier <i>et al.</i> [2008]
Germany, Hainich	<i>Fagus, Fraxinus</i>	2003-2012	-483 \pm 70	1498 \pm 83	1015 \pm 51		Herbst <i>et al.</i> [2015]
UK, Straits Inclosure	<i>Quercus</i>	1999-2010	-486 \pm 115	2034 \pm 228	1548 \pm 192		Wilkinson <i>et al.</i> [2012]
US, Harvard Forest	<i>Acer, Quercus</i>	1992-2004	-242 \pm 100	1400 \pm 164	1153 \pm 105		Urbanski <i>et al.</i> [2007]
US, Duke Forest	<i>Quercus, Carya</i>	2001-2008	-402 \pm 96	1982 \pm 300	1580 \pm 237		Novick <i>et al.</i> [2015]
Croatia, Jastrebarsko	<i>Quercus</i>	2008-2017	-319 \pm 94	1594 \pm 109	1275 \pm 94	819 \pm 89	This research

5. CONCLUSIONS

Micrometeorological eddy covariance experiment was implemented in young pedunculate oak stands to determine net ecosystem exchange of CO₂ between forest and overlying atmosphere. EC technique is far from perfect and strongly prone to errors which were minimized by careful application of all standard filtering procedures and corrections. Measurement instruments were installed at 23 m and later at 27 m high tower which is located approximately 6 km near the town of Jastrebarsko, Croatia. Footprint analysis showed that the contribution to the measured fluxes arriving from areas outside of the forest (i.e., agricultural areas, highway, and the town of Jastrebarsko with distances from EC tower of 1.2 km W, 2.4 km NW, and 5 km NW, respectively) is likely negligible. Measurements lasted 10 years, from 1st of January 2008 to 31st of December 2017. Over the study period, young pedunculate oak stands were total sink of carbon of $-3195 \text{ gC m}^{-2} (10\text{yr})^{-1}$, while the average value of net sink was $-319 \pm 30 \text{ gC m}^{-2} \text{ yr}^{-1}$. *NEE* showed high inter-annual variability. Highest carbon sink of $-496 \pm 15 \text{ gC m}^{-2} \text{ yr}^{-1}$ was measured in 2009, while the lowest sink of $-147 \pm 13 \text{ gC m}^{-2} \text{ yr}^{-1}$ was measured in 2017. Difference between year with highest and a year with the lowest sink of carbon was $349 \text{ gC m}^{-2} \text{ yr}^{-1}$. High inter-annual variability of *NEE* was driven by meteorological conditions and length of growing season.

NEE was partitioned to *GPP*, *RECO* and *NPP*. Observed seasonal variability of carbon fluxes at Jastrebarsko site showed pattern typical for the temperate broadleaved forest in the northern hemisphere. Annual sums of carbon fluxes at Jastrebarsko site are within the range of values for temperate deciduous broadleaved forests [Baldocchi *et al.* 2018]. To validate EC measurements, *NPP* estimated from EC measurements (*NPP_{EC}*) was compared with *NPP* estimated from biometric measurements (*NPP_{BM}*) which were performed on 24 circular plots which are lying in the footprint of the EC tower. Biometric measurements, combined with simple modelling approach on one side, and EC on the other, can provide two independent estimates of *NPP* that are comparable at the annual and within-seasonal scale. The use of simple theoretical model for the replenishment of carbon reserves in the late season greatly improved the seasonal agreement of *NPP_{BM}* and *NPP_{EC}* estimates. The comparison showed good overall agreement ($R^2=0.46$). *NPP_{EC}* was higher than *NPP_{BM}* in every year of measurement which indicates that *NPP* components which were not measured in this research (e.g. fine roots, grasses and understory bushes) significantly contribute to the ecosystem *NPP*. For better agreement *NPP* of fine roots and understory vegetation should be estimated and

added to NPP_{BM} . Furthermore, NPP_{EC} was estimated by using fixed ratio of heterotrophic to ecosystem respiration. Both NPP estimates showed negative trend over the study period. The probable cause of such trend in NPP could be the fact that the stands became denser and competition among trees for resources increased. NPP_{BM} had stronger and more statistically significant trend ($-18.7 \text{ gC m}^{-2} \text{ yr}^{-2}$, $p=0.046$) than NPP_{EC} ($-7.8 \text{ gC m}^{-2} \text{ yr}^{-2}$, $p = 0.290$). Further research is needed on the contribution to NPP of fine roots and understory vegetation, partitioning of the ecosystem respiration into autotrophic and heterotrophic, as well as on the non-structural carbohydrates dynamics.

6. EXTENDED ABSTRACT (in Croatian)

6.1 Uvod

Vodena para (H_2O) i ugljikov dioksid (CO_2) glavni su atmosferski sastojci koji kontroliraju klimu na Zemlji. Dok sadržaj vodene pare u atmosferi nije direktno pod utjecajem antropogene aktivnosti, količina CO_2 u atmosferi, koja je u konstantnom porastu od početka industrijske revolucije, direktno je uvjetovana antropogenom djelatnošću [npr. Schimel 1995]. Od ukupne antropogene emisije CO_2 40% ostaje u atmosferi, dok se preostali postotak emisije CO_2 pohranjuje u oceanima i kopnu [IPCC 2014]. Globalne šume, zajedno s tlom, predstavljaju značajan kopneni ponor ugljika [npr. Pan i sur. 2011]. Procesom fotosinteze šume uzimaju ugljik iz atmosfere te ga ugrađuju u nadzemnu i podzemnu biomasu čime djelomično ublažuju antropogenu emisiju CO_2 te na taj način sudjeluju u regulaciji klime [Janssens i sur. 2003]. Canadell i sur. [2007] procijenili su da su globalne šume u razdoblju od 2000. g. do 2006. g. bile globalni ponor ugljika u iznosu od $2.7 \text{ Pg C (6 god)}^{-1}$ što otprilike čini 30% ukupne antropogene emisije CO_2 u tom periodu. Moguće zasićenje [Nabuurs i sur. 2013], zajedno s klimatskim promjenama, doveli su u pitanje postojanost i snagu ponora ugljika u šumskim ekosustavima. Stoga je, praćenje produktivnosti globalnih šuma, kao i razumijevanje međugodišnje varijabilnosti godišnjih budžeta ugljika u globalnim šumama, postalo važan zadatak brojnih znanstvenika. Međugodišnja varijabilnost produktivnosti šuma rezultat je direktnog odziva drveća na meteorološke uvjete [Gough i sur. 2008], no također sadrži i odgođen odziv koji se često objašnjava postojanjem spremnika ugljika (nestrukturalni ugljikohidrati, NSC) kojeg drveće pohranjuje te ga koristi u nepovoljnim uvjetima [Carbone i sur. 2013, Teets i sur. 2018].

Razvitak mikrometeorološke metode kovarijance turbulentnih vrtloga (eng. *eddy covariance (EC) method*) omogućio je direktno mjerenje tokova ugljika između atmosfere i ekosustava, kao i drugih stakleničkih plinova, i izračun njihovih godišnjih budžeta na razini kompletnog ekosustava [npr. Baldocchi i sur. 2001, Aubinet i sur. 2012]. Tok ugljika određuje se EC metodom pomoću izravnih mjerenja koncentracije CO_2 i 3D komponenti brzine vjetra te označava neto izmjenu CO_2 (eng. *Net Ecosystem Exchange – NEE*). *NEE* je rezultat razlike dva glavna toka ugljika u ekosustavu – bruto primarne produkcije (eng. *Gross Primary Production – GPP*) i respiracije ekosustava (eng. *Ecosystem Respiration – RECO*).

GPP je glavni pozitivni tok ugljika u ekosustavu te označava količinu asimiliranog atmosferskog CO_2 procesom fotosinteze. Glavni negativni tok ugljika, *RECO*, predstavlja količinu ugljika koja je procesima respiracije otpuštena iz ekosustava te se dijeli na autotrofnu (*R_a*) i heterotrofnu (*R_h*) respiraciju. Oduzme li se *NEE* od heterotrofne respiracije, dobiti će se neto primarna produkcija (eng. *Net Primary Production – NPP*) ekosustava koja predstavlja količinu pohranjenog ugljika u biomasi ekosustava u određenom vremenu [Schulze 2005]. *NPP* uključuje produkciju nadzemne i podzemne drvene biomase (*NPP_{WBI}*), lista (*NPP_L*) i ploda (*NPP_{FR}*). Ukoliko je količina ugljika koji je asimiliran iz atmosfere veća od količine ugljika koji je otpušten iz ekosustava, ekosustav je ponor ugljika, dok u obrnutom slučaju ekosustav predstavlja izvor ugljika.

EC metoda je mikrometeorološka metoda za direktno mjerenje izmjene impulsa, mase i topline između ravne horizontalno-homogene površine i atmosfere [npr. Aubinet 2012]. U takvim uvjetima neto transport između površine i atmosfere je jedno-dimenzionalan pa se vertikalni tok može izračunati kovarijancom između turbulentnih fluktuacija vertikalne komponente vjetrova i skalarne varijable od interesa (jedn. 1.6). EC mjerenja se tipično vrše u površinskom sloju (eng. *surface layer*). Površinski sloj zauzima prvih 5-10% atmosferskog graničnog sloja. Atmosferski granični sloj najniži je dio troposfere te je pod direktnim termalnim i mehaničkim utjecajem Zemljine površine. Debljina mu varira od nekoliko metara u uvjetima snažne stabilne stratifikacije do otprilike 3 km u slučaju snažne nestabilne stratifikacije [npr. Stull 1988]. Dominantan mehanizam transporta u površinskom sloju je turbulencija koja se sastoji od mnoštva vrtloga različitih veličina od kojih svaki ima tri komponente brzine koje se mogu mjeriti pomoću EC sustava. Za mjerenje 3D brzine vjetrova koriste se ultrazvučni anemometri koji mogu mjeriti na frekvencijama od 10 Hz i više, dok se za mjerenje koncentracije CO_2 , kao i drugih stakleničkih plinova, u zraku koriste infra crveni plinski analizatori (IRGA). Mjerenja nisu savršena te su vrlo podložna pogreškama. Visokofrekventni podaci često sadrže podatke koji strše (eng. *spike*), konstantne, ne-fizičke vrijednosti i šum. Izvori loših podataka su instrumentalne poteškoće, problemi u električnom napajanju, životinjski utjecaj, te kiša, magla i snijeg. Takvi podaci trebaju biti detektirani te izbačeni prije računanja turbulentnih tokova kako bi izračunati tokovi bili visoke kvalitete. Detekcija i odbacivanje loših podataka vrši se kroz brojne procedure filtriranja. Najveći problemi nastaju tijekom mirnih noći kada je stabilni noćni sloj u potpunosti razvijen. U takvim uvjetima nema vertikalnog transporta jer je turbulencija slaba pa se zrak obogaćen CO_2 nakuplja u sloju ispod mjernih instrumenata. EC metoda u takvim slučajevima

podcjenjuje CO₂ tok što može dovesti do precjenjivanja *NEE*-a na godišnjoj razini jer se tijekom noći ekosustav ponaša kao izvor ugljika. Takvi tokovi također trebaju biti detektirani i izbačeni iz daljnje obrade. Kvarovi mjernog sustava, zajedno s odbačenim mjerenjima koja nisu prošla kontrolu kvalitete, stvaraju praznine u vremenskim nizovima koje se popunjavaju raznim metodama popunjavanja praznina (eng. *gap-filling methods*) [Falge i sur. 2001, Reichstein i sur. 2005]. EC metoda nije savršena te je prilikom njene primjene potrebno pažljivo provesti sve potrebne procedure filtriranja i korekcija. Obzirom da prednosti metode uvelike nadjačavaju njene mane, EC metoda je danas postala standardan alat za izmjeru tokova stakleničkih plinova [Burba 2013]. Sukladno tome, u ovom radu su tokovi ugljika izračunati EC metodom.

Nizinske šume hrasta lužnjaka spadaju u najproduktivnije ekosustave u Hrvatskoj te predstavljaju važan ekonomski resurs za državu. Iz tog je razloga, praćenje njihove produktivnosti te odziva na klimatske promjene značajno. U sklopu projekta CarbonPro, Hrvatski šumarski institut je u 2007. g. montirao mjernu stanicu u mladoj sastojini hrasta lužnjaka (*Quercus robur* L.) kojom od tada provode EC i meteorološka mjerenja. Cilj ovog rada je: (1) odrediti *NEE* ugljikovog dioksida između sastojine hrasta lužnjaka i atmosfere na temelju desetogodišnjih mjerenja (2008-2017.); (2) ispitati uzroke dugoročne i kratkoročne varijabilnosti tokova ugljika; (3) ispitati utjecaj vremenskih ekstrema kao što su poplave i suše na tokove ugljika; (4) odrediti *NPP* na temelju desetogodišnjih biometrijskih izmjera i usporediti ga s EC procjenom *NPP*-a.

6.2 Područje istraživanja i materijali

Istraživanje je provedeno u mladim (~35-44 godina starim) sastojinama hrasta lužnjaka koje su dio 13600 ha velikog šumskog kompleksa bazena rijeke Kupe (sl. 2.1). Na EC tornju, koji je visok 27 m (od 2011. godine, u početku je bio visok 23 m) montirani su ultrazvučni anemometar i IRGA otvorenog tipa koji mjere na frekvenciji od 20 Hz, te ostali senzori kojima se mjere meteorološke varijable. Na udaljenosti od otprilike 2 km jugozapadno od EC tornja postavljena je pomoćna manja meteorološka stanica čija mjerenja su korištena za popunjavanje praznina u meteorološkim mjerenjima s EC tornja. Tijekom zimskih mjeseci 2007. i 2008. godine mreža od 65 trajnih kružnih ploha postavljena je u okolini EC tornja. Nakon preliminarnе analize područja otiska toka (eng. *footprint area*), na 24 plohe koje su imale najveću vjerojatnost da će biti u dosegu EC tornja, instalirani su dendrometri (sl. 2.6) na

stabla čiji je prsni promjer bio veći od 7.5 cm i to prema metodologiji opisanoj u radu Keelanda i Younga [2004]. Tijekom vegetacijske sezone, na tjednoj ili dvotjednoj bazi, provođena su mjerenja kumulativnog prirasta na dendrometrima. Osim toga, na kraju svake vegetacijske sezone izmjerene su visine i prsni promjeri svakog označenog stabla. Skupljan je i šumski otpad (grančice, plodovi, lišće) iz košara (45 cm u promjeru) nekoliko puta tokom i na kraju vegetacijske sezone. Spomenuta biometrijska izmjera poslužila je za izračun *NPP*-a biometrijskom metodom.

6.3 Metodologija

6.3.1 Tretiranje sirovih podataka

EC sirovi podaci spremeni su u jednosatne binarne datoteke. Prije obrade podataka napravljena je kontrola kvalitete sirovih podataka te su iz daljnje obrade izbačene sve jednosatne binarne datoteke unutar kojih mjerenja nisu zadovoljila kontrolu kvalitete.

6.3.2 Izračun tokova ugljika EC metodom

Za izračun tokova CO₂ korišten je računalni program otvorenog tipa EdiRe koji sadrži sve standardne korekcije koje su potrebite kako bi izračunati tokovi bili visokokvalitetni. Tokovi su izračunati prema EUROFLUX metodologiji [Aubinet i sur. 2000, 2012]. Prvi korak u izračunu tokova CO₂ EC metodom jest čišćenje visokofrekventnih podataka od šuma, podataka koji strše te konstantnih i ne fizikalnih vrijednosti. Ta procedura je izgadila vremenske nizove te izbacila sve loše podatke koji su eventualno prošli preliminarnu kontrolu podataka. Novonastale praznine popunjene su linearnom interpolacijom susjednih vrijednosti. Obzirom da su senzori za mjerenje koncentracije CO₂ i brzine vjetra udaljeni, izmjera u istom trenutku nije moguća, pa nastaje kratko kašnjenje jer je zraku potrebno određeno vrijeme da prođe udaljenost između ta dva senzora što dovodi do toga da se dio toka gubi. Kako do toga ne bi došlo, izvršena je procedura uklanjanja vremena kašnjenja [Lee i sur. 1994]. Ultrazvučni anemometar nemoguće je savršeno poravnati na način da vertikalna os *z* bude okomita na srednji tok, tj. na strujnice srednjeg vjetra. Kao posljedica neporavnatog anemometra javlja se kontaminacija vertikalne komponente vjetra horizontalnim komponentama što dovodi do velikih pogrešaka u mjerenju tokova. Problem je riješen primjenom metoda planarnog uklapanja (eng. *planar fit*) [Wilczak i sur. 2001]. Tok CO₂ je izračunat kovariancom fluktuacija vertikalne komponente brzine vjetra i koncentracije CO₂ (jedn. 3.23). Vrijednosti

su spremljene kao polusatni srednjaci. EC mjerni sustav uklanja i nisko- i visoko frekventne komponente signala. Nisko-frekventni gubitci rezultat su ograničenja mjernih instrumenata koji ne dopuštaju uzorkovanje cijelih turbulentnih fluktuacija pa period usrednjavanja može biti prekratak da obuhvati sve relevantne niske frekvencije. S druge strane, visoko frekventni gubitci nastaju npr. uslijed separacije senzora, te neadekvatnog frekventnog odziva mjernog instrumenta. [Aubinet i sur. 2012]. Ti gubitci su u mjernim sustavima otvorenog tipa obično mali i iznose 5-10% ukupnog toka. Kako bi se taj gubitak kompenzirao izračunate su funkcije prijenosa koje opisuju gubitke na svakoj frekvenciji. Izračunat je korekcijski faktor koji se pomnoži s tokom kako bi se dobio korigirani tok. Na kraju, da bi se kompenzirale fluktuacije u gustoći CO₂ i vodene pare koje su rezultat fluktuacija temperature i vodene pare a koje nisu reprezentativne za mjereni tok, provedena je WPL (Webb, Pearmann i Leuning) korekcija. Nadalje, obzirom da EC metoda zahtjeva stacionarnost procesa, proveden je test stacionarnosti te su svi polusatni tokovi koji nisu prošli test izbačeni iz daljnje obrade. Kako bi odredili *NEE*, izračunatom toku CO₂ trebalo je dodati član uslijed promjene zalihe ugljika u sloju zraka ispod IRGA uređaja (eng. *CO₂ flux storage term*). Tok zbog promjene zalihe izračunate na temelju mjerenja vertikalnog profila koncentracija CO₂ na šest visina (1, 2, 4, 8, 16, 23 m tj. 27 m) posebnim sustavom, odnosno korištenjem koncentracija izmjerenih pomoću IRGA uređaja (jedn. 3.42) u slučaju da su mjerenja profila koncentracija zakazala.

Izračunati tokovi iz EdiRe-a još su jednom podvrgnuti testovima kako bi na kraju ostali isključivo visokokvalitetni tokovi. Najprije je napravljen test apsolutnih granica te su svi tokovi koji nisu bili unutar definiranih granica izbačeni. Nakon toga provedena je procedura sekundarnog uklanjanja podataka koji strše u vremenskim nizovima *NEE*-a prema radu Papale i sur. [2006]. Potom je provedeno u_* filtriranje kojim su izbačeni svi loši tokovi nastali tijekom statički stabilnih noći.

Kvarovi mjernog sustava, zajedno s filtriranjima koja su izbacila mnoštvo podataka, rezultirali su velikim brojem praznina u vremenskim nizovima *NEE*-a. Kako bi odredili godišnje sume *NEE*-a praznine su popunjene standardnom metodom popunjavanja praznina (MDS – *Marginal Distribution Sampling*) koju su predstavili Reichstein i sur. [2005] a koja je dostupna kao mrežni (eng. *online*) alat. Metoda je pokazala konzistentno dobar učinak te se danas standardno koristi prilikom obrade EC podataka pa je tako korištena i u ovome radu. Isti mrežni alat iskorišten je za raspodjelu (engl. *partitioning*) *NEE* toka u *GPP* i *RECO*. Respiracija je određena kao funkcija temperature zraka eksponencijalnim regresijskim

modelom [Lloyd i Taylor 1994] iz noćnih podataka (jedn. 3.47), dok je GPP izračunat prema (jedn. 3.48).

6.3.3 Izračun neto primarne produkcije EC metodom (NPP_{EC})

Da bi odredili NPP EC metodom, R_{ECO} je razdijeljena u autotrofnu (R_a) i heterotrofnu respiraciju (R_h), a NPP_{EC} je određen oduzimanjem NEE -a od heterotrofne respiracije (jedn. 3.49).

6.3.4 Izračun neto primarne produkcije biometrijskom metodom (NPP_{BM})

NPP_{BM} je određen zbrojem neto produkcije ukupne drvne biomase (NPP_{WBi}) te neto produkcije lišća (NPP_L) i plodova (NPP_{FR}). Produkcija debla je izračunata iz mjerenja prirasta na dendrometrima. Nakon što je iz mjerenja određen promjer na prsnoj razini za svaki termin mjerenja, Schumacher Hall-ovom jednadžbom [Schumacher i Hall 1933] izračunat je volumen debla i grana do 3 cm promjera. Pretpostavljeno je da volumen sitnih grančica iznosi 5% volumena debla [Balboa-Murias i sur. 2006] te je dodan volumenu debla. Volumen korijenja izračunat je množenjem volumena debla i sitnih grančica s omjerom podzemnog i nadzemnog dijela stabla (engl. *root-to-shoot ratio*) koji je iznosio 0.257. Omjer podzemno/nadzemno izračunat je kao srednja vrijednost omjera za sastojine s hrastom lužnjakom objavljenih u Cairns i sur. [1997]. Volumen korijena dodan je volumenu debla i sitnih grančica, te je taj ukupni volumen pretvoren u biomasu korištenjem specifičnih drvnih gustoća za svaku vrstu drveća posebno [Šumarska enciklopedija 1959]. Biomasa je zatim preračunata u masu ugljika množenjem s faktorom 0.5 [IPCC 2003, IPCC 2006]. Ukupni NPP_{WBi} izračunat je kao srednja vrijednost od svih NPP_{WBi} na 24 plohe. Prikupljeni šumski otpad iz košara razvrstan je na lišće, grančice i plodove. Uzorci su osušeni i izvagani te je masa suhe biomase pomnožena s faktorom 0.5 kako bi se odredio NPP lista i ploda. Na kraju su NPP_L i NPP_{FR} zbrojeni te dodani NPP_{WBi} -u kako bi se odredio NPP_{BM} . Unutar-sezonska dinamika NPP_{BM} -a aproksimirana je logističkom funkcijom (jedn. 3.70).

6.4 Rezultati i diskusija

6.4.1 Meteorološki uvjeti u periodu 2008-2017

Srednja temperatura zraka tijekom 10 godina mjerenja iznosila je 11.24 °C što je za 0.62 °C više od tridesetogodišnjeg (1981-2010.) prosjeka od 10.62 °C [podaci od Državnog

hidrometeorološkog zavoda za postaju Jastrebarsko]. 2010. godina, s prosječnom temperaturom zraka od 10.22 °C, je bila jedina godina s prosječnom temperaturom zraka nižom od tridesetogodišnjeg prosjeka. Prosječna godišnja oborina tijekom perioda istraživanja iznosila 1058 mm. Glavnina oborine pala je u ljetnim mjesecima i ranu jesen. 2011. godina, s ukupnom godišnjom oborinom od 576 mm, je bila najsuša godina, dok je 2014. godina bila najkišovitija, s ukupnom godišnjom oborinom od 1727 mm. Štoviše, ukupna oborina tijekom vegetacijske sezone 2014. je premašila čak i tridesetogodišnji prosjek za godišnju oborinu od 962 mm. To je značajno utjecalo na sadržaj vode u tlu (SWC) koji je gotovo tijekom cijele 2014-te, bio blizu zasićenja (60%) (sl. 4.3). Valja ukazati i na tri epizode suše koje su se dogodile tijekom ljetnih mjeseci u 2011. i 2012. godini, te u proljeće 2017-te godine.

6.4.2 Neto izmjena CO₂ - *NEE*

NEE ugljikovog dioksida je pokazao jasan godišnjih hod (sl. 4.12). Tijekom sezone mirovanja dnevne vrijednosti *NEE*-a su bile minimalne i kretale su se oko nule. Ekosustav je u tom periodu bio izvor ugljika što ukazuje na aktivnu respiraciju čak i tijekom hladnih zimskih mjeseci. Nadalje, tijekom zimskih mjeseci mogle su se uočiti nešto veće negativne vrijednosti *NEE*-a koje se vjerojatno posljedica fotosinteze trava i manjih zimzelenih grmova. U rano proljeće, razvitkom trave i ranog lišća, počela je asimilacija ugljika iz atmosfere što se očitovalo naglim rastom magnitude *NEE*-a koji je bio izrazito snažan u svibnju, a vrhunac postigao u lipnju. Uočeni su i dani tijekom kojih je u jeku vegetacijske sezone ekosustav bio izvor ugljika što ukazuje na to da je respiracija bila snažnija od asimilacije ugljika, a najvjerojatniji razlog za to su nepovoljni vremenski uvjeti (razmjerno niska razina svjetlosti ili suša te visoka temperatura, posebice tla). U jesen je slabljenje *NEE*-a pratilo postupno žućenje i naposljetku odbacivanje lista.

Na dnevnoj bazi, asimilacija ugljika iz atmosfere počela je ubrzo nakon izlaska sunca te je maksimum postizala oko podneva. Nakon zalaska sunca asimilacija je prestala te je ekosustav postao izvor ugljika uslijed kontinuirane respiracije. Srednja dnevna varijacija *NEE*-a po mjesecima prikazana je na sl. 4.11.

Mlada sastojina hrasta lužnjaka je u periodu 2008-2017 bila ukupni ponor ugljika u iznosu od $-3195 \text{ gC m}^{-2} (10\text{god})^{-1}$. *NEE* ugljikovog dioksida je pokazala izrazitu međugodišnju varijabilnost te je bila uvjetovana meteorološkim uvjetima kao i trajanjem vegetacijske sezone. Najviše godišnje sume *NEE*-a od $-496 \pm 15 \text{ gC m}^{-2} \text{ god}^{-1}$ postignute su u 2009. godini, dok su najniže ($-147 \pm 11 \text{ gC m}^{-2} \text{ god}^{-1}$) postignute u 2017. godini (tablica 4.4).

Srednja vrijednost ponora ugljika tijekom proučavanog desetogodišnjeg perioda iznosila je $-319 \pm 30 \text{ gC m}^{-2} \text{ god}^{-1}$. Analiza otiska toka, tj. područja koje obuhvaća izvore i ponore koji daju najznačajniji doprinos mjerenom toku, isključila je obližnja industrijska postrojenja u Jastrebarskom kao i autoput Zagreb - Rijeka kao antropogene doprinose mjerenom toku. Također, analiza otiska toka je pokazala da je usporedba biometrijskih mjerenja s EC mjerenjima opravdana jer se sve 24 plohe na kojima su se obavljala biometrijska izmjere nalaze unutar 90% otiska toka (sl. 4.8).

6.4.3 Razdijeljeni tokovi ugljika GPP , R_{ECO} i NPP

Neto izmjena CO_2 razdijeljena je u dva glavna toka ugljika u šumskim ekosustavima, GPP i R_{ECO} . NPP je određen kao razlika između heterotrofne respiracije i NEE -a. Tokovi ugljika u mladoj sastojini hrasta lužnjaka pokazali su jasnu sezonsku varijabilnost koja je tipična za umjerene listopadne šume sjeverne hemisfere [Carrara i sur. 2004]. Tijekom sezone mirovanja dnevne vrijednosti GPP -a kretale su se blizu nule (sl. 4.15). U rano proljeće, s razvitkom lista, dnevne vrijednosti GPP -a naglo su porasle, a najviše vrijednosti postignute su u lipnju. Nakon vrhunca u rano ljeto GPP je polako počeo opadati te se ponovno spustio na vrijednosti oko nule nakon što je lišće otpalo. Najviše dnevne vrijednosti R_{ECO} -a postignute su tijekom ljetnih mjeseci (sl. 4.13), a tijekom zime R_{ECO} je imao najniže vrijednosti. U jesen su se mogli uočiti sekundarni vrhunci koji su najvjerojatnije rezultat pojačanog razlaganja uslijed svježeg otpalog lista. Godišnji hod NPP_{EC} -a je slijedio godišnji tok GPP -a (sl. 4.17). Tijekom hladnog dijela godine vrijednosti NPP_{EC} su često bile negativne što ukazuje na to da je autotrofna respiracija premašivala GPP . Usporedba s izmjerama u drugim šumama sjeverne hemisfere pokazala je dobro slaganje, te se izmjerene godišnje vrijednosti tokova ugljika nalaze unutar okvira rezultata objavljenim u drugim radovima (Tablica 4.14).

6.4 Usporedba EC mjerenja s biometrijskim mjerenjima

Na kraju rada uspoređena je izmjera neto produkcije šume EC metodom (NPP_{EC}) s biometrijskom metodom (NPP_{BM}). Usporedba je pokazala dobro slaganje u rezultatima ($R^2=0.46$, sl. 4.27). Godišnje sume NPP_{EC} su u svim godinama (Tablica 4.13). bile više od godišnjih suma NPP_{BM} . Razlog tome najvjerojatnije leži u činjenici da NPP izmjeren EC metodom predstavlja NPP cijelog ekosustava, dok NPP_{BM} predstavlja samo produkciju drveća te ne uključuje produkciju trava, manjih grmova i sitnog korijenja. Prema tome, razlika

između dvije izmjere NPP -a najvjerojatnije je nastala zbog neizmjerene produkcije trava, grmova i sitnog korijenja. Drugi mogući izvor neslaganja je razdjeljivanje respiracije pri čemu je heterotrofna respiracija izračunata kao fiksni postotak ukupne respiracije ekosustava ($R_h=0.3919 \cdot R_{ECO}$). U tom slučaju autotrofna respiracija iznosila je $R_a=0.6081 \cdot R_{ECO}$. Autotrofna respiracija uvelike ovisi i o specifikacijama područja istraživanja, a neki autori predlažu da bi autotrofna respiracija trebala ovisiti o biomasi [Mori i sur. 2010]. Obje izmjere pokazale su negativan trend NPP -a (sl. 4.28). NPP_{BM} je pokazao jači negativni trend ($-18.7 \text{ gC m}^{-2} \text{ god}^{-1}$) u odnosu na NPP_{EC} ($-10.7 \text{ gC m}^{-2} \text{ god}^{-1}$). Za bolje slaganje tih dviju nezavisnih izmjere potrebno je pronaći bolji način kojim bi se ukupna respiracija ekosustava razdijelila na heterotrofni i autotrofni dio. Analiza sezonske dinamike NPP -a (sl. 4.29) pokazala je jasne razlike u sezonskom kretanju NPP .

6.5 Zaključak

U radu je obavljen opsežan pregled mjerenja tokova CO_2 u mladoj sastojini hrasta lužnjaka. Rezultati su pokazali da je varijabilnost tokova ugljika usko povezana s okolišnim pokretačima. Drugi uzrok varijabilnosti tokova ugljika bilo je trajanje vegetacijske sezone. Mlada sastojina hrasta lužnjaka bila je u periodu 2008-2017. prosječni ponor ugljika od $-319 \pm 30 \text{ gC m}^{-2} \text{ god}^{-1}$. Izmjereni NEE razdijeljen je u R_{ECO} , GPP i NPP . Izmjera NPP -a EC metodom validirana je NPP -om određenim iz biometrijskih mjerenja. Obje metode pokazale su negativan trend NPP -a koji je u slučaju biometrijske izmjere bio izraženiji. Usporedba rezultata dobivenih EC i biometrijskim mjerenjima pokazala je dobro slaganje ($R^2=0.46$). Bolje slaganje može se očekivati ukoliko se biometrijskoj izmjeri NPP -a pridoda NPP trave, grmova i sitnog korijenja koji u ovom radu nisu mjereni, te ukoliko se nađe bolji način kojim bi se ukupna respiracija ekosustava razdijelila na heterotrofni i autotrofni dio.

REFERENCES

- Anthoni P.; Law B.E.; Unsworth M.H. Carbon and water vapor exchange of an open-canopied ponderosa pine ecosystem. *Agric. For. Meteorol.*, **1999**, *95*, 151-168
- Aubinet M.; Grelle A.; Ibrom A.; Rannik Ü.; Moncrieff J.; Foken T.; Kowalski A.S.; Martin P.H.; Berbigier P.; Bernhofer C. *et al.* Estimates of the annual net carbon and water exchange of European forests: the EUROFLUX methodology. *Adv. Ecol. Res.*, **2000**, *30*, 113-175
- Aubinet M.; Feigenwinter C.; Heinsech B.; Bernhofer C.; Canepa E.; Lindroth A.; Montagnani L.; Rebmann C.; Sedlak P.; Van Gorsel E. Direct advection measurements do not help to solve the night-time CO₂ closure problem: Evidence from three different forests, *Agric. For. Meteorol.*, **2010**, *150*, 655-664
- Aubinet, M.; Vesala, T.; Papale, D. Eddy covariance: a practical guide to measurement and data analysis. **2012**, Springer, Dordrecht, Berlin, Heidelberg, New York, 451 pp
- Babić, K. Low-level turbulence characteristics over inhomogeneous surface during wintertime. **2016**, Doctoral thesis, Faculty of Science, University of Zagreb, 147 pp
- Balboa-Murias, M.A.; Rojo, A.; Alvarez, J.G.; Merino A. Carbon and nutrient stocks in mature *Quercus Robur* L. stands in NW Spain. *Ann. For. Sci.* **2006**, *63*, 557-565
- Baldocchi D.; Falge E.; Gu L.; Olson R.; Hollinger D.; Running S.; Anthoni P.; Bernhofer C.; Davis K.; Evans R. *et al.* FLUXNET: a new tool to study the temporal and spatial variability of ecosystem-scale carbon dioxide, water vapor, and energy flux densities. *Bull. Am. Meteorol. Soc.*, **2001**, *82*, 2415-2434
- Baldocchi D. Assessing the eddy covariance technique for evaluating carbon dioxide exchange rates of ecosystems: past, present and future. *Glob. Change. Biol.* **2003**, *9*, 1-14
- Baldocchi, D.; Chu, H.; Reichstein, M. Inter-annual variability of net and gross ecosystem carbon fluxes: A review. *Agric. For. Meteorol.* **2018**, *249*, 520-533
- Barcza Z. Long term atmosphere/biosphere exchange of CO₂ in Hungary. **2001**, Doctoral dissertation, 115 pp

- Begum, S.; Kudo, K.; Rahman, M.H.; Nakaba, S.; Yamagishi, Y.; Nabeshima, E.; Nugroho, W.D.; Oribe, Y.; Kitin, P.; Jin, H.O., et al. Climate change and the regulation of wood formation in trees by temperature. *Trees-Struct. Funct.* **2018**, *32*, 3-15.
- Bond-Lamberty, B.; Bailey, V.L.; Chen, M.; Gough, C.M.; Vargas, R. Globally rising soil heterotrophic respiration over recent decades. *Nature* **2018**, *560*, 80-83
- Burba G., McDermitt D.K., Grelle A., Anderson D.J., Xu L. Addressing the influence of instrument surface heat exchange on the measurements of CO₂ flux from open-path gas analyzers. *Glob. Change. Biol.* **2008**, *14*, 1854-1876
- Burba G. Eddy Covariance Method for Scientific, Industrial, Agricultural and Regulatory Applications, **2013**, LI-COR Biosciences, 329 pp
- Cairns M.A., Brown S., Helmer E.H., Baumgardner G.A. Root biomass allocation in the world's upland forests. *Oecologia* **1997**, *111*, 1-11
- Campioli, M.; Malhi, Y.; Vicca, S.; Luysaert, S.; Papale, D.; Penuelas, J.; Reichstein, M.; Migliavacca, M.; Arain, M.A.; Janssens, I.A. Evaluating the convergence between eddy-covariance and biometric methods for assessing carbon budgets of forests. *Nat. Commun.* **2016**, *7*
- Canadell, J.G.; Le Quere, C.; Raupach, M.R.; Field, C.B.; Buitenhuis E.T.; Ciais, P.; Conway, T.J.; Gillett, N.P.; Houghton, R.A.; Marland G. Contributions to accelerating atmospheric CO₂ growth from economic activity, carbon intensity, and efficiency of natural sinks. *Proc. Natl. Acad. Sci.* **2007**, *104*(47), 18866-18870
- Carbone M.S.; Czimczik C.I.; Keenan T.F.; Murakami P.F.; Pederson N.; Schaberg P.G.; Xu X.; Richardson A.D. Age, allocation and availability of nonstructural carbon in mature red maple trees. *New. Phytol.* **2013**, *200*, 1145–1155
- Carrara, A.; Janssens, I.A.; Curiel Yuste, J.; Ceulemans, R. Seasonal changes in photosynthesis, respiration and nee of a mixed temperate forest. *Agric. For. Meteorol.* **2004**, *126*, 15-31
- Cestar, D. and Kovačić, Đ. Wood volume tables for Black Alder and Black Locust. *Rad. Šum. inst. Jastrebarsko* **1982**, *49*, 1-149 (In Croatian with English summary)

- Cestar, D. and Kovačić, Đ. Wood volume tables for Narrow-leaved Ash (*Fraxinus parvifolia* Auct.). *Rad Šum inst Jastrebarsko* **1984**, *60*, 1-178 (In Croatian with English summary)
- Croatian Forests Ltd.: Zagreb, Croatia, **2017**; Available online: <http://www.mps.hr/hr/sume/sumarstvo/sumskogospodarska-osnova-2016-2025>, 859 pp
- Curtis, P.S.; Gough, C.M. Forest aging, disturbance and the carbon cycle. *New Phytol.* **2018**, *219*, 1188–1193.
- Delpierre, N.; Berveiller, D.; Granda, E.; Dufrene, E. Wood phenology, not carbon input, controls the interannual variability of wood growth in a temperate oak forest. *New Phytol.* **2016**, *210*, 459-470.
- Dietze, M.C.; Sala, A.; Carbone, M.S.; Czimeczik, C.I.; Mantooth, J.A.; Richardson, A.D.; Vargas, R. Nonstructural carbon in woody plants. *Annu. Rev. Plant. Biol.* **2014**, *65*, 667-687
- EdiRe software: <http://www.geos.ed.ac.uk/homes/jbm/micromet/EdiRe>
- EddyPro Software Instruction Manual, LI-COR
- Falge E.; Baldocchi D.; Olson R.; Anthoni P.; Aubinet M.; Bernhofer C.; Burba G.; Ceulemans R.; Clement R.; Dolman H.; Granier A. et al. Gap filling strategies for defensible annual sums of net ecosystem exchange. *Agric. For. Meteorol.* **2001**, *107*, 43-69
- Felber R.; Münger A.; Neftel A.; Amman C. Eddy covariance methane flux measurements over a grazed pasture: effect of cows as moving point sources. *Biogeosciences* **2015**, *12*, 3925-3940
- Finnigan J.J.; Clement R.; Malhi Y.; Leuning R.; Cleugh H.A. A re-evaluation of long-term flux measurement techniques – Part 1: averaging and coordinate rotation. *Boundary Layer Meteorology*, **2003**, *107* (1), 1-48
- Flux Footprint Prediction (FFP) online data processing. Available online: <http://geography.swansea.ac.uk/nkljun/ffp/www/>
- FLUXNET2015 Dataset. Available online: <http://fluxnet.fluxdata.org/data/>

- Foken T. Micrometeorology. **2008** Springer 308 pp.
- Gan S. and Amasino R. Making Sense of Senescence. *Plant Physiol*, **1997**, *113*, 313-319
- Gaudinski, J.B.; Torn, M.S.; Riley, W.J.; Swanston, C.; Trumbore, S.E.; Joslin, J.D.; Majdi, H.; Dawson, T.E.; Hanson, P.J. Use of stored carbon reserves in growth of temperate tree roots and leaf buds: Analyses using radiocarbon measurements and modeling. *Glob. Chang. Biol.* **2009**, *15*, 992–1014
- Gough, C.M.; Vogel, C.S.; Schmid, H.P.; Curtis, P.S. Controls on annual forest carbon storage: Lessons from the past and predictions for the future. *Bioscience* **2008**, *58*, 609-622.
- Gough, C.M.; Vogel, C.S.; Schmid, H.P.; Su, H.B.; Curtis, P.S. Multi-year convergence of biometric and meteorological estimates of forest carbon storage. *Agric. For. Meteorol.* **2008**, *148*, 158-170.
- Gough, C.M.; Flower, C.E.; Vogel, C.S.; Dragoni, D.; Curtis, P.S. Whole-ecosystem labile carbon production in a north temperate deciduous forest. *Agric. For. Meteorol.* **2009**, *149*, 1531–1540
- Goulden M.L.; Munger, J.W.; Fan S.-M.; Daube B.C.; Wofsy S.C. Measurements of carbon sequestration by long-term eddy covariance: methods and a critical evaluation of accuracy. *Glob Chang Biol*, **1996a**, *2*, 169-182
- Goulden M.L.; Munger, J.W.; Fan S.-M.; Daube B.C.; Wofsy S.C. Exchange of carbon dioxide by a deciduous forest: response to interannual climate variability. *Science*, **1996b**, *271*, 1576-1578
- Granier A., Ceschia E., Damesin C., Dufrene E., Epron D., Gross P., Lebaube S., Le Dantec V., Le Goff N., Lemoine D., Lucot E., Ottorini J.M., Pontailler J.Y., Saugier B. The carbon balance of a young Beech forest, **2001**, *14*, 312-325
- Granier A.; Breda N.; Longdoz B.; Gross P.; Ngao J. Ten years of fluxes and stand growth in a young beech forest at Hesse, North-eastern France. *Ann For Sci* **2008**, *65*, 704-717.
- Hanewinkel M.; Cullman D.A.; Schelhaas M.J.; Nabuurs G.J.; Zimmermann N.E. Climate change may cause severe loss in the economic value of European forest land. *Nature Clim. Change* **2013**, *3*, 203-207

- Haszpra L.; Barcza Z.; Bakwin P.S.; Berger B.W.; Davis K.J.; Weidinger T. Measuring system for the long-term monitoring of biosphere/atmosphere exchange of carbon dioxide. *J. Geophys. Res.* **2001**, *106D*, 3057-3070
- Herbst, M.; Mund, M.; Tamrakar, R.; Knohl, A. Differences in carbon uptake and water use between a managed and an unmanaged beech forest in central Germany. *For. Ecol. Manage.* **2015**, *355*, 101-108.
- Højstrup J. A statistical data screening procedure. *Meas. Sci. Technol.* **1993**, *4*, 153-157
- Indir K. Optimalni način prikupljanja i obrade podataka kontrolnom metodom u inventuri šuma. **2004**, Master's thesis, Faculty of Forestry, University of Zagreb, Zagreb, 117 pp (In Croatian with English summary)
- IPCC. *Good Practice Guidance for Land Use, Land-Use Change and Forestry*; Penman, J.; Gytarsky, M.; Hiraishi, T.; Kruger, D.; Pipatti, R.; Buendia, L.; Miwa, K.; Ngara, T.; Tanabe, K.; Wagner, F. et al.; IPCC/IGES: Hayama, Japan, **2003**
- IPCC. *2006 IPCC Guidelines for National Greenhouse Inventories*; Eggleston, H.S.; Buendia, L.; Miwa, K.; Ngara, T.; Tanabe, K.; Eds. IGES: Kobe, Japan, **2006**
- IPCC Climate Change 2014: Synthesis Report. Contribution of Working Groups I, II and III to the Fifth Assessment Report of the Intergovernmental Panel on Climate Change [Core Writing Team, R.K. Pachauri and L.A. Meyer (eds.)]. IPCC, Geneva, Switzerland, **2014**
- Janssens I. A.; Freibauer A.; Ciais P.; Smith P.; Nabuurs G. J.; Folberth G.; Schlamadinger B.; Hutjes R. W. A.; Ceulemans R.; Schulze E. D.; Valentini R.; Dolman A. J. Europe's Terrestrial Biosphere Absorbs 7 to 12% of European Anthropogenic CO₂ Emissions. *Science* **2003**, *300*, 1538-1542
- Jena online tool - Eddy covariance gap-filling & flux-partitioning tool. Available online: <https://www.bgc-jena.mpg.de/bgi/index.php/Services/REddyProcWeb>
- Kaimal J.C.; Wyngaard J.C.; Izumi J.; Cote O.R. Spectral characteristics of surface layer turbulence. *Q. J. Royal Meteorol. Soc.* **1972**, *98*, 563-589
- Kaimal J.C.; Finnigan J.J. Atmospheric Boundary Layer Flows: Their Structure and Measurement. **1994**, Oxford University Press, New York, pp 289

- Keeland B. D. and Young J. Construction and installation of dendrometer bands for periodic tree-growth measurement. **2006** National Wetlands Research Center, Lafayette, LA
- Keeling, C.D.; Piper, S.C.; Heimann, M. Global and hemispheric CO₂ sinks deduced from changes in atmospheric O₂ concentration. *Nature*, **1996**, *381*, 218-221
- Klepac, D. Introduction. In Pedunculate oak in Croatia, 1st ed.; Klepac, D., Dundović, J., Gračan, J., Eds.; Croatian Academy of Arts and Sciences, Centre for Scientific Work: Vinkovci and Croatian forests Ltd: Zagreb, Croatia, **1996**; pp. 9-12
- Kljun N., Rotach M.W., Schmid H.P. A 3-D backward Lagrangian footprint model for a wide range of boundary layer stratifications. *Bound.-Layer Meteorol.* **2002**, *103*, 205-226
- Kljun, N.; Calanca, P.; Rotach, M.W.; Schmid, H.P. A simple two-dimensional parameterisation for Flux Footprint Prediction (FFP). *Geosci. Model Dev.* **2015**, *8*, 3695-3713
- Kozłowski T.T. and Pallardy S.G. Physiology of woody plants, **1997**, 2nd edition. Academic Press, San Diego
- Lasslop G.; Reichstein M.; Papale D.; Richardson A.D.; Arneth A.; Barr A.; Stoy P.; Wohlfahrt G. Separation of net ecosystem exchange into assimilation and respiration using a light response curve approach: critical issues and global evaluation. *Glob. Change Biol.* **2010**, *16*, 187-208
- Law, B.E.; Falge, E.; Gu, L.; Baldocchi, D.D.; Bakwin, P.; Berbigier, P.; Davis, K.; Dolman, A.J.; Falk, M.; Fuentes, J.D., et al. Environmental controls over carbon dioxide and water vapor exchange of terrestrial vegetation. *Agric. For. Meteorol.* **2002**, *113*, 97-120.
- Lee X.; Black T.A. Relating eddy correlation sensible heat flux to horizontal sensor separation in the unstable atmospheric surface layer, *J. Geophys. Res.* **1994**, *99(D8)*, 18545-18553

- Liu H. Z.; Feng J. W.; Jarvi L.; Vesala T. Four year (2006-2009) eddy covariance measurements of CO₂ flux over an urban area in Beijing. *Atmospheric. Chem. Phys.* **2012**, *12*, 7881-7892
- Lloyd J. and Taylor J.A. On the temperature dependence of soil temperature. *Funct. Ecol.* **1994**, *8*, 315-323
- Malhi Y.; Baldocchi D.D.; Jarvis P.G. The carbon balance of tropical, temperate and boreal forests. *Plant Cell Environ.* **1999**, *22*, 715-740
- Marjanović H. Modeliranje razvoja stabala i elemenata strukture u mladim sastojinama hrasta lužnjaka (*Quercus Robur* L.), **2009**, Doctoral dissertation, Faculty of Forestry, University of Zagreb, Zagreb, 213 pp (In Croatian with English summary)
- Marjanović H.; Ostrogović M.Z.; Alberti G.; Balenović I.; Paladinić E.; Indir K.; Peresotti A.; Vuletić D. Carbon dynamics in younger stands of Pedunculate oak during two vegetation periods (in Croatian with English summary). *Šum. list*, **2011**, *135*, 59-73
- Marjanović, H.; Alberti, G.; Balogh, J., Czóbel, S.; Horváth, L.; Jagodics, A.; Nagy, Z.; Ostrogović, M.Z.; Peressotti, A.; Führer, E.; Measurements and estimations of biosphere-atmosphere exchange of greenhouse gases - Forests, In: L. Haszpra (ed.), Atmospheric Greenhouse Gases: The Hungarian Perspective, **2011**, Springer, pp. 65–90
- Markkanen T.; Rannik Ü.; Keronen P.; Suni T.; Vesala T. Eddy covariance fluxes over a boreal Scots pine forest, *Bor. Environ. Res.* **2001**, *6*, 65-78
- Martínez-Vilalta, J. Carbon storage in trees: pathogens have their say. *Tree Physiol.* **2014**, *34*, 215–217
- Mauder M., Foken T. Documentation and instruction manual of the eddy covariance software package TK2, **2004**, vol 26, Arbeitsergebnisse, Universität Bayreuth, Abteilung Mikrometeorologie. 42 pp
- Mayer, B. Hydropedological relations in the region of lowland forests of the Pokupsko basin (In: Lowland forests of the Pokupsko basin, Ed: B. Mayer]. *Rad. Šumar. ins. Jastrebarsko*, **1996**, 37-89 (in Croatian)

- Michailoff, I. Zahlenmäßiges Verfahren für die Ausführung der Bestandeshöhenkurven. [Numerical algorithm for the implementation of stand height curves]. *Forstw. Cbl. u Thar. Jahrb.* **1943**, 6, 273–279 [In German]
- Moffat A.M.; Papale D.; Reichstein M.; Hollinger D.Y.; Richardson A.D.; Barr A.G.; Beckstein C.; Brasswell B.H.; Churkina G.; Desai A.R.; Falge E.; Gove J.H.; Heimann M.; Hui D.; Jarvis A.J.; Kattge J.; Noormets A.; Stauch V.J. Comprehensive comparison of gap-filling techniques for eddy covariance net carbon fluxes. *Agric. For. Meteorol.* **2007**, 147, 209-232
- Molen M.K.; Dolman A.J.; Ciais P.; Eglin T.; Gobron N.; Law B.E.; Meir P.; Peters W., et al. Drought and ecosystem carbon cycling. *Agric. For. Meteorol.* **2011** 151 (7): 765-773
- Moncrieff J.B.; Malhi Y.; Leuning R. The propagation of errors in long-term measurements of land atmosphere fluxes of carbon and water. *Glob. Change. Biol.* **1996**, 2, 231-240
- Montgomery R.B. Vertical eddy flux of heat in the atmosphere, *Journal of Meteorology* **1948**, 5, 265-274
- Moore C.J. Frequency response corrections for eddy correlation systems. *Bound.-Layer Meteorol.* **1986**, 37, 17-35
- Mori S.; Yamaji K.; Ishida A.; Prokushkin S.G.; Masyagina O.V.; Hagihara A.; Hoque A.; Suwa R.; Osawa A.; Nishizono T. Mixed-power scaling of whole-plant respiration from seedlings to giant trees. *Proc. Natl. Acad. Sci. USA* **2010**, 107: 1447-1451
- Nabuurs G.-J.; Lindner M.; Verkerk P.J.; Gunia P.J.; Deda P.; Michalak R.; Grassi G. First signs of carbon sink saturation in European forest biomass. *Nature Clim. Change.* **2013**, 3, 792-796
- Novick, K.A.; Oishi, A.C.; Ward, E.J.; Siqueira M.B.S.; Juang, J.-Y.; Stoy, P.C. On the difference in the net ecosystem exchange of CO₂ between deciduous and evergreen forests in the southeastern United States. *Glob. Change Biol.* **2015**, 21(2), 827-842.
- Obukhov A.M. Charakteristiki mikrostruktury vetra v prizemnom sloju atmosfery (Characteristics of the micro-structure of the wind in the surface layer of the atmosphere) *Izv AN SSSR ser Geofiz* **1951**, 3, 49-68

- Ohtsuka, T.; Mo, W.H.; Satomura, T.; Inatomi, M.; Koizumi, H. Biometric based carbon flux measurements and net ecosystem production (NEP) in a temperate deciduous broad-leaved forest beneath a flux tower. *Ecosystems* **2007**, *10*, 324-334.
- Ohtsuka, T.; Saigusa, N.; Koizumi, H. On linking multiyear biometric measurements of tree growth with eddy covariance-based net ecosystem production. *Glob. Change Biol.* **2009**, *15*, 1015-1024.
- Oke T.R. *Boundary Layer Climates*, **1987**, chapter 8, pages 262-303, Routledge, 2nd edition
- Owen N.A.; Choncubhair O.N.; Males J.; Del Real Laborde J.I.; Rubio-Cortes R.; Griffiths H.; Lanigan G. Eddy covariance captures four-phase crassulacean acid metabolism (CAM) gas exchange signature in Agave. *Plant Cell Environ.* **2016**, *39*, 295-309
- Palacio, S.; Camarero, J.J.; Maestro, M.; Alla, A.Q.; Lahoz, E.; Montserrat-Martí, G. Are storage and tree growth related? Seasonal nutrient and carbohydrate dynamics in evergreen and deciduous Mediterranean oaks. *Trees*, **2018**, *32*, 777-790
- Pan Y.D.; Birdsey R.A.; Fang J.Y.; Houghton R.; Kauppi P.E.; Kurz W.A.; Phillips O.L.; Shvidenko A.; Lewis S.L.; Canadell J.G.; Ciais P.; Jackson R.B.; Pacala S.W.; Mcguire A.D.; Piao S.L.; Rautiainen A.; Sitch S.; Hayes D. A large and persistent carbon sink in the world's forests. *Science* **2011**, *333*, 988-993
- Panofsky H.A. and Dutton J.A. *Atmospheric Turbulence – models and methods for engineering applications*. **1984**, Wiley, New York, pp 397
- Papale, D.; Reichstein, M.; Aubinet, M.; Canfora, E.; Bernhofer, C.; Kutsch, W.; Longdoz, B.; Rambal, S.; Valentini, R.; Vesala, T.; Yakir, D. Towards a standardized processing of Net Ecosystem Exchange measured with eddy covariance technique: algorithms and uncertainty estimation. *Biogeosciences* **2006**, *3*, 571-583
- Pilegaard K.; Hummelshøj P.; Jensen N.O.; Chen Z. Two years of continuous CO₂ eddy flux measurement over a Danish beech forest. *Agric. For. Meteorol.* **2001**, *107*, 29-41
- Pilegaard, K.; Ibrom, A.; Courtney, M.S.; Hummelshøj, P.; Jensen, N.O. Increasing net CO₂ uptake by a Danish beech forest during the period from 1996 to 2009. *Agric. For. Meteorol.* **2011**, *151(7)*, 934-946.

- Pregitzer K.S. and Euskirchen E.S. Carbon cycling and storage in world forests: biome patterns related to forest age. *Glob. Change Biol.* **2004**, *10(1)*, 1-26
- Raupach M.R. Anomalies in flux-gradient relationships over forests, *Bound.-Layer Meteorol.* **1979**, *16*, 467-486
- Reichstein M.; Falge E.; Baldocchi D.; Papale D.; Aubinet M.; Berbigier P.; Bernhofer P.; Buchmann N.; Gilmanov T.; Granier A. et al. On the separation of net ecosystem exchange into assimilation and ecosystem respiration: review and improved algorithm. *Glob. Change Biology.* **2005**, *11*, 1424-1439
- Richardson, A.D.; Keenan, T.F.; Migliavacca, M.; Ryu, Y.; Sonnentag, O.; Toomey, M. Climate change, phenology, and phenological control of vegetation feedbacks to the climate system. *Agric. For. Meteorol.* **2013**, *169*, 156-173
- Roth M. Review of atmospheric turbulence over cities, *Q. J. Royal Meteorol. Soc.* **2000**, *126*, 941-990
- Schimel D.S. Terrestrial ecosystems and the carbon cycle. *Glob. Change. Biol.* **1995**, *1*, 77-91
- Schmid H.P.; Grimmond S.B.; Cropley F.; Offerle B.; Su H.-B. Measurement of CO₂ and energy fluxes over a mixed hardwood forest in the mid-western United States. *Agric. For. Meteorol.* **2000**, *103*, 357-374
- Schulze E.-D.; Beck E.; Müller-Hohenstein K. *Plant Ecology*, **2005**, Springer, 679 pp
- Schumacher, F.X. and Hall, F.D.S. Logarithmic expression of timber-tree volume. *J. Agric. Res.* **1933**, *47*, 719-734
- Stoy, P.C.; Katul, G.G.; Siqueira M.B.S.; Juang, J.-Y.; Novick, K.A.; Uebelherr, J.M.; Oren, R. An evaluation of models for partitioning eddy covariance-measured net ecosystem exchange into photosynthesis and respiration. *Agric. For. Meteorol.* **2006**, *141*, 2-18.
- Stull R.B. *An introduction to Boundary Layer Meteorology*, **1988** Springer, 670 pp
- Subke, J.A.; Inglima, I.; Cotrufo, M.F. Trends and methodological impacts in soil CO₂ efflux partitioning: A meta-analytical review. *Glob. Change Biol.* **2006**, *12*, 1813-1813.

- Sulman, B.N.; Roman, D.T.; Scanlon, T.M.; Wang, L.; Novick, K.A. Comparing methods for partitioning a decade of carbon dioxide and water vapor fluxes in a temperate forest. *Agric. For. Meteorol.* **2016**, *226-227*, 229-245.
- Swinbank W.C. The measurement of vertical transfer of heat and water vapor by eddies in the lower atmosphere. *Journal of Meteorology*, **1951**, *8*, 135-145
- Špiranec, M. Wood volume tables. *Rad. Šum. inst. Jastrebarsko* **1975**, *22*, 1-262 (In Croatian with German summary)
- Šumarska enciklopedija (1959) 1st edition, Leksikografski zavod FNRJ
- Teets A.; Fraver S.; Hollinger D.Y.; Weiskittel A.R.; Seymour R.S.; Richardson A.D. Linking annual tree growth with eddy-flux measures of net ecosystem productivity across twenty years of observation in a mixed conifer forest. *Agric. For. Meteorol.* **2018**, *249*, 479-487
- Tennekes H. and Lumley J.L. A First Course in Turbulence, **1972**, M.I.T. Press, 300 pp
- Thomas M.V.; Malhi Y.; Fenn K.M.; Fisher J.B.; Morecroft M.D.; Lloyd C.R.; Taylor M.E.; McNeill D.D. Carbon dioxide fluxes over an ancient broadleaved deciduous woodland in southern England, *Biogeosciences* **2011**, *8*, 1595-1613
- Thomson, D.J. Criteria for the selection of Stochastic Models of Particle Trajectories in Turbulent Flows. *J. Fluid Mech.* **1987**, *180*, 529-556
- Trinajstić I. Taksonomska problematika hrasta lužnjaka u hrvatskoj, U: D. Klepac (gl. ur.), Hrast lužnjak u Hrvatskoj, **1996**, HAZU Centar za znanstveni rad Vinkovci i HŠ p.o., 96-101, Zagreb
- Urbanski, S.; Barford, C.; Wofsy, S.; Kucharik, C.; Pyle, E.; Budney, J.; McKain, K.; Fitzjarrald, D.; Czikowsky, M.; Munger, W. Factors controlling CO₂ exchange on timescales from hourly to decadal at Harvard Forest. *J. Geophys. Res.* **2007**, *112*, G02020
- Van Dijk, A.J.I.M. and Dolman, A.J. Estimates of CO₂ uptake and release among European forests based on eddy covariance data. *Glob. Change Biol.* **2004**, *10*, 1445-1459

-
- Vickers, D.; Mahrt, L. Quality Control and Flux Sampling Problems for Tower and Aircraft Data. *J. Atmos. Ocean. Technol.* **1997**, *14*, 512-526
- Web E.K.; Pearman G.I.; Leuning R. Correction of the flux measurement for density effects due to heat and water vapour transfer. *Q. J. Royal Meteorol. Soc.* **1980**, *106*, 85-100
- Wilczak, J.M.; Oncley S.P. Sonic anemometer tilt correction algorithms. *Bound.-Layer Meteorol.* **2001**, *99*, 127-150
- Wilkinson, M.; Eaton, E.L.; Broadmeadow, M.S.J.; Morison, J.I.L. Inter-annual variation of carbon uptake by a plantation oak woodland in south-eastern England. *Biogeosciences* **2012**, *9*, 5373-5389
- WRB - World Reference Base for Soil Resources 2014 International soil classification system for naming soils and creating legends for soil maps, update 2015. World Soil Resources Reports No. 106. FAO: Rome, Italy, **2015**, pp 192

CURRICULUM VITAE

Mislav Anić was born on 19th of April 1988 in Koprivnica where he finished Fran Galović gymnasium in 2006. He graduated at Faculty of Science, University of Zagreb, on 17th of December 2013, at the Department of Geophysics. In May of 2014 he started internship at Croatian forest research institute, at Department for forest management and forestry economics. With the beginning of 2015 he became assistant on the project EFFEffectivity (Estimating and Forecasting Forest Ecosystems Productivity by Integrating Field Measurements, Remote Sensing and Modelling) and enrolled in postgraduate doctoral program Physics, at the Faculty of Science, University of Zagreb, direction Geophysics.

List of publications:

Anić, M.; Ostrogović Sever, M.Z.; Alberti, G.; Balenović, I.; Paladinić, E.; Peresotti, A.; Tljan, G.; Večenaj, Ž.; Vuletić, D.; Marjanović, H. Eddy covariance vs. biometric based estimates of Net Primary Productivity of pedunculated oak (*Quercus robur* L.) forest in Croatia during 10 years. *Forests* **2018**, *9*, 764

Ostrogović Sever, M.Z.; Paladinić, E.; Barcza, Z.; Hidy, D.; Kern, A.; Anić, M.; Marjanović, H. Biogeochemical Modelling vs. Tree-Ring Measurements – Comparison of Growth Dynamic Estimates at Two Distinct Oak Forests in Croatia. *SEEFOR*, **2017**, *8(2)*, 71-84

Kern, A.; Marjanović, H.; Dobor, L.; Anić, M.; Hlasny, T.; Barcza, Z. Identification of Years with Extreme Vegetation State in Central Europe Based on Remote Sensing and Meteorological Data. *SEEFOR*, **2017**, *8(1)*, 1-20